POWER REACTOR TECHNOLOGY

A Quarterly Technical Progress Review

Prepared for DIVISION OF TECHNICAL INFORMATION, USAEC, by
W. H. ZINN and J. R. DIETRICH, GENERAL NUCLEAR ENGINEERING CORPORATION

Spring 1964

● VOLUME 7

● NUMBER 2

FEATURE ARTICLE:

Neutron Physics Considerations in Large Fast Reactors

TECHNICAL PROGRESS REVIEWS

To meet the needs of industry for concise summaries of current atomic developments, the Atomic Energy Commission is publishing this series, Technical Progress Reviews. Issued quarterly, each of the reviews digests and evaluates the latest findings in a specific area of nuclear technology and science.

The five journals published in this series are:

Isotopes and Radiation Technology, P. S. Baker, A. F. Rupp, and associates, Oak Ridge National Laboratory

Nuclear Safety, Wm. B. Cottrell, W. H. Jordan, and associates, Oak Ridge National Laboratory

Power Reactor Technology, W. H. Zinn and J. R. Dietrich, General Nuclear Engineering Corporation

Reactor Fuel Processing, Stephen Lawroski and associates, Chemical Engineering Division, Argonne National Laboratory

Reactor Materials, R. W. Dayton, E. M. Simons, and associates, Battelle Memorial Institute

Each journal may be purchased from the Superintendent of Documents, U. S. Government Printing Office, Washington, D. C., 20402. *Isotopes and Radiation Technology* at $2.00 per year for subscription or $0.55 for individual issues; the other four journals at $2.50 per year and $0.70 per issue. See back cover for remittance instructions and foreign postage requirements.

Availability of Reports Cited in This Review

Unclassified AEC reports are available for inspection at AEC depository libraries and are sold by the Office of Technical Services, Department of Commerce, Washington, D. C., 20230. Some of the reports cited are not available owing to their preliminary nature; however, the information contained in them will eventually be made available in formal progress or topical reports.

Unclassified reports issued by other Government agencies or private organizations should be requested from the originator.

Unclassified British and Canadian reports may be inspected at AEC depository libraries. British reports are sold by the British Information Service, 45 Rockefeller Plaza, New York, N. Y.; Canadian reports (AECL series) are sold by the Scientific Document Distribution Office, Atomic Energy of Canada, Ltd., Chalk River, Ontario, Canada.

Classified U. S. and foreign reports identified in this journal as Classified may be purchased by properly cleared Access Permit Holders from the Division of Technical Information Extension, U. S. Atomic Energy Commission, P. O. Box 1001, Oak Ridge, Tenn., 37831. Such reports may be inspected at classified AEC depository libraries.

POWER REACTOR TECHNOLOGY

A REVIEW OF RECENT DEVELOPMENTS

Prepared for DIVISION OF TECHNICAL INFORMATION, USAEC,
by W. H. ZINN and J. R. DIETRICH,
GENERAL NUCLEAR ENGINEERING CORPORATION

SPRING 1964

VOLUME 7

NUMBER 2

Foreword

This quarterly review of reactor development has been prepared at the request of the Division of Technical Information of the U. S. Atomic Energy Commission. Its purpose is to assist interested organizations in the task of keeping abreast of new results in reactor technology for civilian application.

Power Reactor Technology contains reviews of selected recently published reports that are judged noteworthy in the fields of power-reactor research and development, power-reactor applications, design practice, and operating experience. It is not meant to be a comprehensive abstract of all material published during the quarter, nor is it meant to be a treatise on any part of the subject. However, related reports from different sources are often treated together to yield reviews having some breadth of scope, and background material may be added to place recent developments in perspective. Occasionally the reviews are written by guest authors. Reviews having unusual breadth or significance are placed at the front of the issue as Feature Articles.

The intention is to cover the various areas of reactor development from the general viewpoint of the reactor designer rather than from the more detailed points of view of specialists in the individual areas. To whatever extent the coverage of *Power Reactor Technology* may occasionally overlap the fields of the other Technical Progress Reviews, the overlaps will be motivated by this objective of viewing current progress through the eyes of the reactor designer.

A degree of critical appraisal and some interpretation of results are often necessary to define the significance of reported work. Any such appraisal or interpretation represents only the opinion of the reviewer and (in the usual case, when the review is written by General Nuclear Engineering Corporation staff) the Editor. When the review is predominantly interpretive, the reviewer is named; unless identified as a guest author, he is a member of the General Nuclear Engineering Corporation staff. Readers are urged to consult the original references to obtain all the background of the work reported and to obtain the interpretation of the results given by the original authors.

For timely coverage, *Power Reactor Technology* must often review fragmentary material. The fixed subject headings listed below have been adopted in the hope of maintaining some continuity and order in the material from one issue to another: all reviews except Feature Articles will be arranged under these headings. A particular issue will not necessarily contain all the headings but only those under which material is reviewed.

Economics, Applications, Programs
Resources and Fuel Cycles
Physics
Fluid and Thermal Technology
Fuel Elements
Materials
Control and Dynamics
Containment, Radiation Control, and Siting
Systems Technology
Components
Design and Construction Practice
Operating Experience
Specific Reactor Types
Specific Applications
Unconventional Approaches

W. H. Zinn, President
J. R. Dietrich, Vice-President and Editor
General Nuclear Engineering Corporation

Contents

FEATURE ARTICLE

(Note: The pagination of this journal will henceforth be consecutive throughout the four issues of each volume.)

Issued quarterly by the U. S. Atomic Energy Commission. Use of funds for printing this publication approved by the Director of the Bureau of the Budget on October 14, 1963.

FEATURE ARTICLE

Neutron Physics Considerations in Large Fast Reactors

By David Okrent*

(Editor's Note: Of all reactor types the fast reactor probably depends most strongly for successful design on correct and adequate consideration of the neutron physics relations. We are fortunate to have Dr. Okrent as a guest reviewer for that subject. Because of his long experience and his familiarity with a broad range of both calculational and experimental results, he has been able to cover even the subtler aspects of neutron-physics behavior without demanding of the reader more than a qualitative knowledge of reactor physics. We believe the review will be interesting and useful to the general reader as well as to the reactor physicist, and we expect to make good use of it as a background for future reviews of progress in fast reactor development.)

Introduction

The term "fast reactor" is a broad one, covering a host of reactor types and sizes. The common attribute of fast reactors has usually† been taken to be the absence of moderating material deliberately introduced to lower the neutron energy. The sodium, oxygen, or carbon that may be incidentally present does affect the neutron energy spectrum, but the moderating power of these elements is too small to reduce neutron energies to thermal values before capture or leakage occurs. In a very small, high-metal-density fast reactor, inelastic scattering will reduce the average fission energy of about 2 Mev only to several hundred kilovolts before fission or leakage occurs. In a very large ceramic-fueled fast reactor, on the other hand, a large fraction of the fission events in the fissile isotope, such as Pu^{239}, may occur at energies between 1 and 100 kv, and some neu-

*David Okrent received the Mechanical Engineering degree from Stevens Institute of Technology in 1943 and the Ph.D. in Physics from Harvard University in 1951. Since January 1951 he has been with the Argonne National Laboratory. He served as chief physicist in the design and startup of ZPR-III and as chief physicist during the design of EBR-II. As manager of the Fast Reactor Safety Program for several years, he originated the TREAT Reactor and experimental program and also worked on theoretical problems in the physics and safety of fast reactors. Dr. Okrent became a Senior Physicist at Argonne in 1957 and is currently a member of the Laboratory Director's Office. He is also a member of the AEC Advisory Committee on Reactor Safeguards.

In 1955 he was a delegate to the first Atoms for Peace conference in Geneva. In 1958 he served with the United Nations as a Scientific Secretary for the second Geneva Conference. In 1961–1962 he held a Guggenheim fellowship at the University of Cambridge. Dr. Okrent is a Fellow of the American Physical Society and a member of the American Nuclear Society. He is currently vice-chairman of the Mathematics and Computing Division of ANS.

† In conceptual designs of some large metal and ceramic fueled fast reactors, modest amounts of moderating material have recently been deliberately added to the reactor core to enhance the Doppler coefficient and to modify other physics parameters. The moderation introduced is insufficient to thermalize a significant fraction of the neutrons.

trons may be found in the few-electron-volt range. In general, inelastic scattering is effective in reducing the energy of neutrons above 100 kv. The number of neutrons found much below this energy will depend directly on the ratio of moderating power to total absorption.

Fast reactors differ from thermal reactors in that the cross sections for fission at these energies are of the order of 100 times smaller than at thermal energies. However, the high concentration of fissionable atoms needed to maintain criticality is what permits the use of large quantities of structural materials, such as steel, in the core with only slight effect on the breeding ratio. Per atom, the ratio of capture in iron to fission in plutonium is similar for fast and for thermal reactors. The effect on breeding then depends primarily on the relative numbers of atoms of steel and plutonium; 50 times as much plutonium per unit volume of fast reactor core permits the use of 50 times as much steel.

Relatively speaking, the fission and capture cross sections are slowly varying in this energy range. There are no huge capture resonances, and hence no special reactivity effects are associated with xenon and samarium. There is no very strong absorber, such as cadmium in a thermal reactor, which is black to neutrons and from which one can design control rods in the form of thin plates. The neutron absorption cross section for B^{10}, the usual fast reactor control-rod poison, is less than 1 barn at 500 kev. Total cross sections are relatively small, and neutron mean free paths are relatively long. To a first approximation the reactor can usually be considered homogeneous for purposes of reactor physics analysis. There are no very steep gradients in flux, even near control rods.

The absence of thermal neutrons means that there is no thermal group whose mean energy will change with changes in moderator temperature. Small but important changes in spectrum can occur, however, with gross changes in core composition, such as partial or complete loss or expulsion of the sodium coolant from the core. Changes in the relative probability of fission and capture with such a shift in spectrum can be accompanied by important reactivity effects.

Fast reactors are relatively small, and, excepting the Doppler effect and the spectral shift on loss of sodium, most changes in reactivity with increase in temperature are associated with changes in leakage probability attributable to sodium and fuel expansion or to small motions of the fuel elements. A reduction in the fuel density in the core leads to a loss of reactivity. A reduction in sodium density allows more neutrons to leak; however, for large fast reactors this reactivity loss may be counterbalanced by a reactivity gain associated with the hardening of the neutron energy spectrum.

Table 1 VARIATION IN NEUTRON ENERGY SPECTRUM WITH REACTOR SIZE AND COMPOSITION

	Fraction of flux in each range			
Energy range	Fission spectrum	EBR-II	Large metal	Large oxide
1 to 10 Mev	0.69	0.20	0.09	0.08
0.1 to 1	0.30	0.70	0.67	0.54
0.01 to 0.1	0.01	0.10	0.22	0.30
0 to 0.01			0.02	0.08

There is a correlation between the size of the reactor, its k_∞,* and the mechanisms of control that are available. Very small reactors must be highly enriched; they will have a high k_∞ in the vicinity of 2 and hence a high leakage probability. Large changes in reactivity can be accomplished by the motion of reasonable masses of material next to the core, i.e., by reflector control. As core size increases, k_∞ and the probability of neutron leakage decrease. Increasingly impractical quantities of reflector material must be moved to achieve the necessary degree of reactor control. One then ordinarily resorts to fuel removal or the introduction of a strong neutron absorber, usually B^{10}.

The amount of control required can vary considerably with reactor type, design, and manner of operation. Things such as temperature and power coefficients, internal breeding ratio, maximum allowable burnup, and frequency of partial reloading all play major roles.

Although cross sections do vary relatively slowly, both the absolute and the relative values of cross sections change significantly over the broad energy range of importance, and this has a direct effect on the performance of various

* The term k_∞ is the number of neutrons emitted per neutron absorbed, averaged over all materials of the core.

reactors. In Table 1 the relative amounts of neutron flux to be found in four different energy ranges are given for the EBR-II reactor, for a large metal-fueled reactor, and for a large ceramic-fueled reactor. In Fig. 1 the neutron energy spectra of these reactors are compared graphically. The differences are considerable. Note that the curves of Fig. 1 represent smoothed-out versions of the true spectra. As is illustrated in Fig. 2 for an 800-liter metal-fueled reactor, the scattering resonances in materials like sodium and iron produce many more large wiggles in the curve than are shown in Fig. 1.

Many aspects of fast reactor performance depend strongly on reactor size and spectrum. Some reactors will be sensitive to neutron cross sections at high energies, whereas others will depend strongly on cross sections below 10 kv. The high concentration of fissile isotopes in very small reactors may allow the use of considerable quantities of structural materials that have high capture cross sections, whereas in a large ceramic-fueled reactor, equal volume fractions of the same structural material would prove disastrous to the breeding ratio. Similarly, the hard spectrum of small reactors will lead to small Doppler coefficients, and large reactors that have some extra moderation may have large Doppler coefficients.

Most of the nuclear safety studies on fast reactors in the past[1] have dealt with moderate-sized reactors using one-piece, freely expanding uranium metal fuel elements. The rapid shutoff coefficient with axial expansion, the absence of an appreciably positive Doppler coefficient, and the presence of a negative reactivity coefficient for loss of sodium all helped in efforts to demonstrate the safety of this reactor type.

However, development work for large fast reactors today is centered primarily on a restrained metallic fuel element or on some form of ceramic fuel, neither of which seems certain to provide a reliable, negative, prompt thermal-expansion effect on reactivity of sufficient mag-

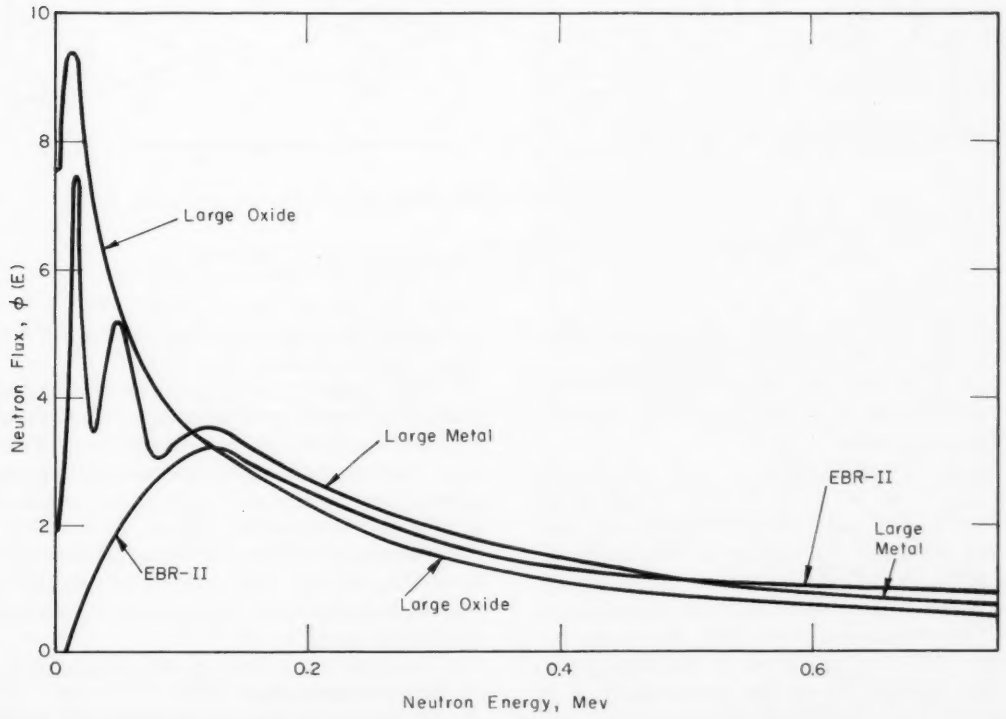

Fig. 1 Neutron energy spectra for EBR-II, for a large metal-fueled reactor, and for a very large oxide-fueled reactor.

nitude. Hence attention has shifted, and increased importance has been attached, to the Doppler effect, which promises to be large, and to the sodium void coefficient, which threatens to be positive.

Reviews of physics of small and intermediate-sized fast reactors were made by Okrent et al.[2] in 1955, by Codd et al.[3] in 1956, and by Loewenstein and Okrent[4] in 1958. Several papers on reactors received considerable attention at that seminar, as they did at the Conference on Breeding, Economics, and Safety in Large Fast Power Reactors in 1963.[13]

This review article deals primarily with the steady-state nuclear performance characteristics of large fast power reactors. The treatment given is descriptive and qualitative. Most of the results used for purposes of illustration

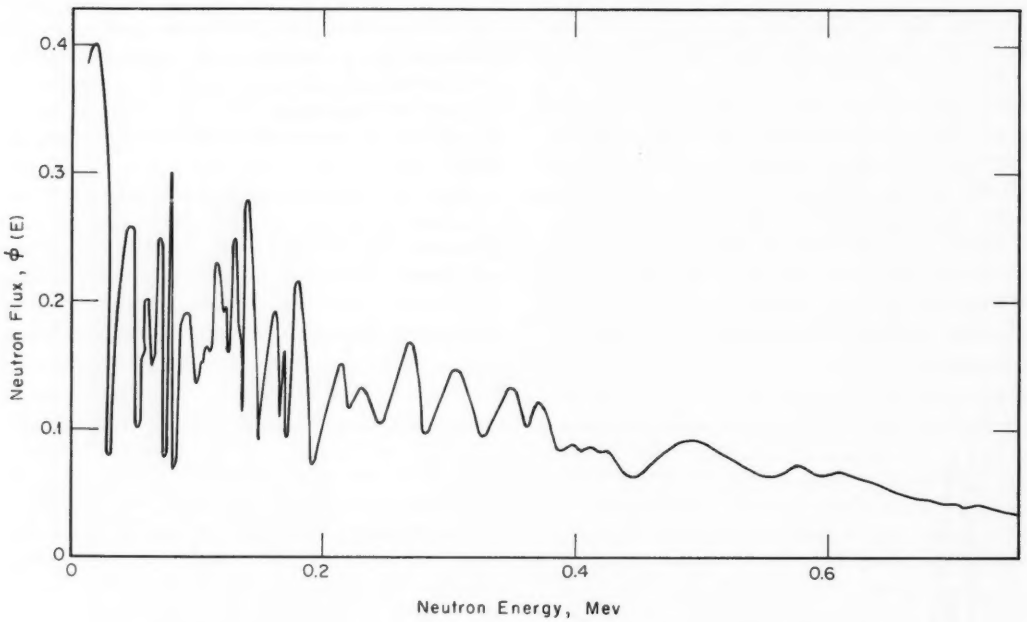

Fig. 2 Detailed neutron energy spectrum for a large metal-fueled reactor.

varied topics in fast reactor physics were given at the Second United Nations International Conference on the Peaceful Uses of Atomic Energy in 1958[5–8] and at the Conference on the Physics of Breeding in 1959.[9]

A major review of work on small fast critical assemblies was given by Paxton[10] in 1959 and in the series of papers by members of the Los Alamos Scientific Laboratory in the December 1960 issue of *Nuclear Science and Engineering*. Fast reactor cross sections were examined in detail by Yiftah et al.[11] in 1960. The most extensive collection of papers in the field of fast reactor physics is in the proceedings of a seminar, *Physics of Fast and Intermediate Reactors*, sponsored by the IAEA in Vienna in 1961.[12] Physics problems of large fast power

are drawn from the published literature. The subsections that follow deal with:

1. The important cross sections of the major fissile and fertile isotopes in relation to the neutron energy spectrum in typical fast reactors. The relative reactivity worth and breeding potential of the various isotopes are explained in terms of these cross sections.

2. Performance-related characteristics, such as breeding ratio, critical mass, and long-term reactivity changes, as functions of reactor size and composition.

3. Safety-related characteristics, namely, the reactivity coefficients.

4. A number of design variables and design considerations in relation to these neutron physics characteristics. Included among the

topics treated are hybrid fuel systems and the relative nuclear performance of various cladding and structural materials.

Basic Cross Sections

The fission cross sections for Pu^{239}, U^{233}, and U^{235} are plotted in Fig. 3 as functions of neutron energy. The cross sections are rather flat at high energies and rise slowly with decreasing energy below 100 kv. At low energies, U^{233} is seen to have a considerably higher cross section than Pu^{239}. The cross section for Pu^{241} is roughly similar to that for U^{233}.

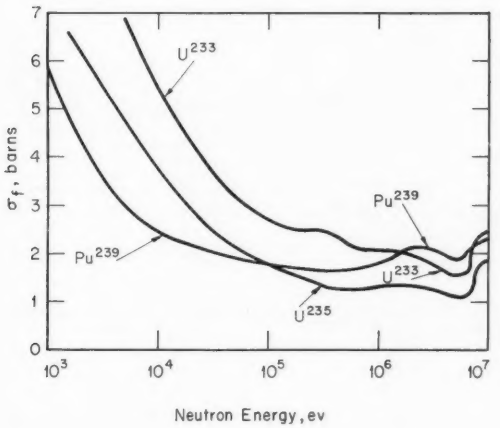

Fig. 3 Fission cross sections of U^{233}, U^{235}, and Pu^{239}.

The fission cross sections for Th^{232}, U^{238}, and Pu^{240} are compared in Fig. 4. The cross section for the plutonium isotope, which is very similar to that for U^{234}, has a much lower threshold energy and a much greater magnitude than that for U^{238}. Thorium has a very high threshold energy and a very small cross section, so that fission in thorium will be very small.

The ratios of capture to fission (α) for Pu^{239}, U^{233}, and U^{235} are plotted as functions of energy[14] in Fig. 5. This ratio has a major effect on breeding potential. Alpha for U^{233} is small and shows very little variation with energy above 10 kev. Alpha for Pu^{239}, on the other hand, is quite large and furthermore exhibits a large change with energy in the vicinity of 50 kv. One can expect considerable differences in breeding ratio for plutonium-fueled reactors

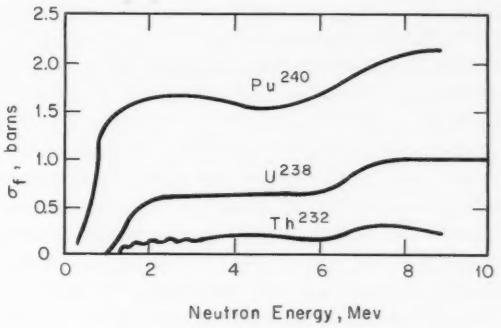

Fig. 4 Fission cross sections of Th^{232}, U^{238}, and Pu^{240}.

that have fluxes lying primarily above or primarily below this energy.

The capture cross section for U^{238} is plotted in Fig. 6. The capture cross section for thorium is similar. Over much of the energy range, the ratio of capture in the fertile materials to the sum of fission plus capture in the fissile isotope is roughly 1:10. Hence a fuel enrichment of 10% gives an internal breeding ratio in the vicinity of unity.

The number of neutrons emitted per fission, ν, rises with energy, as is demonstrated[11,15] for Pu^{239} in Fig. 7. A similar behavior is expected for all fissionable isotopes. However, the number of neutrons emitted per fission varies from isotope to isotope, as is illustrated in Table 2 for a specific neutron energy, 1.5 Mev.

Direct consequences of the cross sections, for example, are that Pu^{241} is more reactive

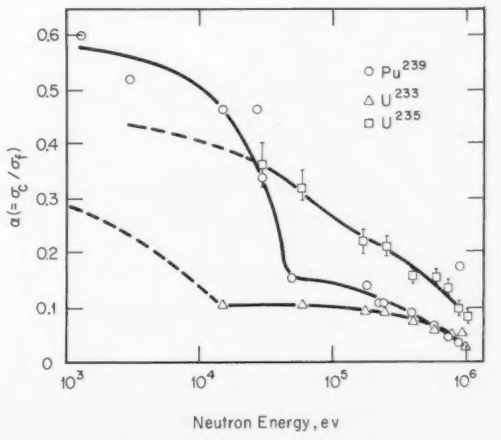

Fig. 5 Alpha for U^{233}, U^{235}, and Pu^{239}.

than Pu^{239} and that Pu^{240} is more reactive than U^{238}. The parameter ($\nu\sigma_{fission} - \sigma_{fission} - \sigma_{capture}$), which provides a partial measure of the relative reactivity worth of these isotopes, has been plotted (per atom) for U^{233}, U^{235}, and Pu^{239} in Fig. 8, and for U^{238} and Pu^{240} in Fig. 9. The curve for thorium would be similar to that for U^{238}, except that it would show less rise at higher energies because of its smaller fission cross section. Of course, below the threshold energy for fission, the parameter is negative ($= -\sigma_c$) for the fertile isotopes.

The same parameter has been averaged over the core spectrum for four reactors that have widely different spectra. The results are listed in Table 3 for U^{238}, Pu^{239}, Pu^{240}, and Pu^{241}. The rapid variation with reactor spectrum for threshold fissionable materials is obvious. Indeed, for large reactors, where the effect of scattering on neutron leakage is not very great, the total reactivity effect of the U^{238} in the core

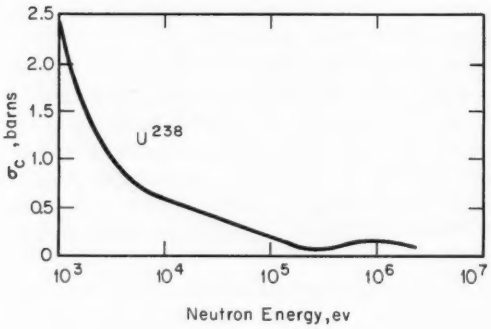

Fig. 6 Capture cross section of U^{238}.

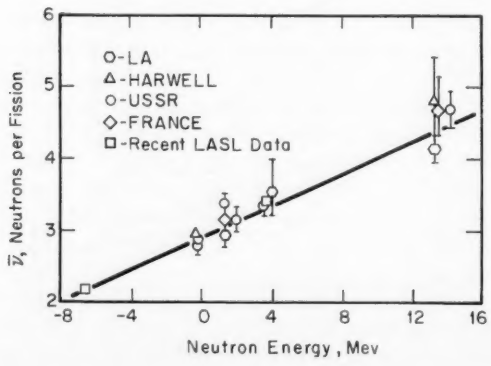

Fig. 7 ν (neutrons per fission) for Pu^{239}.

Table 2 NEUTRONS EMITTED PER FISSION (ν) PRODUCED BY 1.5-Mev NEUTRONS

Isotope	ν
Thorium	2.2
U^{233}	2.66
U^{235}	2.58
U^{238}	2.57
Pu^{239}	3.09
Pu^{240}	3.1
Pu^{241}	3.2

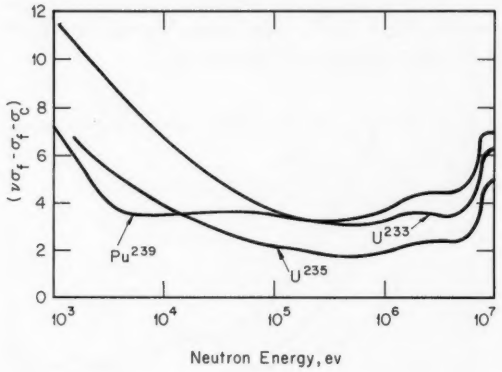

Fig. 8 Reactivity parameter ($\nu\sigma_f - \sigma_f - \sigma_c$) for U^{233}, U^{235}, and Pu^{239}.

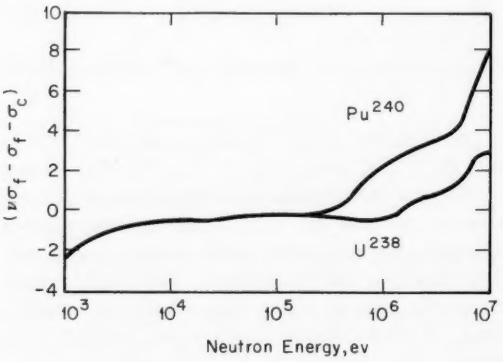

Fig. 9 Reactivity parameter ($\nu\sigma_f - \sigma_f - \sigma_c$) for U^{238} and Pu^{240}.

may be a loss of reactivity; in other words, reactors that have less U^{238} in the core will have a lower critical mass, other things being equal.

The breeding ratio of any particular reactor can be expressed by the formula

$$\text{Breeding ratio} = \frac{\nu - 1 - \alpha - A - L + (\nu' - 1)F}{1 + \alpha}$$

where the numerator measures the number of neutrons left for breeding purposes (by capture in fertile material) per fission in the thermally fissionable isotope. The symbols A, L, and F each signify the number of neutron events of a specific kind per fission in the thermally fissionable isotope. A is the parasitic absorption of neutrons in nonfissile and nonfertile materials, L is the leakage of neutrons from the blanket, and F is the number of fissions in fertile material, each giving off ν' neutrons.

Table 3 AVERAGE VALUES OF $(\nu\sigma_f - \sigma_f - \sigma_c)$ IN SEVERAL FAST-REACTOR SPECTRA

Reactor spectrum type	U^{238}	Pu^{239}	Pu^{240}	Pu^{241}
EBR-II	0.03	3.47	1.05	4.00
Fermi	−0.06	3.39	0.66	4.25
800-liter metal	−0.19	3.44	0.26	5.13
1500-liter oxide	−0.19	3.44	0.22	5.24

The term $[(\nu - 1 - \alpha)/(1 + \alpha)]$ measures the breeding potential of the primary fissionable material. The term $(\nu' - 1)\sigma_{\text{fission}}$ measures the fast fission bonus to breeding from the fertile material. These terms, averaged over the spectra of four different reactors, are compared for the appropriate isotopes in Table 4. For these reactors Pu^{239} and Pu^{241} have a considerably greater breeding potential than that of U^{233}. The breeding potential for U^{235} is below all of these. All the isotopes show some loss of breeding potential as the neutron spectrum is lowered. However, since the alpha for U^{233} is relatively flat with neutron energy, it is possible that for intermediate spectrum reactors having an average energy considerably lower than any of those examined in Table 4, the breeding potential for U^{233} will exceed that of Pu^{239}.

Table 4 BREEDING POTENTIAL OF VARIOUS ISOTOPES IN DIFFERING SPECTRA

Reactor spectrum	$(\nu - 1 - \alpha)/1 + \alpha$				$(\nu_f - 1)\sigma_f$			
	Pu^{239}	Pu^{241}	U^{233}	U^{235}	U^{238}	Pu^{240}	Pu^{242}	Th
EBR-II	1.79	1.86	1.44	1.17	0.19	1.35	1.30	0.034
Fermi	1.71	1.81	1.39	1.12	0.12	1.01	0.98	0.021
800-liter metal	1.56	1.76	1.33	1.04	0.081	0.75	0.72	0.014
1500-liter oxide	1.55	1.75	1.32	1.03	0.087	0.71	0.69	0.015

Table 5 NEUTRON BALANCE FOR 800-LITER METAL-FUELED REACTORS*

(On Basis of 1 Fission in Plutonium

	25% steel in core		25% tantalum in core	
	Core	Blanket	Core	Blanket
Fissions in Pu^{239}	1.0		1.0	
Captures in Pu^{239}	0.19		0.17	
Fissions in U^{238}	0.21	0.076	0.13	0.051
Captures in U^{238}	0.87	1.29	0.44	0.75
Na captures	0.005	0.001	0.001	
Structural captures	0.053	0.023	0.90	0.013
Neutrons escaping from blanket	0.038		0.025	
Ratio of fertile to fissile atoms in core	7.9		5.5	

*Core contains 25% fuel (Pu^{239} + U^{238}), 25% structure, and 50% sodium. Blanket is 45 cm thick and is well reflected. Blanket contains 60% U^{238}, 20% steel, and 20% sodium.

Among the fertile materials Pu^{240} can provide a much greater fast fission bonus than that of U^{238}, thanks to its higher fission cross section. The fast fission bonus from thorium is very small.

Some orientation as to the relative size of different contributions to the breeding ratio formula, given earlier, can be obtained from Table 5. The neutron balance for an 800 liter metal-fueled reactor, having an efficient well-reflected blanket, is presented here for two cases involving different structural and cladding materials—steel and tantalum. Capture in the sodium is very small, but the structural parasitic absorption depends very strongly on the material used. Leakage from the blanket can be kept small, but whether it is economical to

do this must be evaluated separately. An appreciable fast fission bonus is achievable with either structural material.

Performance: Related Characteristics

Critical Mass and Breeding Ratio

Knowledge of the critical mass and breeding ratio is basic to a determination of the economic performance of a fast reactor. The total fuel inventory will consist of a critical mass plus the requirements for fuel held up in cooling, shipping, reprocessing, refabrication, etc. Frequently an estimate of two critical masses as the total inventory is made for computing interest charges on the fuel.

The breeding gain (i.e., the breeding ratio minus 1) enters into a determination of reactor income through sale of excess fissile isotope. Also, for a given specific power (say, in units of kilowatts per kilogram of fissile isotope) the doubling time of the reactor is inversely proportional to the ratio of the breeding gain to the critical mass.[16]

Breeding may take place primarily in the core, primarily in the blanket, or may be divided roughly equally between the two, depending on reactor design. From the long-term reactivity point of view, an internal breeding ratio of about unity is desirable. However, accomplishing this characteristic may lead to an undesirable safety-related effect, namely, a sodium reactivity coefficient that corresponds to an increase of reactivity upon loss of sodium. This will be discussed later.

The performance of a broad range of large fast power reactors was computed by Yiftah and Okrent[17] in 1960, using cross sections representing the then best evaluation of available cross-section measurements.[11] Some representative results are reproduced herein to demonstrate performance trends. The calculations were all made in spherical geometry on reactor systems having typical but arbitrary compositions. The breeding ratio has been defined as the ratio of thermally fissionable isotopes made to those used, and the breeding ratio and critical mass of thermally fissionable isotopes are for the new, clean just-critical reactor. The details of geometry, composition, and density are given in Table 6.

Equal core volume does not signify equal reactor-power capability for different kinds of fuel. It should also be observed that the blanket material was always assumed to be metallic, and that the blanket fertile material volume fractions used in these calculations are quite high, probably too high when one allows for the low-density blankets usually required in the path of core coolant flow. The core volume fraction of 0.25 for structural material may also be on the high side. No allowance could be made in these idealized calculations for control-rod holes and transition regions. However, for reactors using stainless steel as the structural material, the results obtained are nevertheless typical.

The critical mass, breeding ratio, internal breeding ratio, and average alpha of Pu^{239} are listed for Pu^{239}-U^{238} metal-, oxide-, and carbide-fueled reactors as functions of core volume in the first section of Table 7.

Table 6 REACTOR SPECIFICATIONS FOR PERFORMANCE CALCULATIONS[17]

Core volume fractions	
Fuel and fertile material	0.25
Structural material	0.25
Sodium	0.5
Assumed density fuels, g/cm^3	
Pu-U^{238}	19.0
U^{235}-U^{238}	18.7
PuO_2-UO_2	8.4
PuC-UC	11.4
Thorium	11.6
ThO_2-UO_2	8.4
Blanket thickness, cm	45 (U); 54 (Th)
Blanket volume fractions	
U^{238} or Th	0.6
Steel	0.2
Sodium	0.2

The plutonium is pure Pu^{239}. The critical masses rise with reactor size, whereas the breeding ratios fall off slightly because of a rise in alpha of Pu^{239}, with a degradation in average neutron energy. The absence of a moderator such as oxygen or carbon and the higher concentration of a strong absorber such as U^{238} both cause the metal-fueled reactor to have fewer neutrons in the low energy range. Consequently the average alpha is lower for the metal fuel. This factor, plus the larger fast fission bonus that accompanies a higher concentration of U^{238}, leads to a considerably

higher breeding ratio for the metal fuels, other things being equal.

A similar set of results for U^{233}-thorium fueled reactors is also listed in Table 7. For these reactors the breeding ratio is found generally to lie between 1.2 and 1.3. Alpha for U^{233} is found to vary only slightly over the wide range of reactors studied. The breeding ratio is lower for these reactors than for the Pu^{239}-U^{238} fueled systems, not only because of the

Table 7 PERFORMANCE CHARACTERISTICS OF FAST REACTORS* USING STEEL STRUCTURE, SODIUM COOLANT, AND METAL, OXIDE, OR CARBIDE FUEL[17]

(See Table 6 for Reactor Specifications)

Reactor core volume, liters	Fuel	Critical mass, kg	Breeding ratio	Internal breeding ratio	α of fissile isotope
		U^{238}-Pu^{239} Fuel			
800	Metal	430	1.82	0.73	0.19
	Oxide	370	1.55	0.31	0.23
	Carbide	400	1.62	0.46	0.22
1500	Metal	690	1.79	0.91	0.20
	Oxide	560	1.47	0.44	0.25
	Carbide	610	1.56	0.61	0.24
2500	Metal	1030	1.76	1.04	0.21
	Oxide	810	1.42	0.54	0.27
	Carbide	900	1.52	0.73	0.25
		U^{238}-U^{235} Fuel			
800	Metal	650	1.32	0.49	0.21
1500	Metal	1010	1.30	0.62	0.22
	Oxide	790	1.09	0.27	0.24
	Carbide	860	1.15	0.40	0.24
2500	Oxide	1110	1.05	0.35	0.25
		Th-U^{233} Fuel			
800	Metal	450	1.29	0.38	0.09
	Oxide	370	1.23	0.27	0.10
	Carbide	410	1.26	0.38	0.10
1500	Metal	680	1.28	0.50	0.09
	Oxide	540	1.21	0.39	0.11
	Carbide	620	1.24	0.52	0.10
2500	Metal	970	1.28	0.61	0.09
	Oxide	760	1.19	0.49	0.11
	Carbide	890	1.23	0.62	0.11
		Th-U^{235} Fuel			
800	Metal	790	1.03	0.28	0.20
1500	Metal	1190	1.02	0.37	0.20
	Carbide	1060	0.97	0.36	0.23

$$\text{Breeding ratio} = \frac{U^{238}\ (\text{or } Th^{232}) \text{ captures in reactor}}{Pu^{239}\ (\text{or } U^{233} \text{ or } U^{235}) \text{ captures + fissions in reactor}}$$

$$\text{Internal breeding ratio} = \frac{\text{production of thermally fissionable isotopes in core}}{\text{destruction of thermally fissionable isotopes}}$$

$$\alpha = \frac{\sigma_{\text{capture}}}{\sigma_{\text{fission}}}$$

* All reactors have 25% fuel, 25% steel, and 50% sodium in the core. Blankets have 60% fertile isotope (metallic), 20% steel, and 20% sodium. Calculations were made in spherical geometry.

reduced breeding potential of U^{233} at these neutron energies but because of the very small fast fission bonus obtained with thorium as the fertile material in the core.

For comparative purposes the performances of some U^{235}-fueled reactors are also given in Table 7. In general, with U^{235} the critical mass is higher and the breeding ratio lower. This is directly attributable to its smaller fission cross section, its smaller ν relative to that measured for Pu^{239}, and its higher α relative to that for U^{233}.

Effects of Fission Products

The detailed capture cross sections of all the fission products have not been measured, but one can make theoretical estimates thereof.[18–21] The effect of fission products on breeding ratio and critical mass are listed in Table 8 for typical metal-, oxide-, and carbide-fueled plutonium reactors of 1500 liters core volume.[22] In each case the same number of fission products, 0.0008×10^{24} atoms/cm^3, have been added to the core. This many atoms would accumulate if 3⅓% of the combined Pu + U^{238} had fissioned in the metal reactor considered. The corresponding heavy atom burnup is 8.6% for the carbide case. The effect on breeding of this considerable fission-product accumulation is small, although not negligible.

The performance of reactors lacking any internal breeding is not examined here in detail. Enriched oxide or metal dispersions in a matrix of stainless steel would fall into this category. In large sizes, reactors of this type will generally have much lower critical masses and much lower breeding ratios. In a very large reactor, capture in U^{238} or thorium causes the reactor to lose reactivity, hence the reduction in critical mass for systems without fertile material in the core. However, there is a nearly complete loss of fast-fission bonus (a small blanket contribution remains), and parasitic capture in plutonium fuel would rise appreciably. The result can be a drop of 0.6 in the breeding ratio of the usual plutonium metal-fueled system. A U^{233}-fueled reactor would not be hurt as much on breeding ratio.

Table 8 EFFECT OF FISSION PRODUCTS (0.0008×10^{24} atoms/cm^3) ON PERFORMANCE OF 1500 LITER REACTORS*[22]

Reactor type	Critical mass		Breeding ratio	
	New reactor	With fission products	New reactor	With fission products
Metal	686	700	1.79	1.74
Oxide	562	592	1.47	1.39
Carbide	613	630	1.56	1.47

* All reactors have 25% fuel, 25% steel, and 50% sodium in core. The blankets all have 60% uranium metal, 20% steel, and 20% sodium.

Long-Term Reactivity Effects

The reactivity loss associated with a net uniform burnout of a fraction $\delta M_c/M_c$ of the original critical mass is given approximately by the relation

$$\frac{\delta k/k}{\delta M_c/M_c} \approx (0.4 \text{ to } 0.5)$$

$$\delta M_c = M_c \times \frac{\%\text{ burnup of fuel alloy}}{\%\text{ enrichment of fuel alloy}} \times \left(\frac{1}{1+F_c}\right) \times (1+\alpha)(1-\text{IBR})$$

where F_c = fissions in core fertile isotopes per fission in core fissile isotopes
α = ratio of capture to fission in fissile isotope
IBR = internal breeding ratio = (fissile atoms produced in core)/[fissile atoms destroyed (by capture and fission) in core]

In this report burnup means fission. The definition of IBR used herein applies to this formula, even if some thermally fissile isotope exists and is destroyed in the blanket. The real definition of the term "internal breeding ratio" becomes somewhat obscure in that event.

The change in reactivity is a function primarily of the product of the percent burnup of fuel alloy and the term (1 – IBR). Of course, if the fissile isotope produced is different from that destroyed, the relative reactivity worths of the two isotopes must be factored into the equation.

Radial growth of the fuel within its jacket under irradiation should produce only slight reactivity effects, corresponding to a small displacement of sodium bond, for example. Axial growth, on the other hand, corresponds to a net reduction in the fuel density in the

overall core. Its reactivity effect can be estimated roughly by a relation like

$$\frac{\delta k}{k} \approx -0.3\,\frac{\delta L}{L}$$

where $\delta L/L$ is the fractional increase in core length with fixed core radius and fixed mass of fuel. The numerical coefficient in the equation will vary with parameters like core size and ratio of core height to diameter.

strongly toward placing conservative limits on the shim reactivity requirements. Partial reloading helps in this respect but not without costs in shutdown time. (Fortunately, there is no xenon-override problem.) But a constant reactivity core seems highly desirable, and, in principle, it is not beyond reach in large fast power reactors. Internal breeding ratios can be raised simply by increasing either the density or volume fraction of the fuel mixture. There is relatively little change in critical mass

Table 9 LONG-TERM REACTIVITY EFFECTS*[22]

Reactor type	Breeding ratio	Internal breeding ratio	Atoms/cm^3 of Pu + U ($\times 10^{-24}$)	Burnup, % of Pu + U fissioned	$\delta k/k$ Burnout in core	Buildup in blanket	Fission product buildup	Total
800-liter metal	1.82	0.73	0.012	5	−0.054	+0.026	−0.017	−0.045
1500-liter oxide	1.47	0.44	0.00467	10	−0.169	+0.025	−0.037	−0.181
1500-liter carbide	1.56	0.61	0.0069	10	−0.147	+0.031	−0.028	−0.144

* All reactors have 25% fuel, 25% steel, and 50% coolant in the core.

The long-term reactivity losses due to a net burnup of fuel and fission-product accumulation in the core, and the reactivity gain due to buildup of plutonium in the blanket, have been listed for three typical reactors[22] in Table 9. Heavy atom burnups of 5% for the metal fuel and 10% for the oxide and carbide have been arbitrarily chosen for purposes of illustration. The major reactivity loss lies in net core burnup for all three reactors. The loss is huge for the oxide and carbide since the chosen compositions yield relatively low internal breeding ratios. The fission-product buildup has only a moderate effect on reactivity and is approximately balanced by the gain associated with blanket plutonium buildup.

Changes in plutonium isotopic composition with recycle affect the long-term reactivity loss by changing the net core burnup of fuel. The reactivity loss is generally greater for pure Pu^{239} than for the equilibrium plutonium mixture obtained with recycle. The difference between the two is about the same order of magnitude as the loss due to fission-product accumulation.[22]

Even a 2 or 3% reactivity loss can be a considerable amount to balance with control rods in a fast reactor. The small core dimensions and the unavailability of strong absorbers for control-rod materials, coupled with complicating considerations of reactor safety, all tend

or overall breeding ratio as a consequence. The move would be an obvious one except for the adverse effect it has on a vital dynamic characteristic, the sodium reactivity coefficient, which will be discussed in the following section.

Safety-Related Characteristics

The prompt-neutron lifetime in fast reactors is relatively short, i.e., the time between successive generations of neutrons emitted promptly at the time of fission will usually be less than 5×10^{-7} sec. For such a reactor an excess reactivity of only 0.0035 $\delta k/k$ above prompt critical would lead to a doubling of the power every 100 μsec. Hence any single super-prompt-critical burst in a fast reactor will take its course long before mechanically induced control-rod motion can be effective, and the inherent fast-acting reactivity coefficients of the reactor will determine whether the burst will be terminated without excessive damage or will lead to a violent disassembly with pressures comparable to those generated by a high explosive.

Thus nuclear safety must be factored into the design of the fast reactor from its very incep-

tion. A major portion of this safety consideration deals with the three reactivity coefficients due to fuel expansion, to coolant expansion, and to the Doppler effect.

Fuel Expansion

Fuel expansion leading to an increase in core length and a decrease in fuel density reduces reactivity. For a one-piece, unrestrained metallic fuel pin in a reactor such as EBR-II, this mechanism provides a large, negative prompt-acting reactivity effect that plays a major role in guaranteeing the safety of the reactor. Calculations indicate that the fuel expansion effect for a fuel element of similar type in a large reactor having a core height-to-diameter ratio of unity would still be appreciable, as is illustrated[23] in Table 10. For pancake-shaped reactors with an $H:D$ ratio of $\frac{1}{4}$, however, the fuel expansion reactivity coefficient may be much reduced.

Table 10 FUEL EXPANSION REACTIVITY COEFFICIENTS*[23]

Core size, liters	$H:D$	$\frac{\Delta k/k}{\Delta T} \times 10^6$
50	1	−4.5
	$\frac{1}{4}$	−0.9
3000	1	−3.4
	$\frac{1}{4}$	−0.9

*All reactors contain 25% PuC-$U^{238}C$, 16% steel, and 59% Na in the core.

Unfortunately most of the fuel-element types actively under development for use in large fast power reactors may be unable to provide a large prompt-acting axial expansion of the fuel. The fuel may be restrained, preventing axial motion. It may be multipiece with no definite average reduction in fuel density upon local expansion. It may crumble or crack with irradiation and thermal cycling. Care must be taken to ensure that fuel motion with heating does not add reactivity for some fuel-element types.

Sodium Void Reactivity Effects[17,24–27]

The loss of some or all the sodium from the reactor influences reactivity in three ways:

—Less neutrons are captured in sodium, adding reactivity. This is generally a small effect, since the sodium capture cross section is very small. Sodium has a large resonance at 3 kev, however, and the reactivity gained from the reduction in absorption cannot be neglected for large ceramic-fueled fast reactors.

—Neutrons tending to escape from the core will no longer be scattered into different directions by the sodium. Their leakage probability is increased, and their reactivity is decreased. The major contribution to this effect will come from the sodium near the core boundary; a change in neutron direction near the core center has less influence on the chance of its leaking. Small reactors having more leakage will be more sensitive than large reactors to the change in scattering probability. Reactors in which sodium contributes a higher fraction of the scattering will have a greater increase in neutron leakage with sodium loss.

—The loss of inelastic scattering and elastic moderation by the sodium results in a harder neutron energy spectrum. Fission becomes more probable in the fertile isotopes like U^{238} and Pu^{240}, and capture and fission in all isotopes occur at a higher average energy. However, the capture cross section of Pu^{239} falls off much more rapidly with increasing energy than does the Pu^{239} fission cross section, as do also the capture cross sections of most other highly absorbing isotopes, for example, niobium and U^{238}. Hence the average number of neutrons produced per absorption (fission and capture)

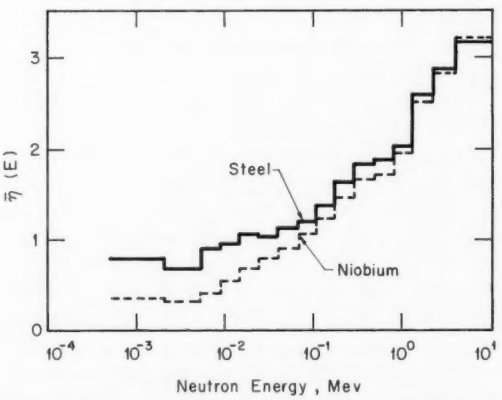

Fig. 10 $\bar{\eta}$ as a function of neutron energy for 1500-liter plutonium carbide-fueled reactors with steel or niobium structure. $\bar{\eta}$ is the average number of neutrons emitted per absorption in all core materials.

in all core materials rises as the spectrum hardens, and this effect generally produces a reactivity gain. The effect is illustrated in Fig. 10 for 1500-liter reactors fueled with PuC-UC and using steel or niobium as the structural material.[17] Using more sophisticated calculation techniques,[25] Hummel et al.[28] recently reported a similar result, as illustrated in Fig. 11, where the adjoint flux (i.e., the relative reactivity worth of a neutron) is plotted for two large oxide-fueled reactors. The situation is much aggravated when the enrichment is reduced, or when Pu^{240} and fission products are present.

The net sodium void reactivity effect will be negative if the contribution from enhanced neutron leakage predominates. This is the case for the EBR-II and the Enrico Fermi reactors.

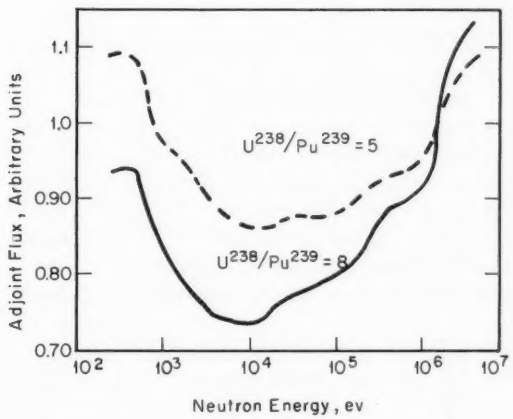

Fig. 11 Adjoint flux (neutron reactivity worth) for large $Pu^{239}O_2$-$U^{238}O_2$ fueled reactors. (Reactors have 70 vol.% sodium effect of Pu^{240} and fission products if not included.)

As is shown in Fig. 12, the sodium void coefficient becomes less negative (or more positive) as reactor size is increased for a given reactor composition.[17] For each composition there is some size at which the spectral effect predominates and the net effect becomes positive. The reactors of Fig. 12 are fueled with plutonium-uranium metal, using steel or niobium as the structural material. Sodium occupies 50% of the core. With steel structure the threshold for a positive coefficient is about 1200 liters, whereas with niobium the threshold falls below 500 liters. The calculations were

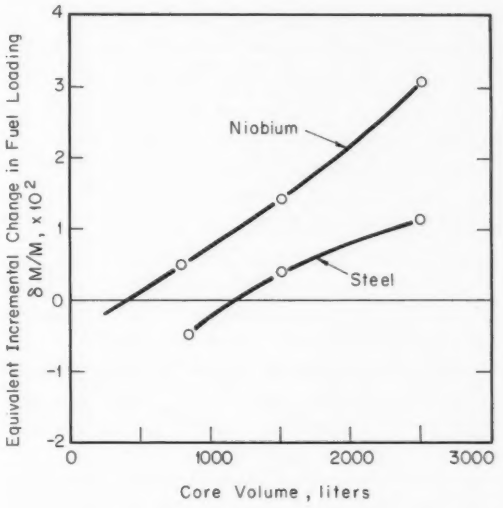

Fig. 12 Reactivity change effected by removal of 40% of sodium from plutonium-metal-fueled cores with steel or niobium structure.

made in spherical geometry, and the sodium coefficient was computed for the loss of core sodium only.

When a fuel material of lower density is used, less U^{238} will be present in the fuel elements, and the sodium void coefficient turns positive at a larger core size. In Fig. 13 the coefficient has been plotted against reactor size for some specific carbide- and oxide-fueled reactors. In the case of PuC-UC the threshold volume for a positive coefficient was calculated to be near 2000 liters, whereas for the oxide it was above 3000 liters.

The spatial dependence of the sodium void coefficient is also an important consideration. As shown in Fig. 14, Nims and Zweifel[24] calculated that the net coefficient for the Fermi reactor was negative at all core radii. In this relatively small U^{235}-fueled* reactor, spectral hardening was calculated to cause a reactivity loss rather than a gain. In a larger reactor fueled with PuO_2 dispersed in a uranium-molybdenum matrix, however, as is shown in Fig. 15, only neutron leakage contributed nega-

* The flatter variation of α with energy and the rapid fall of σ_f with increasing neutron energy for energies below 300 kev with U^{235} lead one to expect this isotope to be less inclined toward positive sodium coefficients than is Pu^{239}.

tively to the sodium void coefficient. The net coefficient varied from highly positive at the core center to slightly negative at the core edge.

Hence for a reactor having a zero value for the overall sodium coefficient, there is a strong positive component from the inner portions of the core which is balanced by a negative contribution from the blanket and from outer parts

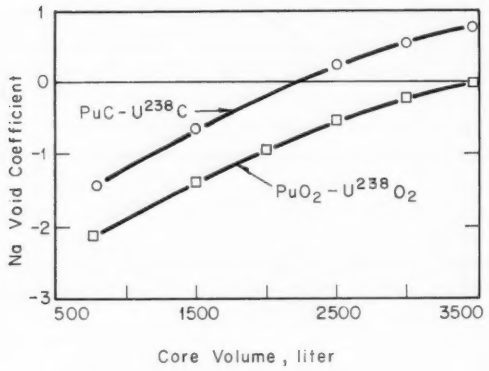

Fig. 13 Sodium coefficient as a function of core volume for oxide and carbide-fueled reactors. (Reactor composition is 25% fuel, 25% steel, and 50% sodium.)

of the core. Thus expulsion of sodium initially from the center of the core can lead to a reactivity excursion. This effect is illustrated[29] in Fig. 16. The change in reactivity with progressive axial loss of sodium is plotted for each of two oxide-fueled reactors. In Case A, where a total loss of sodium leads to a gain of reactivity of 0.008 $\Delta k/k$, there is a peak gain of more than twice this amount when two-thirds of the core is the only region voided. Case B describes a reactor to which some beryllium oxide has been added. The addition of this small amount of moderator serves two purposes. First, it makes the sodium coefficient less positive by shifting the neutron energy spectrum downward and by reducing the dependence of the spectrum on the presence or absence of sodium. Second, by increasing the fraction of low-energy neutrons present at all times—both in the presence and absence of sodium—it ensures a considerably larger negative Doppler coefficient than would be present in Case A. However, the beryllium oxide addition has a bad side effect. The breeding ratio[29] drops from about 1.3 to about 1.1.

If the magnitude of the reactivity which might be gained through the loss of sodium were always less than that which could be balanced by other reactivity effects, the sodium void reactivity effect might not assume very great importance in large fast power-reactor design. However, one generally has only a fraction of 1% $\Delta k/k$ available for shutdown from the Doppler effect or from fuel expansion, even if the latter mechanism is still operative at high fuel temperatures. On the other hand, the reactivity gains from the total loss of sodium have been calculated to be well in excess of 3% $\Delta k/k$ for some core compositions in large sizes.

What are the avenues available if one wishes to achieve a negative sodium coefficient, or a coefficient that is only slightly positive, in a 1000-Mw(e) reactor fueled with plutonium plus U^{238}? Core volumes ranging from 3000 to 6000 liters and perhaps more are needed for such an output.

As shown[27] in Fig. 17, the sodium coefficient depends strongly on the sodium volume fraction for a given core composition and volume. For compositions typical of large reactors, the sodium coefficient is slightly positive for small sodium volume fractions, increasing as the volume fraction of sodium is increased, until, somewhere between 50 and 70 vol.% sodium, the coefficient falls sharply and becomes negative. The greater the core height (the greater

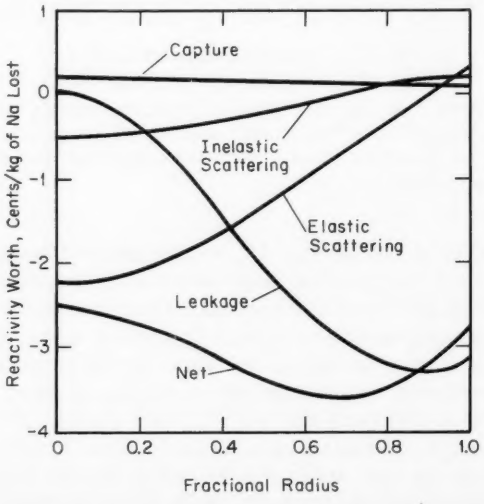

Fig. 14 Components of sodium density coefficient of reactivity for Fermi reactor as a function of core radius.

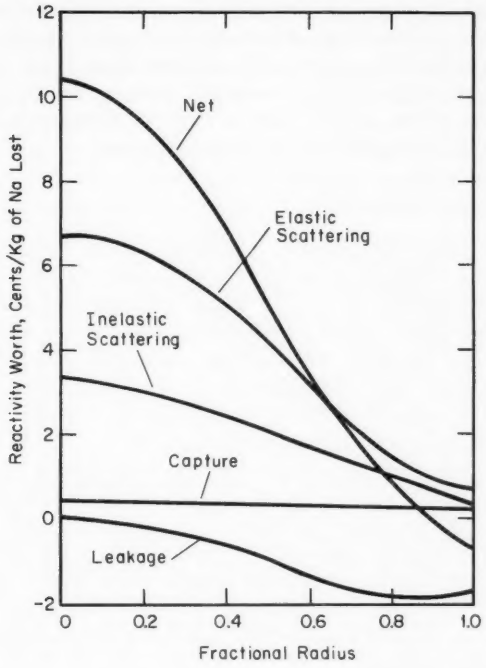

Fig. 15 Components of sodium density coefficient of reactivity for a 800-liter cermet-fueled (PuO_2 in U^{238} + Mo) reactor as a function of core radius.

the core volume) the greater the sodium volume fraction needed to achieve a negative sodium coefficient.

Figure 17 is for oxide-fueled reactors. For plutonium-U^{238} metal-fueled reactors that have the same overall volume fractions in the core, the sodium coefficients would be more positive for each reactor design, thanks to the higher concentration of U^{238} in the fuel.

The high sodium volume fractions necessary to give a negative coefficient will lead to reduced breeding ratios. A lower fast fission bonus from the U^{238} is a major cause. The efficiency of the blanket for capturing neutrons may also be impaired. And the internal breeding in the core will drop in direct relation to the ratio of U^{238} to Pu^{239}, leading to greater reactivity losses for the same degree of heavy atom burnup.

Also, high sodium volume fractions may lead to undesirably large positive reactivity contributions, in the event that only the central regions of the core should lose sodium.

Various geometric configurations may afford the opportunity of tailoring the sodium coefficient to more desirable specifications. Pancake-shaped, or thin, annular cores lead to higher enrichment, greater neutron leakage, and hence some improvement in the sodium coefficient.

Calculations indicate that the reactivity effect due to loss of sodium from the core alone tends to be relatively insensitive to the blanket design.[28,30] However, the reactivity loss accompanying loss of sodium from the blanket is quite large for a relatively thin blanket having a high volume fraction of sodium. Unfortunately such a blanket is not efficient in capturing neutrons, and its use might lead to an appreciable reduction in breeding ratio. Modifications in the relation between blanket and core, i.e., the introduction of a sodium transition region between the two, may be a better way to help achieve an overall negative sodium void effect.

At the Argonne conference on large fast power reactors[13] in October 1963, studies were reported by Cohen[29] and by Zaleski[31] on the safety characteristics of large fast reactors having positive sodium void effects. Zaleski found that with a large negative Doppler coefficient the reactor would still be stable in the presence of a positive sodium void coefficient. Cohen and Zaleski both found that the course of an accident involving the expulsion of sodium by boiling depends very strongly on the manner in which the sodium is lost from the reactor. For a mild power transient or a partial loss of flow, boiling might be limited to the upper core regions

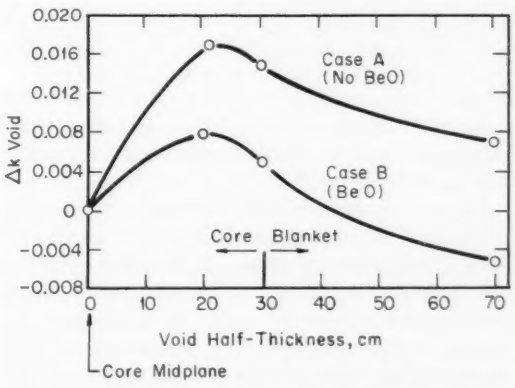

Fig. 16 Spatial dependence of reactivity change for progressive axial loss of sodium, starting at core midplane. (Case *A* is a large oxide-fueled reactor. Case *B* is a similar reactor to which some BeO has been added to improve Doppler and sodium density coefficients.)

and upper blanket. In this case boiling would decrease reactivity. However, model experiments, using water,[32] have exhibited a chugging behavior that leads to periodic voiding of the central regions of subassemblies; hence further study is needed here.

For the hypothetical accident involving full loss of coolant flow and a delay in scram, boiling may begin at the core center. The course of such an event would depend strongly on the

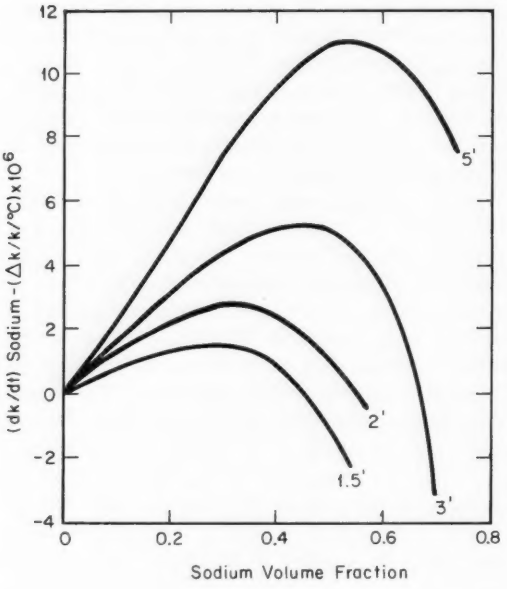

Fig. 17 Sodium coefficient as a function of core height and sodium volume fraction for pancake-shaped reactors (vol.% fuel/vol.% steel = 2).

magnitude of the Doppler effect and the variation in sodium void reactivity effect with position in the reactor.[29]

Clearly, intensive study is needed on the role of positive sodium void effects in the safety of large fast power reactors. If, in order to go to the 1000-Mw(e) size, one has to pay a large penalty in the form of reduced breeding ratio, higher fuel-cycle costs, or greater capital investment for containment purposes, it may be that two 500-Mw(e) reactors at a common site will prove more desirable. Or an increased emphasis on higher power densities, leading to smaller reactor sizes, may result.

In any event, it is clear that the determination of the sodium void effect, the evaluation of the effect to determine what are its acceptable magnitudes, and the accomplishment of acceptable effects without spoiling other reactor performance characteristics combine to form one of the major reactor physics problems of large fast power-reactor design today.

Other Coolants

Since the positive character of the sodium void coefficient is introduced primarily by its moderating power, it might be expected that this effect would be alleviated with the use of a heavy coolant. Calculations have been made of coolant void coefficient for several large reactors cooled with a lead-bismuth eutectic.[17] These magic number elements have low neutron-capture cross sections and high thresholds for inelastic scattering, making them ideal in this respect. Highly negative coolant void coefficients were obtained with lead-bismuth for reactors in which sodium coolant would lead to a highly positive coefficient. A coolant like potassium should also have a less positive tendency than sodium.

Lithium has also been examined as a potential fast reactor coolant.[33] As one expects, even the weakly absorbing Li^7 isotope gives a more positive coolant void coefficient in large reactors than sodium, as a consequence of its stronger moderating powers. The presence of Li^6 isotope in small amounts in the lithium makes the situation still less attractive. Since Li^6 is a strong neutron absorber, its explusion, of course, leads to considerable reactivity gains.

Fast reactors cooled with helium gas or carbon dioxide are not expected to have sizable reactivity effects associated with coolant pressure changes.[34] Fast reactors cooled with steam or water at supercritical pressure, however, apparently can face a problem similar to that encountered with sodium.[35]

Doppler Effect[27,36–41]

Heating of the fuel changes the velocity of atomic vibration, leading to a changed distribution of relative velocities between neutron and atom. Any self-shielding in cross-section resonances is reduced, and the increased reaction rates are reflected in reactivity changes. If only fissile material is heated, it has been expected that a gain in reactivity would result, due to the increased probability of absorption

compared to leakage. When an isotope like U^{238}, having a high cross section for neutron capture, is intimately mixed with the fissile isotope in sufficient quantity, the Doppler effect associated with fuel heating will lead to a reactivity loss.

The EBR-I reactor with the Mark I and II loadings exhibited a prompt positive power coefficient of reactivity[42] that was thought possibly to arise from a positive Doppler coefficient. Although later experiments demonstrated that the positive coefficient arose from bowing of the fuel rods,[43,44] attempts were made to calculate and to measure[45,46] a Doppler effect. The results of both calculation and experiment indicated that the Doppler coefficient was so small as to be negligible in EBR-I.

Self-shielding of resonances is small at the higher neutron energies. A greater resonance width, a higher level density, and a reduced resonance strength combine to produce a generally overlapping character. In reactors of moderate size such as the EBR-II and the Enrico Fermi, with relatively high fuel enrichment and a hard neutron energy spectrum, the Doppler effect on reactivity is believed to be small, much smaller than the negative reactivity effect of fuel expansion for these reactors.

In large fast reactors, on the other hand, particularly those fueled with a ceramic such as the oxide or carbide, the ratio of moderating power to neutron absorption is large enough to provide significant fractions of neutrons below 10 kev, and the Doppler effect can be appreciable. Doppler coefficients such as $-1 \times 10^{-5}\ \Delta k/k$ per °C at fuel operating temperatures have been calculated for some designs.[27] Such a reactor would lose about 0.015 $\Delta k/k$ when the fuel went from room temperature to operating temperatures, and would lose about 0.007 $\Delta k/k$ when the fuel went from operating temperatures to the melting point. In this temperature range the Doppler coefficient of such a reactor falls off with rising temperatures roughly as $1/T$.

A prompt-acting, large negative Doppler coefficient imposes some extra control requirements. However, it affords a powerful tool for reactor safety and eases the problem of reactor stability.[31] It reduces the chances that the accidental rapid insertion of reactivity will lead to excessive fuel temperatures. If the accident is so severe that explosive pressures and violent disassembly are needed to terminate the affair, an appreciably negative Doppler effect can markedly reduce the severity of the accident.[47,48] Hence the Doppler effect is a very important parameter to consider when optimizing overall performance. For example, the neutron energy spectrum in a large metal-fueled fast reactor can be adjusted downward by the deliberate introduction of small quantities of moderating material. The reactor would then have both the Doppler effect and the breeding ratio of a ceramic-fueled reactor that has the same ratio of fertile-to-fissile material.

Conversely the loss of sodium from the core hardens the spectrum and reduces the Doppler effect that would result from further fuel heating. Bhide and Hummel[49] have calculated that the Doppler coefficient may be reduced by a factor of 2 on loss of sodium from large ceramic-fueled reactors that have an initial sodium fraction of 52 vol.%. Some of their results are reproduced in Table 11.

For reactors having 70 vol.% sodium initially present, Hummel has recently calculated a reduction in Doppler coefficient by nearly a factor of 5 upon loss of sodium.[50] This sharp reduction in the Doppler effect is serious, since the effect is already smaller than the possible total amount of reactivity to be gained from the loss of sodium for some larger reactor concepts. Moreover, the reduction of Doppler effect itself corresponds to an increase in the reactivity gained upon loss of sodium, if this loss occurs when the fuel is hotter than normal. The problem has led to the consideration of the deliberate introduction of some fixed moderator, possibly in the form of beryllium oxide.[51] The moderation augments the normal Doppler coefficient by providing more neutrons between 500 and 5000 volts, and it does make the Doppler coefficient less sensitive to the loss of sodium. However, as mentioned earlier, it also results in a considerable reduction in the breeding ratio for plutonium-fueled reactors.

It seems very likely that large fast power reactors can be designed to have a substantially negative Doppler coefficient. The fertile U^{238} (or thorium) has been calculated to provide large negative reactivity effects upon heating (see Refs. 27, 40, 49, 52–54), and this is being confirmed in recent experiments.[52,55] Also, a negative Doppler effect has been measured upon heating a U^{235} sample in a U^{235}-thorium fast assembly.[52] Furthermore, recent improvements in theoretical methods,[56–60] in which allowance has been made for the overlapping effect be-

Table 11 DOPPLER REACTIVITY EFFECTS AND COEFFICIENTS FOR LARGE[49] FAST REACTORS FUELED WITH PuO_2-$U^{238}O_2$ AND PuC-$U^{238}C$

Ratio of Pu to U^{238}	Sodium present?	300 to 2500°K		300 to 750°K		1500 to 2500°K	
		$-\%\ \Delta k$	$-\frac{\Delta k}{\Delta T}\times 10^5$	$-\%\ \Delta k$	$-\frac{\Delta k}{\Delta T}\times 10^5$	$-\%\ \Delta k$	$-\frac{\Delta k}{\Delta T}\times 10^5$
				Oxide Case			
1:9	Yes	2.63	1.15	1.09	2.40	0.59	0.59
1:9	No	1.44	0.65	0.63	1.40	0.29	0.29
1:7	Yes	1.81	0.79	0.77	1.73	0.40	0.40
1:7	No	0.92	0.40	0.39	0.87	0.18	0.18
				Carbide Case			
1:9	Yes	1.95	0.89	0.82	1.82	0.40	0.40
1:9	No	1.11	0.48	0.47	1.05	0.20	0.20
1:7	Yes	1.30	0.59	0.54	1.20	0.29	0.29
1:7	No	0.63	0.29	0.27	0.60	0.12	0.12

tween resonances of the same isotope, as well as for overlapping between resonances of different isotopes, indicate that the reactivity contribution from the fissile isotope should be very small and possibly slightly negative upon heating a mixture of fertile and fissile material, typifying the fuel of a large reactor.

For reactors of medium enrichment (30 to 50%), a small negative Doppler effect has usually been calculated.[50,61] Of course, detailed analysis is required for each design.

Other Fuel Cycles

Since the world's fission-energy resources consist primarily of thorium and U^{238}, one can anticipate that each of these fertile isotopes will find its way into future breeder reactors and that both U^{233} and Pu^{239} will serve as fissionable isotopes. It has been conventional to speak in terms of the U^{238}-Pu^{239} cycle and the Th^{232}-U^{233} cycle. The latter combination has been calculated to provide a breeding ratio of 1.20 : 1.25 in clean large fast reactors, smaller than that for U^{238}-Pu^{239} but still well above unity. However, it may be that a more desirable set of overall performance characteristics can be obtained with mixed fuel systems such as Th-Pu^{239} or U^{238}-U^{233}.

The fission cross section of U^{233} falls off more steeply with increasing energy between 5 and 100 kev than that of Pu^{239}. Also, the ratio of capture to fission for fast neutrons is thought to be small and slowly varying with energy for U^{233}, whereas that of Pu^{239} shows a rapid decrease between 30 and 300 kev. Consequently the reactivity increase due to the spectral hardening that accompanies the loss of sodium should be much smaller when U^{233} rather than Pu^{239} is used as the fissionable isotope. A reactor fueled with U^{233} should therefore exhibit less difficulty with positive sodium coefficients.

Thorium has a much smaller fission cross section and a higher threshold energy for fission than U^{238}. Consequently thorium provides very little fast fission bonus to the breeding ratio. However, it also contributes a smaller reactivity gain due to increased fast fission upon loss of sodium; hence it should tend to give a more negative sodium void coefficient. Also, in the metallic form thorium is less dense than uranium. Two metal-fueled reactors that use the same volume fractions of thorium or uranium will exhibit less capture and scattering from the fertile isotope in the thorium case. This again makes the sodium void coefficient more negative for thorium than for uranium.

Reactors using thorium in the core do suffer from an important control problem. Upon capture of a neutron in thorium, Pa^{233} is first formed; it decays to U^{233} with a 27.4-day half-life. (The corresponding link in the U^{238}-Pu^{239} chain, Np^{239}, decays with only a 2.33-day half-life.) Consequently a considerable buildup of Pa^{233} will occur in a thorium-bearing reactor. When such a reactor is shut down after long-term operation at high power, considerable reactivity will be released if this Pa^{233} is allowed to decay in the core. For one Th-U^{233} conceptual design, Goldman[61] has calculated that $1\frac{3}{4}\%\ \Delta k/k$ would be released in 22 days and that a total of $4\%\ \Delta k/k$ was available. This reactivity, of course, is initially lost during

operation of the reactor, leading to greater reactivity shim requirements for burnup. Goldman has estimated that even with an internal breeding ratio of unity, such a reactor would lose considerable reactivity during operation. In the concept studied, a large portion of the thorium absorptions would not produce U^{233} until after the fuel element had been unloaded. Thus considerably more shutdown and operational reactivity are required if thorium is the fertile material in the core. Thorium in the blanket would produce an effect much smaller in magnitude, since the reactivity worth of fissionable isotopes there is less.

The buildup of Pu^{240} or U^{234} with recycle generally makes the sodium coefficient more positive. Both these isotopes have larger fission cross sections and lower threshold energies for fission than U^{238}. In this respect, U^{233} can again be expected to fare better than Pu^{239}. Because of the lower ratio of capture to fission in U^{233}, the buildup of U^{234} at equilibrium, when U^{233} is the fuel, will be much less than the buildup of Pu^{240} when Pu^{239} is the fuel, other things being equal.

What does this all mean so far as hybrid fuel cycles are concerned? In Table 12 the breeding ratio and sodium void reactivity effect are compared for 3000-liter metal-fueled spherical reactors for different fertile-fissile combinations.[30]* The sodium void effect for uniform loss from the core is negative for all but the U^{238}-Pu^{239} fuel type. The breeding ratio is about 0.2 higher when U^{238} rather than thorium is used in the cores of these reactors.

This is at least preliminary evidence that for metal-fueled large reactors, the sodium void problem with Pu^{239} may be significantly eased if thorium is used as the fertile material in the core, at some expense to breeding ratio and with the creation of some additional control problems. Less improvement in the sodium coefficient would be expected upon the substitution of thorium into oxide or carbide fuels, since the density advantage would not be present.

The excellent characteristics of the U^{238}-U^{233}-fueled reactor are of particular interest. The breeding ratio is much better than for the conventional thorium-U^{233} concept, the control problem due to Pa^{233} buildup is alleviated,* and the sodium coefficient is quite negative. Thus one can reasonably expect to be able to go to somewhat higher fuel alloy concentrations (and a still higher breeding ratio) or to larger core volumes, or to both, without getting a positive sodium void coefficient. An internal breeding ratio of about unity may be possible. Furthermore, the relatively flat alpha of U^{233} leads one to expect only a moderate drop in breeding ratio upon going from the metallic form to the oxide or carbide of the U^{238}-U^{233} mixture. Also, only moderate differences in sodium coefficient are expected for equal concentrations of U^{238} in metal, oxide, or carbide reactors of the same size.

Table 12 CRITICAL MASS, BREEDING RATIO, AND SODIUM VOID[30] EFFECT FOR 3000-LITER METAL-FUELED FAST REACTORS*

Fuel type	Critical mass, kg	Breeding ratio	Sodium void effect, $\Delta k/k$†
Th-U^{233}	918	1.27	−0.031
U^{238}-U^{233}	878	1.50	−0.012
Th-Pu^{239}	1060	1.36	−0.013
U^{238}-Pu^{239}	1030	1.60	+0.0025
Th-U^{235}	1580	1.02	−0.030
U^{238}-U^{235}	1460	1.16	−0.016

* All reactors have 15 vol.% fuel, 18 vol.% steel, and 67 vol.% sodium in the core. The blanket has 40% uranium, is 45 in. thick, and is reflected.

† Reactivity effect produced by removing 40% of sodium in core.

These expectations are confirmed by the calculated results listed in Table 13. At 3000 liters and fuel concentrations up to 27%, the U^{238}-U^{233} combination in metal, oxide, or carbide form gives negative core sodium void effects. With the metal an internal breeding ratio above unity is calculated, with an overall breeding ratio of 1.67. Even for the oxide the breeding ratio exceeds 1.4. At 6000 liters in spherical geometry, negative sodium coefficients are calculated for fuel concentrations between 15 and 20%.

It may be that nature has been doubly kind. Fuel elements of uranium in metallic, oxide,

* For ready comparison, the sodium coefficient and other characteristics are also listed in Table 12 for U^{235}-fueled reactors of similar composition. Note that U^{235} seems to give a sodium coefficient similar to that with U^{233}.

* The U^{238}-U^{233} reactor would also have a larger delayed-neutron fraction than the corresponding thorium-U^{233} reactor, thanks to the appreciable delayed-neutron contribution from U^{238}.

Table 13 PERFORMANCE CHARACTERISTICS OF REACTORS USING U^{238}-U^{233} FUEL IN METALLIC, OXIDE, OR CARBIDE FORM*

Reactor type	Blanket of 40% U^{238}, 45% Na					
	Ratio U^{238} to U^{233}	Critical mass, kg	Na void effect, $\Delta k/k$		Breeding ratio	
			Core only	Core + blanket	Internal	Total
3000-liter metal						
20% fuel, 67% Na	11.1	940	−0.0068	−0.0091	0.87	1.61
27% fuel, 57% Na	13.7	1050	−0.0001	−0.0016	1.05	1.67
6000-liter metal						
20% fuel, 67% Na	13.1	1620	+0.0020	+0.0007	1.04	1.61
27% fuel, 57% Na	15.6	1850	+0.0061	+0.0053	1.22	1.67
3000-liter oxide						
20% fuel, 67% Na	6.1	840	−0.0150	−0.0180		
27% fuel, 57% Na	8.0	900	−0.0048	−0.0068	0.69	1.41
6000-liter oxide						
20% fuel, 67% Na	7.7	1390	−0.0034	−0.0051	0.69	1.35
27% fuel, 57% Na	9.6	1540	+0.0040	+0.0029	0.85	1.39
3000-liter carbide						
20% fuel, 67% Na	8.0	870	−0.0096	−0.0121	0.68	1.45
27% fuel, 57% Na	10.1	950	−0.0015	−0.0033	0.85	1.50
6000-liter carbide						
15% fuel, 70% Na	7.7	1350	−0.0059	−0.0078	0.68	1.35
20% fuel, 67% Na	10.0	1470	+0.0006	−0.0008	0.87	1.46
27% fuel, 57% Na	11.7	1660	+0.0058	+0.0048	1.01	1.48

* Structure is steel in core and blanket. Blanket is 45 cm thick and reflected. Density of metal, oxide, and carbide are 19, 10, and 13 g/cm^3, respectively. The sodium void effect is computed by removing 40% of the sodium originally present in region.

carbide, and sulfide form have all exhibited considerable potential in irradiation tests to date.

Thus there is reason to believe that, in the long run, U^{238}-U^{233} in some form may well be one of the two primary fuel types for fast power reactors. Such a reactor type, in concert with the optimum plutonium-burning design, could consume the world's supply of fissionable material. The blanket of each reactor type could be built with thorium or U^{238}, or both, as the need arose for specific fissile isotopes.

Very Large Reactors

From the point of view of coolant void coefficients, the thorium-U^{233} combination should lend itself particularly well to the very large reactors mentioned in connection with the desalinization of water. In Table 14 sodium void coefficients and other nuclear characteristics are given for 25,000- and 50,000-liter spherical reactors containing 15% thorium-U^{233} and 70% sodium in the core.[62] The sodium void effect for the core alone still appears to be negative at 25,000 liters.

With lead as the coolant, the coolant void effect is more negative than for sodium. At 25,000 liters, where the sodium void effect is essentially zero, lead (or lead-bismuth) gives a substantially negative result. By 50,000 liters in spherical geometry, however, even lead is calculated to have a slightly positive void coefficient with U^{233}-thorium fuel. The coefficient would be more strongly positive if U^{238} were the fertile material.

It must be noted that the multigroup cross sections[11] used in these calculations were prepared with smaller reactors, having a harder

Table 14 PERFORMANCE OF VERY LARGE REACTORS[62] USING THORIUM-U^{233}*

Core size, liters	Coolant	Critical mass, kg	Breeding ratio		Coolant void effect,† $\Delta k/k$
			Internal	Total	
25,000	Na	4600	0.82	1.03	−0.00005
50,000	Na	8440	0.91	1.06	+0.012
25,000	Pb	4070	0.89	1.08	−0.010
50,000	Pb	7600	0.97	1.10	+0.0005

* All reactors are spherical and contain 15% metal fuel, 15% steel, and 70% coolant in core.

† Reactivity change on removing 40% of coolant from core.

spectrum, in mind. Particularly for the very large sodium-cooled reactors, the results can only be taken as indicative, not definitive.

Fuel Recycle Effects

The equilibrium fuel isotopic composition with continuous recycling will depend only on the reactor design and the feed material used to replenish core burnout. The initial composition will influence the time needed to get close to equilibrium but not the final composition.

The equilibrium composition upon recycle has been computed with three different feed materials for some of the Pu^{239}-U^{238}-fueled reactors discussed earlier in the section on reactor performance, assuming in each case that the feed plutonium composition is the same as that initially present in the core.[22] Representative results are given in Table 15. When the feed material is Pu-A (pure Pu^{239}), very little Pu^{242} has a chance to build up, and only about 5% of Pu^{241} is present at equilibrium for all the cases considered. When the feed material has a large proportion of higher isotopes, the final constitution depends sharply on the internal breeding ratio. Internal breeding adds primarily Pu^{239}, and, when the internal breeding ratio is high, less of the feed material rich in higher isotopes is used. Thus the metal-fueled core, with larger internal breeding, has less Pu^{241} and Pu^{242} at equilibrium than the oxide, when Pu-C is the feed.

Table 16 COMPARISON OF INITIAL AND EQUILIBRIUM CRITICAL MASS AND BREEDING RATIO FOR 1500-LITER OXIDE REACTOR[22]

Feed type	Critical mass*		Breeding ratio†	
	Initial	Equilibrium	Initial	Equilibrium
Pu-A	562	496	1.47	1.67
Pu-B	514	468	1.57	1.80
Pu-C	442	421	1.72	1.96

* Kilograms of (Pu^{239} + Pu^{241}).
† (Pu^{239} + Pu^{241} produced)/(Pu^{239} + Pu^{241} consumed.)

A comparison of initial and equilibrium critical mass and breeding ratio is given in Table 16 for a 1500-liter oxide-fuel reactor using Pu-A, -B, or -C, respectively, as the initial fuel and the feed. In all three cases the critical mass is lowered and the breeding ratio is increased on the transition to an equilibrium composition. It is interesting to note that the breeding ratio for equilibrium composition with Pu-C feed is 0.49 above that for a reactor using pure Pu^{239}, whereas the critical mass (of thermally fissile isotopes) is only three-fourths as large. The large fast fission bonus in Pu^{240} and Pu^{242} leads to some of this large difference in performance. The remainder is attributable to the relatively greater reactivity and breeding potential which Pu^{241} is believed to have, relative to Pu^{239}.

However, not all qualities of a reactor improve with the change in plutonium isotopic composition on recycle. If pure Pu^{239} is taken

Table 15 EQUILIBRIUM COMPOSITION OF FUEL WITH PLUTONIUM RECYCLE[22]

Reactor type	Type of feed Pu	Pu^{239}	Pu^{240}	Pu^{241}	Pu^{242}	Atoms of Pu/ atoms of U^{238} (at equilibrium)	Atoms of Pu/ atoms of Pu^{238} (initially)
800-liter metal	Pu-A	0.653	0.293	0.041	0.013	0.172	0.128
800-liter metal	Pu-C	0.544	0.281	0.066	0.109	0.189	0.163
800-liter oxide	Pu-A	0.609	0.324	0.049	0.018	0.510	0.336
800-liter oxide	Pu-C	0.288	0.266	0.121	0.325	0.795	0.439
1500-liter oxide	Pu-A	0.582	0.343	0.054	0.021	0.391	0.253
1500-liter oxide	Pu-B	0.481	0.372	0.088	0.059	0.425	0.269
1500-liter oxide	Pu-C	0.329	0.287	0.109	0.275	0.542	0.323

Pu Composition of Feed

Feed type	Atom %			
	Pu^{239}	Pu^{240}	Pu^{241}	Pu^{242}
Pu-A	100	0	0	0
Pu-B	74.7	10.2	12.4	2.7
Pu-C	40.0	10.0	25.0	25.0

as the starting point, the sodium void reactivity coefficient gets appreciably more positive (or less negative) during the transition to equilibrium composition.

Some Considerations of Practical Design and Blanket Management

The performance figures presented earlier were all for idealized spherical reactors. Actual reactors of the same core volume will all have larger critical masses for a variety of reasons. Control-rod channels, coolant-flow transition regions, and, in particular, the transition from spherical to cylindrical geometry, may combine to raise the critical mass by 20% or more.

The overall breeding ratio should not be affected significantly by these considerations if the blanket is kept an efficient capturer of neutrons. However, various practical considerations also enter herein. If the residence time of the upper and lower blanket is determined by fuel-element burnup considerations rather than by optimum blanket economics, thick end blankets may prove to be uneconomical. Again, if blanket fabrication and reprocessing costs are excessive, or if the blanket fluxes are very low because of a low core power density, the outer portions of a radial blanket may prove uneconomical.[63]

In the cases where flux levels are low or residence times are limited, the introduction of moderator into the blanket, with a consequent reduction in fertile material requirements, may help appreciably. A blanket cycle involving inward radial motion of elements during their total residence time may sometimes improve the economics, but this depends strongly on the specific conditions present.

In an unmoderated blanket of a fast reactor, one can expect a buildup of 2 or 3% Pu^{240} in the bred Pu^{239} for optimum cycling. Since the core physics performance is good for essentially any plutonium isotopic composition (disregarding sodium coefficient and possibly Doppler effect considerations), the reactor can be used to convert "dirty" plutonium* to "clean" plutonium by feeding the core with the former from thermal reactors and extracting the latter from the blanket for use in thermal reactors, should suitable designs develop.

Burnout does not appear to be limited by considerations of reactivity in fast reactors, even if the internal breeding ratios are low. There will be economic penalties imposed, however, due to (1) the higher frequency of reactor shutdown imposed by the need of partial reloading and (2) the loss of neutrons to shim type control rods, which will be needed to supply the reactivity loss between partial unloadings, assuming control is via a neutron absorber such as boron, tantalum, or tungsten.

If the latter problem becomes important, the use of moderator (or moderator plus fertile material) type shim rods may help.[30]

Neutron Physics Effects of Structural Materials

General Cross-Section Considerations

The effect of structural materials on fast reactor performance is determined by the magnitude and variation with energy of three cross sections: those for elastic scattering, inelastic scattering, and neutron capture.

The use of a structural material with a high cross section for elastic scattering reduces the leakage reactivity controlled by the sodium coolant, other things being equal. That phenomenon leading to a negative component in the sodium void reactivity effect is thus reduced, making the overall sodium void coefficient more positive.

Inelastic scattering affects the critical mass by moving neutrons from a higher energy to a lower energy, where the probability of leakage from the core is usually smaller but the probability of producing a fission may be smaller or larger, depending on the particular conditions involved. The introduction of a structural material with much inelastic scattering can also influence the sodium coefficient or the Doppler coefficient by producing more low-energy neutrons.

Inelastic scattering affects the breeding ratio in two ways: (1) by moving neutrons to a region of lower energy where alpha for Pu^{239} is higher and (2) by reducing the probability of fast fis-

* The expression "dirty plutonium" is used to categorize plutonium having a considerable buildup of the higher isotopes.

sion in the fertile material and hence the fast fission bonus.

Neutron capture in the structural materials exhibits a regular behavior and a systematic variation with atomic number, Z. For all structural materials neutron capture is usually much smaller than the fission cross section of Pu^{239} over the energy range from 10 kev to 10 Mev. There are no huge resonances as are found for xenon and samarium in the thermal-energy region. Only tantalum has a cross section about equal to that for fission in Pu^{239}, and this is only below 15 kev.

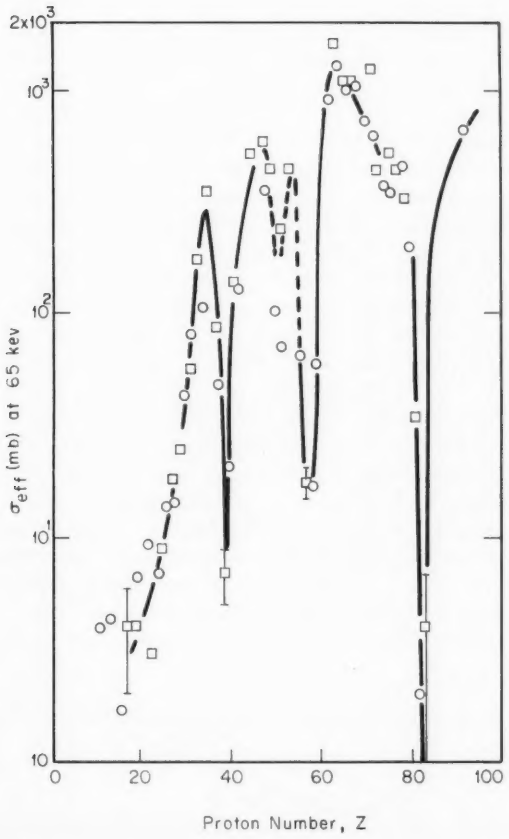

(The squares correspond to results for odd-Z elements. The circles, corresponding to results for even-Z elements, would generally fall below the curve drawn through the squares, except that the results for even-Z elements have been multiplied by a factor of 2.2, to make the data overlap. This even-odd effect is related to the average difference in resonance-level spacing for even vs. odd nuclei. The large dips in the cross section occur for isotopes with complete neutron shells, corresponding to the "magic" numbers 50, 82, and 126.)

Fig. 18 Average radiative capture cross sections for 65-kev neutrons as a function of atomic number.

The capture cross section will vary from element to element, as well as among isotopes of a particular element, but there is a general behavior pattern. The capture cross section tends to increase with atomic number. It is larger for nuclei having an odd number of protons or neutrons (odd-even) than for those having even numbers of both protons and neutrons (even-even). And it is very small for the so-called "magic nuclei." This systematic behavior pattern of neutron capture is illustrated in Fig. 18, where measurements of σ_c at 65 kev are plotted against Z over a large range of elements.[64] The values plotted in Fig. 18 are listed in Table 17, along with similar measurements of 30 kev.

In Fig. 19 the capture cross sections of three important structural elements, iron, niobium, and tantalum, are plotted vs. neutron energy. Of the two odd-even isotopes, the heavier Ta^{181} exhibits more capture than Nb^{93}. The capture cross section of U^{238} has been included for comparison purposes. Iron has a small σ_c, as one expects for a lighter element of primarily even-even nuclear structure.

The capture cross sections of tungsten, molybdenum, zirconium, and vanadium are plotted vs. energy in Fig. 20. Tungsten and molybdenum are both even-Z nuclei; the heavier tungsten captures more neutrons. Zirconium and vanadium both have "magic" character; hence one expects them to have small capture cross sections.

The capture cross section usually falls off quite rapidly with increasing neutron energy. Fission cross sections do the same below 100 kv; however, they reach a plateau region and then rise with increasing energy, as illustrated in Fig. 3.

Some Specific Cases

The capture cross sections of various structural* materials have been averaged over the

* The term "structural" is used loosely herein to cover cladding, jacket liners, or subassembly structural components. The calculations, of course, would also apply if the particular element is used as the matrix material for a cermet fuel or as an alloying or additive agent.

Table 17 CAPTURE CROSS SECTION MEASUREMENTS[64] AT 30 AND 65 KEV*

Z	Element	$\sigma_{n,\gamma}(30)$, mb	$\sigma_{n,\gamma}(65)$, mb	Z	Element	$\sigma_{n,\gamma}(30)$, mb	$\sigma_{n,\gamma}(65)$, mb
6	C	<0.2	0.0 ± 0.3	49	In	(763)	(448)
9	F	4.5 ± 1.0		50	Sn	88.0 ± 15.0	51.0 ± 10.0
11	Na	5.0 ± 0.7	0.7 ± 0.3	51	Sb	436	245
12	Mg	0.4 ± 0.2	2.1 ± 0.7	52	Te	97	35
13	Al	2.8 ± 0.7		53	I	733	440
14	Si	13.0 ± 4.0	2.0 ± 0.7	56	Ba	61	33
15	P	7.0 ± 1.0	0.5 ± 0.2	57	La	55.0 ± 10.0	18.0 ± 3.0
16	S	25.0 ± 8.0	0.8 ± 0.6	58	Ce	35.0 ± 5.0	8.0 ± 2.0
17	Cl	11.0 ± 4.0	4.0 ± 2.0	59	Pr	115	59
19	K	16.0 ± 2.0	4.0 ± 1.0	62	Sm	875	450
20	Ca	10.0 ± 1.0	3.0 ± 1.0	63	Eu	2560	1580
22	Ti	29.0 ± 3.0	5.0 ± 1.0	64	Gd	1175	670
23	V	23.0 ± 8.0	3.0 ± 1.0	65	Tb	1850	1070
24	Cr	10.0 ± 3.0	3.5 ± 1.0	66	Dy	775	570
25	Mn	22	9.0 ± 1.0	67	Ho	1720	1070
26	Fe	12.0 ± 3.0	6.3 ± 2.0	68	Er	960	540
27	Co	88.0 ± 30.0	18	69	Tm	1310	700
28	Ni	16.0 ± 4.0	6.5 ± 2.0	70	Yb	575	390
29	Cu	39.0 ± 7.0	25.0 ± 5.0	71	Lu	2520	1200
30	Zn	31.0 ± 6.0	20.0 ± 5.0	72	Hf	510	330
31	Ga	103	56	73	Ta	735	440
32	Ge	74	39.0 ± 6.0	74	W	270	190
33	As	350	175	75	Re	900	525
34	Se	94	51	76	Os	300	175
35	Br	650	345	77	Ir	795	450
37	Rb	180	89	78	Pt	330	234
38	Sr	155	24	79	Au	515	332
39	Y	13.5 ± 3.0	6.9 ± 2.0	80	Hg	295	103
40	Zr	14.0 ± 3.0	10.3 ± 2.0	81	Tl	71	35
41	Cb	264	135	82	Pb	3.0 ± 3.0	1.0 ± 2.0
42	Mo	140	69	83	Bi	1.0 ± 4.0	4.0 ± 3.0
45	Rh	850	540	92	U^{238}	473	302
46	Pd	454	265				
47	Ag	951	586				
48	Cd	330	183				

* The neutron energy resolution was ±7 and ±20 kev at 30 and 65 kev, respectively. The estimated absolute error is ±9% except where noted.

neutron energy spectra of two typical large fast power reactors, one an 800-liter metal-fueled reactor with a relatively hard spectrum and the other a 6000-liter oxide-fueled reactor with a considerably more degraded spectrum. The results are listed in Table 18. Spectrum-averaged values for capture in U^{238} and fission in Pu^{239} are also presented.

The cross sections are listed per atom in units of barns. To compare their effects on reactor performance, one must multiply them by the appropriate concentrations of atoms. These are listed for the pure materials at full density (N) in an adjoining column. For example, 10 vol.% nickel or iron gives about twice the atom concentration that 10 vol.% zirconium would give.

The capture cross sections for thermal neutrons (0.025 ev) have also been listed in Table 17 for the various elements, as has the ratio of $\sigma_{c,\text{thermal}}$ to $\sigma_{c,6000\text{ liters}}$. Except for titanium this ratio is less than the corresponding ratio of the cross section for fission in Pu^{239}. Thus, per atom, capture in structural materials is relatively greater for large fast reactors than for thermal reactors. What makes the use of the various structural materials conceivable is the much higher atom concentration of fissile iso-

tope in fast reactors. The effect on breeding ratio will depend essentially on the ratio

$$\frac{N^{\text{structural}} \cdot \overline{\sigma}_c^{\text{structural}}}{N^{\text{fissile}} \cdot (\overline{\sigma}_f + \overline{\sigma}_c)^{\text{fissile}}}$$

The effect of various structural materials on the critical mass and breeding ratio[17] of an 800-liter U^{238}-Pu^{239} metal-fueled reactor is given in Table 19. Steel, titanium, and zirconium give the lowest critical masses and highest breeding ratios. They are similar in their effect. The higher inelastic scattering cross section in vanadium leads to some reduction in breeding ratio and a small increase in critical mass. Niobium and molybdenum have appreciable capture cross sections, and the breeding ratio is depressed considerably, whereas the large capture cross section of tantalum drops the breeding ratio to near unity. These reactors were all assumed to have 25 vol.% of the structural material; the trends would be similar but the relative differences smaller if, say, 15 vol.% of the structural material were used in the calculation.

The effects of 15 vol.% of various structural elements on a 3000-liter PuC-U^{238}C-fueled reactor are given in Table 20. The general trends are similar to those observed with the smaller metal-fueled reactor. The (n,p) cross section for nickel makes it somewhat less favorable to breeding than iron or chromium.

The choice of structural material in the core also can influence important reactivity coefficients. For example, the magnitude of the Doppler effect is very sensitive to the amount of low-energy flux present. The use of a structural material with a considerable capture cross section, which in turn leads to a higher critical mass, results in a harder neutron energy spectrum. In one large carbide-fuel concept, for example, the use of niobium rather than stainless steel as the cladding material in the core

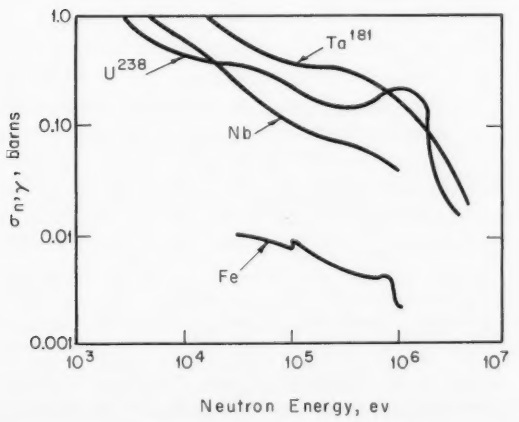

Fig. 19 Capture cross sections of iron, niobium, tantalum, and U^{238}.

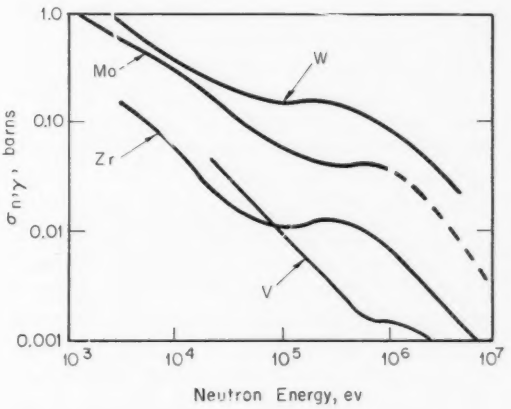

Fig. 20 Capture cross sections of vanadium, zirconium, molybdenum, and tungsten.

led to a reduction[33] of the Doppler coefficient by a factor of 7 (i.e., the coefficient remained negative but was much smaller in magnitude). On the other hand, the use of vanadium or Inconel X instead of steel was calculated to produce little change in the Doppler coefficient for this particular concept.

The effect of various structural materials on the sodium void effect for a 3000-liter PuC-U^{238}C-fueled reactor is illustrated in Table 21. The calculations indicate that the structural elements of low atomic mass are roughly the same in their influence on sodium void effect, at least for this particular reactor choice. A similar behavior among steel, nickel, and vanadium has also been reported for an oxide-fueled concept.[33]

However, it must be emphasized that the results given in Table 20 (as well as in earlier tables on sodium void effect for large reactors) are only qualitative. The techniques used for these calculations were not the most sophisticated,[25] and cross-section information at the lower neutron energies, in particular, is un-

Table 18 AVERAGE CAPTURE CROSS SECTIONS OF STRUCTURAL MATERIALS IN TYPICAL FAST REACTOR SPECTRA

Element	N, atoms per cm^3 of pure element $\times 10^{-24}$	Average capture cross section, barns: 800-liter metal fuel reactor	Average capture cross section, barns: 6000-liter oxide fuel reactor	Capture at 0.025 ev (thermal)	$\sigma_{c,\text{thermal}} / \sigma_{c,6000\text{ liters}}$
Ti	0.0566	0.006	0.012	5.8	483
V	0.0704	0.009	0.019	5.0	263
Cr	0.0822	0.009	0.014	3.1	221
Fe	0.0847	0.006	0.008	2.5	313
Ni	0.0913	0.02*	0.025*	4.8	194
Zr	0.0425	0.011	0.018	0.18	10
Nb	0.0545	0.107	0.245	1.2	5
Mo	0.0640	0.073	0.118	2.7	23
Ta	0.0553	0.322	0.617	21.0	34
U^{238}	0.048	0.202	0.296	2.7	9
$\sigma_f{}^{Pu^{239}}$		1.8	2.0	746.0	373

* Includes 0.01 barn for $\sigma_{n,p}$ reaction.

Table 19 EFFECT OF VARIOUS STRUCTURAL MATERIALS ON PERFORMANCE[17] OF 800-LITER U^{238}-Pu^{239} METAL-FUELED REACTOR*

Structural material	Critical mass, kg	Breeding ratio	Alpha	A†	F†
Stainless steel	431	1.82	0.188	0.082	0.29
Ti	425	1.92	0.180	0.073	0.33
V	456	1.68	0.222	0.11	0.25
Zr	415	1.89	0.181	0.076	0.31
Nb	494	1.51	0.169	0.44	0.25
Mo	502	1.46	0.185	0.41	0.22
Ta	716	1.02	0.170	0.91	0.18

* The core contains 25 vol.% fuel, 25 vol.% structural material, and 50 vol.% sodium. The blanket contains 60% U^{238}, 20% steel, and 20% sodium.

† A = absorptions in structure and coolant per fission in Pu^{239}; F = fissions in U^{238} per fission in Pu^{239}.

Table 20 EFFECT OF VARIOUS STRUCTURAL MATERIALS ON PERFORMANCE OF 3000-LITER PuC-U^{238}C-FUELED REACTOR*

Element	Critical mass, kg	Breeding ratio
Ti	950	1.47
V	1010	1.32
Cr	960	1.42
Fe	950	1.44
Ni	970†	1.33†
Zr	930	1.48
Nb	1190	1.14
Mo	1150	1.14
Ta	1720	0.80

* The core contains 15 vol.% fuel, 15 vol.% structure, and 70 vol.% sodium. The blanket contains 40% U^{238}, 15% steel, and 45% sodium.

† Estimated correction has been made for $\sigma_{n,p}$ in nickel.

Table 21 SODIUM VOID EFFECT FOR 3000-LITER PuC-U^{238}C-FUELED REACTORS* WITH VARIOUS STRUCTURAL MATERIALS

Structural material	Sodium void effect, $\delta k/k$†
Ti	−0.003
V	−0.002
Cr	−0.003
Fe	−0.004
Ni	−0.001‡
Zr	−0.002
Nb	+0.012
Mo	+0.006
Ta	+0.011

* All reactors have 15 vol.% fuel, 15 vol.% structure, and 70 vol.% sodium in core.

† Reactivity change corresponding to removal of 40% sodium initially present in core.

‡ Correction has been estimated and included for $\sigma_{n,p}$ in nickel.

Table 22 EFFECT OF NIOBIUM ON PERFORMANCE OF 6000-LITER THORIUM-U^{233}-FUELED FAST REACTORS*

	Steel structure in core		Niobium structure in core	
Vol.% structure in core	Sodium void effect, $\Delta k/k$ (core only)	Breeding ratio	Sodium void effect, $\Delta k/k$ (core only)	Breeding ratio
15	−0.0258	1.24	−0.0019	0.97
25	−0.0175	1.18	+0.0092	0.79

* All reactors have 15% fuel. All reactors have reflected blanket of 40% U^{238}, 15% steel, and 45% sodium. Sodium void effect is the result of removing 40% of the sodium originally present.

certain. Since the sodium void effect is the result of a balance between two large competing phenomena, considerable error is likely at the present time. Sharper distinctions between the various structural elements of low atomic number may become evident as accuracy of prediction improves.

Molybdenum, niobium, and tantalum all lead to positive sodium void effects, as might be expected from the curves given in Figs. 10 and 11. The capture cross sections for molybdenum and niobium are particularly uncertain at low energies, and the magnitude of these coefficients could change appreciably. It is not expected that they will behave like steel, however, in regard to the sodium coefficient.

The relative effect of steel and niobium structure in the core is again illustrated in Table 22 for 6000-liter thorium-U^{233}-fueled fast reactors. With 15 vol.% structure in the core, for reactors using 15 vol.% fuel, the sodium void effect changes from highly negative with steel to almost zero with niobium. If the core structure is raised to 25 vol.% at the expense of sodium, the sodium void effect is highly negative with steel and is quite positive with niobium. The breeding ratio drops from about 1.2 to below unity upon the change from steel to niobium.

In summary, the choice of materials for purposes of structure, fuel containment, or alloying in large fast power reactors has become increasingly complex from the nuclear point of view. Both the type of fuel and the reactor size can affect the choice. Questions of sodium void reactivity effect and Doppler coefficient, as well as breeding ratio and critical mass, must enter into the judgment. A structural material like niobium may be quite tolerable in all nuclear respects for a small U^{238}-plutonium-fueled reactor of EBR-II size. In a large U^{238}-plutonium metal-fueled reactor, the effect of the niobium on breeding ratio may be acceptable but its effect on sodium void coefficient intolerable. In a large U^{238}-plutonium oxide-fueled reactor, niobium may be intolerable in appreciable quantities on both these counts, as well as because of a large reduction in the Doppler coefficient relative to that which one would have had with steel. In a large thorium-U^{233}-fueled reactor, on the other hand, the influence of niobium on the sodium coefficient may be tolerable, but not its effect on breeding ratio.

Uncertainties in Theoretical Prediction

Although a major improvement in our knowledge of fast-neutron cross sections has come about in the last several years, there remain large gaps in the available information. For Pu^{239}, for example, $\nu(E)$ (neutrons per fission) is believed to be known to 1½ or 2% except at higher energies; $\sigma_{fission}$ is probably known to about 5% except at lower energies where a 10% or greater uncertainty is likely; and the capture cross section is known to about 20% except at lower energies, where the uncertainty is greater. If these few uncertainties all contributed cross-section errors to a calculation in the same direction, the error in reactivity from these sources alone would be 6 or 7% $\Delta k/k$.

The cross sections of most other isotopes and materials of interest to fast reactors are inadequately measured, particularly the capture cross sections. If all these uncertainties were to add up in the same direction, the error in critical mass would be huge. If a careful, objective review of cross sections is made, the errors introduced should be partly random and tend to cancel to a considerable degree. However, considerable discrepancies can and do remain. In one particular 1960 study of this kind on the better measured U^{235}-fueled fast criticals,[11] discrepancies in the prediction of reactivity as large as 4% $\Delta k/k$ appeared between the experiments and calculated results based on an objective cross-section evaluation. Fortunately, recent cross-section measurements have narrowed these differences sharply (see Refs. 11, 15, 65, and 66).

The existence of a considerable body of data from U^{235}-fueled critical experiments enables one to adjust calculations empirically, helping in the prediction of systems not too different in size or composition. However, no similar body of information now exists for plutonium or U^{233}.

The breeding ratio is relatively insensitive to most of the cross-section uncertainties. However, for large oxide- or carbide-fueled reactors, and again for reactors using the thorium-U^{233} cycle, the breeding ratio lies near enough to unity that the uncertainty becomes serious, particularly when doubling time is being evaluated.

Most sensitive to cross-section uncertainties and still in need of further improvement in calculational techniques are the Doppler and sodium void reactivity effects. Both are sensitive to details of reactor spectrum and to the details of cross-section structure in the resonance region. Estimates indicate errors of 50% in the sodium coefficient to be plausible, and even the calculated sign of the coefficient may be in error near the threshold of a positive coefficient.[22] Uncertainties up to 50% are estimated to exist also in the prediction of the Doppler effect.[50,53]

Hence the precise specification of the nuclear characteristics of a large fast power reactor today is essentially impossible. One can only hope to bracket the important parameters.

Concluding Remarks

Only part of the story of large fast power reactor performance has been given here. Conflicts in the simultaneous optimization of design for breeding, for economics, and for safety have been indicated. However, the general subjects of fast reactor safety and fast reactor economics have not been treated. Nor have other considerations, such as heat-transfer characteristics and fuel-element performance, been factored into the discussion.

It has been shown, with reasonable certainty, that breeding is quite feasible in large fast reactors fueled with U^{238}-Pu^{239} or Th^{232}-U^{233}, using any of several structural materials and cooled with sodium. However, materials with large capture cross sections, such as niobium, molybdenum, and tantalum, affect breeding seriously. They also make the attainment of a negative sodium coefficient considerably more difficult for the large reactors.

Breeding is also quite feasible using hybrid fuel systems, such as the combination U^{238}-U^{233}.

It is reasonably certain that large fast reactors can be designed to have significantly negative Doppler coefficients. This desirable characteristic is achievable, in principle, for metal, oxide, or carbide. Small amounts of moderator can be added to enhance the Doppler effect achieved ordinarily but at some penalty to the breeding gain.

It is apparently very difficult to design large fast reactors, especially those fueled with U^{238}-Pu^{239} in some form, so that there is no semblance of a positive sodium void coefficient, even locally. The real importance of the sodium coefficient to fast reactor safety has become the focal point for considerable analysis. Criteria for the determination of safe sodium coefficients (and for safe reactivity gains with the loss of sodium by boiling or other causes) are being sought, always in the light of other existing reactivity coefficients. Despite the difficulties introduced by positive void coefficients, sodium remains, by far, the favorite coolant for large fast power reactors, primarily because of its favorable heat-removal characteristics.

In the process of optimizing the design of large fast power reactors for safety, for economics, and for doubling time, one can anticipate the comparison of reactors having both low and high power densities, of reactors having widely differing geometries, of large reactors with reactors half their size, and of reactors designed with widely differing combinations of reactivity coefficients.

References

1. W. J. McCarthy, Jr., R. B. Nicholson, D. Okrent, and V. Z. Jankus, Studies of Nuclear Accidents in Fast Power Reactors, *Proceedings of the Second United Nations International Conference on the Peaceful Uses of Atomic Energy, Geneva, 1958*, Vol. 12, p. 207, United Nations, Geneva, 1958.
2. D. Okrent, R. Avery, and H. H. Hummel, A Survey of the Theoretical and Experimental Aspects of Fast Reactor Physics, *Proceedings of the International Conference on the Peaceful Uses of Atomic Energy, Geneva*, 1955, Vol. 5, p. 347, United Nations, New York, 1956.
3. J. Codd, L. R. Shepherd, and J. H. Tait, The Physics of Fast Reactors, *Progr. Nucl. Energy*, Ser. I, 1: 251-310 (1956).
4. W. B. Loewenstein and D. Okrent, Physics of Fast Power Reactors, *Proceedings of the Second United Nations International Conference on the Peaceful Uses of Atomic Energy, Geneva*, 1958, Vol. 12, p. 16, United Nations, Geneva, 1958.
5. A. I. Leipunsky, A. I. Abramov, V. N. Andreev, A. I. Baryshnikov, I. I. Bondarenko, N. I. Fetisov, V. I. Galkov, V. I. Golubev, A. D. Gulko, A. G. Guseinov, O. D. Kazachkovsky, N. V. Kozlova, N. V. Krasnoyarov, B. D. Kuziminov, V. N. Morozov, M. N. Nikolaev, L. E. Sherman, G. N. Smirenkin, Iu. Ya. Stavissky, F. I. Ukraintsev, and L. N. Usachev, Studies in the Physics of Fast Neutron Reactors, *Proceedings of the Second United Nations International Conference on the Peaceful*

Uses of Atomic Energy, Geneva, 1958, Vol. 12, p. 3, United Nations, Geneva, 1958.

6. G. E. Hansen, Properties of Elementary Fast-Neutron Critical Assemblies, *Proceedings of the Second United Nations International Conference on the Peaceful Uses of Atomic Energy, Geneva,* 1958, Vol. 12, p. 6, United Nations, Geneva, 1958.
7. R. D. Smith and J. E. Sanders, Experimental Work with Zero Energy Fast Reactors, *Proceedings of the Second United Nations International Conference on the Peaceful Uses of Atomic Energy, Geneva,* 1958, Vol. 12, p. 89, United Nations, Geneva, 1958.
8. J. K. Long, W. B. Loewenstein, C. E. Branyan, G. C. Brunson, F. S. Kirn, D. Okrent, R. E. Rice, and F. W. Thalgott, Fast Neutron Power Reactor Studies with ZPR-III, *Proceedings of the Second United Nations International Conference on the Peaceful Uses of Atomic Energy, Geneva,* 1958, Vol. 12, p. 119, United Nations, Geneva, 1958.
9. G. Fischer, C. Kelber, D. Meneghetti, P. Persiani, D. Shaftman, and A. B. Smith (Eds.), Proceedings of the Conference on the Physics of Breeding, October 19–21, 1959, USAEC Report ANL-6122, Argonne National Laboratory.
10. L. J. Koch and H. C. Paxton, Fast Reactors, in *Ann. Rev. Nucl. Sci.,* 9: 437-472 (1959).
11. S. Yiftah, D. Okrent, and P. A. Moldauer, *Fast Reactor Cross Sections,* Pergamon Press, Inc., New York, 1960.
12. *Physics of Fast and Intermediate Reactors* (3 vols.), International Atomic Energy Agency, Vienna, 1961.
13. Proceedings of the Conference on Breeding, Economics, and Safety in Large, Fast Power Reactors, Report ANL-6792, Argonne National Laboratory, 1963 (to be published).
14. J. C. Hopkins and B. C. Diven, Neutron Capture to Fission Ratios in U^{233}, U^{235} and Pu^{239}, *Nucl. Sci. Eng.,* 12(2): 169 (February 1962).
15. A. B. Smith, Recent Changes in Heavy Element Cross Sections, in Proceedings of the Conference on Breeding, Economics, and Safety in Large, Fast Power Reactors, Report ANL-6792, Argonne National Laboratory, 1963 (to be published).
16. J. R. Dietrich, The Efficient Utilization of Nuclear Fuels, *Power Reactor Technol.,* 6(4): 1 (Fall 1963).
17. S. Yiftah and D. Okrent, Some Physics Calculations on the Performance of Large Fast Breeder Power Reactors, USAEC Report ANL-6212, Argonne National Laboratory, December 1960.
18. P. Greebler, H. Hurwitz, and M. L. Storm, Statistical Evaluation of Fission-Product Absorption Cross Sections of Intermediate and High Energies, *Nucl. Sci. Eng.,* 2(3): 334 (May 1957).
19. U. L. Businaro, S. Gallone, and D. Morgan, On the Dependence upon Energy of Fission Product Poisoning of U^{235}, *J. Nucl. Energy: Pt. A & B,* 4(3): 319 (March 1957).
20. P. A. Moldauer, On the Estimation of Fast Neutron Cross Sections, Proceedings of the Conference on the Physics of Breeding, USAEC Report ANL-6122, pp. 67-76, Argonne National Laboratory, 1959.
21. J. D. Garrison and B. W. Roos, Estimation of Fission Product Capture Cross Sections, *Trans. Am. Nucl. Soc.,* 3(1): 299 (June 1960).
22. D. Okrent, Performance of Large Fast Power Reactors, Including Effects of Higher Isotopes, Recycling and Fission Products, *Physics of Fast and Intermediate Reactors,* Vol. II, International Atomic Energy Agency, Vienna, 1961.
23. A. Smaardyk, T. R. Bump, J. Handwerk, W. J. Kann, E. L. Martinec, P. J. Persiani, G. F. Popper, and S. B. Skladzien, Interim Report: FARET Experimental Program, USAEC Report ANL-6708, Argonne National Laboratory, April 1963.
24. J. B. Nims and P. F. Zweifel, Preliminary Report on Sodium Temperature Coefficients in Large Fast Reactors, USAEC Report APDA-135, Atomic Power Development Associates, Inc., November 1959.
25. H. Hummel and A. Rago, An Accurate Treatment of Resonance Scattering in Light Elements in Fast Reactors, *Physics of Fast and Intermediate Reactors,* Vol. I, International Atomic Energy Agency, Vienna, 1961.
26. M. Bhide and H. H. Hummel, Reactivity Coefficients of Sodium in Some Large Fast Reactors, *Physics of Fast and Intermediate Reactors,* Vol. I, International Atomic Energy Agency, Vienna, 1961.
27. P. Greebler, B. A. Hutchins, and J. R. Sueoka, Calculation of Doppler Coefficient and Other Safety Parameters for A Large Fast Oxide Reactor, USAEC Report GEAP-3646, General Electric Company, Atomic Power Equipment Department, Mar. 23, 1961.
28. H. H. Hummel, K. Phillips, and A. Rago, Calculations of Sodium Void Reactivity Effect for Large Fast Oxide Reactors in Spherical and Slab Geometry, in Proceedings of the Conference on Breeding, Economics, and Safety in Large, Fast Power Reactors, Report ANL-6792, Argonne National Laboratory, 1963 (to be published).
29. K. Cohen et al., Reactor Safety and Considerations of Fuel Cycle Economics for Fast Reactors, in Proceedings of the Conference on Breeding, Economics, and Safety in Large, Fast Power Reactors, Report ANL-6792, Argonne National Laboratory, 1963 (to be published).
30. D. Okrent, Breeding, Safety, and Fuel Cycles, Rome Symposium, 1963.
31. C. P. Zaleski, Some Ideas on the Reactivity Coefficients in Large, Fast Reactors, in Proceedings of the Conference on Breeding, Economics and Safety in Large, Fast Power Reactors, Report ANL-6792, Argonne National Laboratory, 1963 (to be published).

32. P. R. Huebotter, Studies of Simulated Sodium Boiling and Fuel Meltdown, in Proceedings of the Conference on Breeding, Economics, and Safety in Large, Fast Power Reactors, Report ANL-6792, Argonne National Laboratory, 1963 (to be published).
33. K. Horst and B. A. Hutchins, Comparative Study of PuC-UC and PuO_2-UO_2 as Fast Reactor Fuel, Part I, USAEC Report GEAP-3880, General Electric Company, Atomic Power Equipment Department, Jan. 19, 1962.
34. D. Smidt, Discussion, in Proceedings of the Conference on Breeding, Economics, and Safety in Large, Fast Power Reactors, Report ANL-6792, Argonne National Laboratory, 1963 (to be published).
35. R. E. Peterson and S. L. Stewart, Moderator Segmentation: A Core Design for Counteracting Positive Coolant Coefficients in Large Fast Reactors, *Trans. Am. Nucl. Soc.*, 6(2): 260 (November 1963).
36. G. Goertzel, An Estimation of Doppler Effect in Intermediate and Fast Neutron Reactors, *Proceedings of the International Conference on the Peaceful Uses of Atomic Energy, Geneva, 1958*, Vol. 5, p. 472, United Nations, New York, 1956.
37. H. Feshbach, G. Goertzel, and H. Yamauchi, Estimation of Doppler Effect in Fast Reactors, *Nucl. Sci. Eng.*, 1(1): 4 (March 1956).
38. A. M. Lane, J. E. Lynn, and J. S. Syory, An Estimation of the Doppler Effect in Fast Neutron Reactors, British Report AERE-T/M-137, July 1956.
39. H. A. Bethe, On the Doppler Effect in Fast Reactors, USAEC Report APDA-119, Atomic Power Development Associates, Inc., Mar. 11, 1957.
40. R. B. Nicholson, The Doppler Effect in Fast Neutron Reactors (thesis), Report APDA-139, Atomic Power Development Associates, Inc., June 1960.
41. E. A. Fossoul, Effet Doppler du Plutonium 239 dans les Reacteurs Rapides, *Physics of Fast and Intermediate Reactors*, Vol. III, International Atomic Energy Agency, Vienna, 1961.
42. H. V. Lichtenberger, F. W. Thalgott, W. Y. Kato, and M. Novick, Operating Experience and Experimental Results Obtained from a NaK-Cooled Fast Reactor, *Proceedings of the International Conference on the Peaceful Uses of Atomic Energy, Geneva*, 1955, Vol. 3, p. 345, United Nations, New York, 1956.
43. F. W. Thalgott, J. F. Boland, R. O. Brittan, J. C. Carter, F. D. McGinnis, M. Novick, D. Okrent, H. A. Sandmeier, R. R. Smith, and R. E. Rice, Stability Studies on EBR-I, *Proceedings of the Second United Nations International Conference on the Peaceful Uses of Atomic Energy, Geneva*, 1958, Vol. 12, p. 242, United Nations, Geneva, 1958.
44. R. R. Smith, J. F. Boland, F. D. McGinnis, M. Novick, and F. W. Thalgott, Instability Studies with EBR-I, Mark III, USAEC Report ANL-6266, Argonne National Laboratory, December 1960.
45. W. Y. Kato and D. K. Butler, Measurement of the Doppler Temperature Effect in an EBR-I Type Assembly, USAEC Report ANL-5809, Argonne National Laboratory, July 1958.
46. A. R. Baker and T. A. J. Jaques, A Measurement of the Contribution of the Doppler Effect to the Temperature Coefficient of Reactivity in a Fast Reactor, British Report AERE-R/M-168, June 1958.
47. R. B. Nicholson, Methods for Determining the Energy Release in Hypothetical Reactor Meltdown Accidents (thesis), USAEC Report APDA-150, Atomic Power Development Associates, Inc., December 1962.
48. B. Wolfe, N. Friedman, and D. Riley, Influence of the Doppler Effect on the Meltdown Accident, in Proceedings of the Conference on Breeding, Economics, and Safety in Large, Fast Power Reactors, Report ANL-6792, Argonne National Laboratory, 1963 (to be published).
49. M. G. Bhide and H. H. Hummel, Calculations of the Doppler Coefficients of Large Ceramic-Fueled Fast Reactors, USAEC Report ANL-6601, Argonne National Laboratory, August 1962.
50. H. H. Hummel and A. L. Rago, Effect of Parameter Variation in Doppler Effect Calculations, in Proceedings of the Conference on Breeding, Economics, and Safety in Large, Fast Power Reactors, Report ANL-6792, Argonne National Laboratory, 1963 (to be published).
51. P. Greebler, Recent Improvements in Calculations of Doppler and Sodium Reactivity Effects for Large Fast Reactors, in Proceedings of the Conference on Breeding, Economics, and Safety in Large, Fast Reactors, Report ANL-6792, Argonne National Laboratory, 1963 (to be published).
52. T. H. Springer and S. G. Carpenter, Fast Spectrum Doppler Measurements, in Proceedings of the Conference on Breeding, Economics, and Safety in Large, Fast Power Reactors, Report ANL-6792, Argonne National Laboratory, 1963 (to be published).
53. R. Froelich, K. Ott, and J. J. Schmidt, Dependence of Fast Doppler Coefficients on Nuclear Data Uncertainties, in Proceedings of the Conference on Breeding, Economics, and Safety in Large, Fast Power Reactors, Report ANL-6792, Argonne National Laboratory, 1963 (to be published).
54. P. Greebler and E. Goldman, Doppler Calculations for Large, Fast Ceramic Reactors — Effects of Improved Methods and Recent Cross-Section Information, USAEC Report GEAP-4092, General Electric Company, Atomic Power Equipment Department, Dec. 19, 1962.
55. G. J. Fischer, H. H. Hummel, J. R. Folkrod, and D. A. Meneley, Experimental Results for U^{238} Doppler Measurements in Fast Reactor Spectra, in Proceedings of the Conference on Breeding, Economics, and Safety in Large, Fast Power Re-

actors, Report ANL-6792, Argonne National Laboratory, 1963 (to be published).

56. J. Codd and J. P. Collins, Plutonium-239 and Uranium-238 Resonance Interaction Effects in a Dilute Fast Reactor, European Atomic Energy Society Symposium on Advances in Reactor Theory, Karlsruhe, 1963.
57. J. Codd and J. P. Collins, The Influences of Resonance Overlapping on the Doppler Effect in a Dilute Fast Reactor, in Proceedings of the Conference on Breeding, Economics, and Safety in Large, Fast Power Reactors, Report ANL-6792, Argonne National Laboratory, 1963 (to be published).
58. R. N. Hwang, An Improved Method of Doppler Effect Calculations for Fissile Materials in the Intermediate Energy Region, in Proceedings of the Conference on Breeding, Economics, and Safety in Large, Fast Power Reactors, Report ANL-6792, Argonne National Laboratory, 1963 (to be published).
59. R. Froelich, K. Ott, and J. J. Schmidt, Calculation of Doppler Coefficients of Dilute Fast Reactors, in Proceedings of the Conference on Breeding, Economics, and Safety in Large, Fast Power Reactors, Report ANL-6792, Argonne National Laboratory, 1963 (to be published).
60. D. B. Adler and F. T. Adler, Theoretical Representation of Cross Sections of Fissile Isotopes, in Proceedings of the Conference on Breeding, Economics, and Safety in Large, Fast Power Reactors, Report ANL-6792, Argonne National Laboratory, 1963 (to be published).
61. A. J. Goldman, A Feasibility Study of Fast U^{233}-Th Breeder Reactors, USAEC Report NDA-2134-3, Nuclear Development Corporation of America, Oct. 10, 1960.
62. D. Okrent, Nuclear Considerations in the Selection of Materials for Fast Power Reactors, in *Nuclear Metallurgy*, Vol. IX, AIME, 1963.
63. S. A. Hasnain and D. Okrent, On The Design and Management of Fast Reactor Blankets, *Nucl. Sci. Eng.*, 9(3): 314 (March 1961).
64. R. L. Macklin, J. H. Gibbons, and T. Inada, Average Radiative Capture Cross Sections for 30- and 65-keV Neutrons, *Phys. Rev.*, 129(6): 2695 (Mar. 15, 1963).
65. D. Meneghetti, Effect of Resonance Scattering on Criticality Calculations of Fast Assemblies, USAEC Report ANL-6466, Argonne National Laboratory, December 1961.
66. W. G. Davey, k Calculations for 22 ZPR-III Fast Reactor Assemblies Using ANL Cross Section Set 635, USAEC Report ANL-6570, Argonne National Laboratory, May 1962. (See also ANL-6682.)

Section

I

Power Reactor Technology

Economics, Applications, Programs

Desalinization of Water

The use of large blocks of nuclear (thermal) power to produce fresh water from saline water has been under discussion for several months past.[1–6] Both fast[1,2] and thermal[3,4] reactors have been proposed for this purpose, and a recent study[7] has considered a wide range of reactor types and sizes. The reader interested in the general state of water resources in this country—without regard to the nuclear question—may find Refs. 8 and 9 helpful. The discussion here will center around the nuclear energy sources that have been considered for the application.

The plant discussed in Ref. 1 utilizes a fast reactor, fueled with vibration-compacted UO_2-PuO_2, which is described in more detail in Ref. 2. Core specifications are given in Table I-1, and a schematic of the core arrangement is in Fig. I-1. The energy is used entirely for producing distilled water, and the amount produced, 10^9 gal/day, represents about half the consumption of New York City. The water conversion plant discussed in Ref. 2 is a multistage flash evaporation unit consisting of 30 stages, although the seawater plant used in Ref. 1 (Fig. I-2) is a quadruple-effect evaporator. A figure of merit used to describe the relative performance of evaporator plants is the so-called "performance ratio." This is the weight of water evaporated per unit weight of steam consumed and is approximately equal to the number of effects used in a multiple-effect evaporator plant. The performance ratio can also be defined as the weight of fresh water produced per 1000 Btu of heat consumed, and this latter definition is particularly useful for the following conversion:

(Cost of steam, cents/10^6 Btu)(8.33)/(performance ratio) = cost of energy used for distillation, cents/1000 gal of fresh water produced

Table I-1 CORE SPECIFICATIONS[2] OF A PROPOSED FAST REACTOR FOR A WATER DESALINIZATION PLANT

Power, Mw(t) (blanket power neglected)	25,000
Core volume, liters	50,000
Core height, ft	4
Core diameter, ft	24
Core composition	
Fuel material, vol. %	34 (UO_2 + PuO_2)
Coolant, Na, vol. %	50
Steel, vol. %	16
Fuel enrichment, %	15 (total Pu)
Critical mass, kg of Pu (total)	22,000 (at equilibrium)
Fuel and core	
Cladding, outside diameter, in.	0.300
Cladding, thickness, in.	0.020
Fuel diameter, in.	0.260
Pitch, in.	0.396
Elements per subassembly	400
Number of subassemblies (25,000-Mw reference)	1016
Coolant and core	
Maximum/average power density	1.5
Maximum heat flux, Btu/(hr)(sq ft)	10^6
Coolant velocity, ft/sec	25
Average coolant temperature rise, °F	257
Inlet temperature, °F	593
Blanket specifications	
Axial blankets (top and bottom)	
Diameter, ft	24
Thickness, each, ft	3
Composition	34 vol. % UO_2 50 vol. % Na 16 vol. % steel
Radial blanket	
Thickness, ft	1.5
Composition	65 vol. % UO_2 20 vol. % Na 15 vol. % steel
Reactor performance characteristics	
Specific power, Mw/kg of Pu	1.1
Power density, Mw/liter	0.5
Fuel burnup, Mwd/metric ton	100,000
Plutonium production ratio (breeding ratio)	
Total, core and blanket	1.3
Internal (core) breeding ratio	0.75

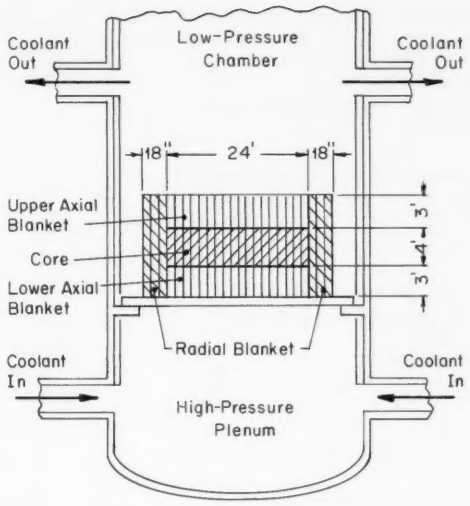

Fig. I-1 Core arrangement of the proposed fast 25,000-Mw reference reactor[2] for conversion of seawater.

This equation expresses the connection between the reactor portion of the seawater conversion plant and the evaporation portion of the plant, at least as far as costs are concerned. If the heat source is expensive, then the cheapest water is produced by an evaporator plant with a high performance ratio. If heat is relatively cheap, then a low performance ratio may be used; the evaporator plant can be cheap also, and the total cost of the fresh water is reduced accordingly. Thus there is an optimum value for the performance ratio which is lower as the cost of heat is lower. For the plant described in Ref. 1, only four effects are postulated, since the cost of steam from the reactor is calculated to be low.

Reference 3 discusses thermal reactors as applied to the production of both electricity and distilled water. The reactor plant consists of three heavy-water-moderated boiling-H_2O reactors, each generating 8333 Mw(t). A simplified flow diagram of the plant is shown in Fig. I-3. The water portion of the plant consumes about 19,800 Mw(t) and 500 Mw(e), and the net power to the switchyard is 4500 Mw(e). Detailed plant designs of the reactors discussed in Ref. 3 are given in Ref. 4. Table I-2 summarizes one of the designs. The heavy-water reactors are refueled under power and employ fuel elements of the concentric tubular type, containing two rings of UO_2 that are each about 0.6 in. thick.

Reference 7 represents a portion of a cooperative effort of a number of governmental agencies to define more closely the costs associated with the dual-purpose plants. Those participating in the overall study are the Atomic Energy Commission (AEC), the Bureau of Reclamation, the Office of Saline Water (Department of Interior), and the Federal Power Commission. The Bechtel Corporation was engaged by the AEC to act as architect-engineer in connection with the AEC portion of the program, and Ref. 7 is the Bechtel report. The total of nine different cases that were studied covered a wide variety of reactors and encompassed a time period from the present to 1980.

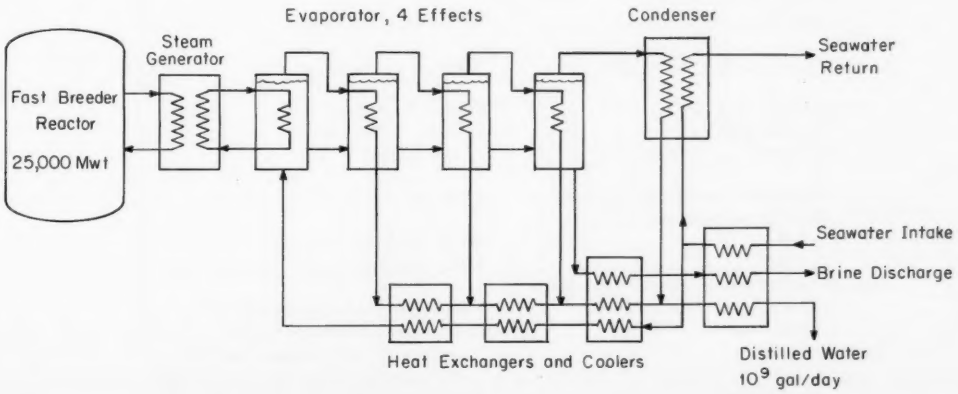

Fig. I-2 Seawater distillation plant employing a fast-breeder reactor.[1]

Table I-2 DESIGN DATA[4] FOR A DUAL-PURPOSE 8333-MW(T) REACTOR

Reactor type	Pressure tube, D_2O moderated, boiling light-water cooled		
Fuel	Vibratory-packed natural UO_2 (below 0.8% U^{235})		
Moderator	D_2O		
Reflector	2 ft of graphite on bottom and sides; 2 ft of D_2O on top of reactor		
Reactor thermal power	25,000 Mw, three 8333-Mw(t) reactors		
Type of refueling	On-line, from below reactor		
Materials			
Density of UO_2 fuel	9.81 g UO_2/cm^3		
Pressure-tube material	Zircaloy-2 tubing; stainless-steel end plugs		
Calandria tube material	Aluminum 6061T6		
Calandria material	Aluminum-clad steel		
Gas between tubes	CO_2		
Reactor dimensions			
Reactor shape	Rectangular parallelepiped with corners removed		
Lattice spacing	Square array on 9-in. pitch		
Nuclear material inventory, each of three reactors			
Uranium, metric tons	747		
D_2O, metric tons	545		
Graphite, metric tons	486		
Core size			
Total number of tubes	1308		
Active core length, ft	28.5		
Active core width, ft	27		
Active core height (along tube length), ft	30		
Calandria vessel			
Length, ft	34.5		
Width, ft	33		
Height, ft	35		
Fuel elements			
Form	Nested concentric tubes of UO_2		
Cladding	0.020-in. Zircaloy-2		
Dimensions of fuel element	Inside diameter, in.	Outside diameter, in.	Length, in.
Inner tube	1.424	2.718	72 nominal
Outer tube	3.152	4.326	72 nominal
Reactor cooling system			
Specific power in uranium	11.2 watts/g (average)		
Heat flux, Btu/(hr)(sq ft)	Average	Maximum	
Inner tube	216,000	248,000	
Outer tube	263,000	303,000	
Burnout (at 12.5% quality)	754,000		
Mass flow rate of coolant, lb/hr	2.21×10^8		
Reactor temperature, pressure			
Inlet	464°F, 720 psia		
Outlet	486°F, 620 psia		
Steam separation system, 8333 Mw(t)			
Method of steam separation	Two-stage centrifugal separators		
First stage	In-line impingement centrifugal separators, one located at end of each pressure tube; exit quality, 90%		
Second stage	Centrifugal separator, 24 per 8333-Mw(t) reactor; exit quality > 99.25%		

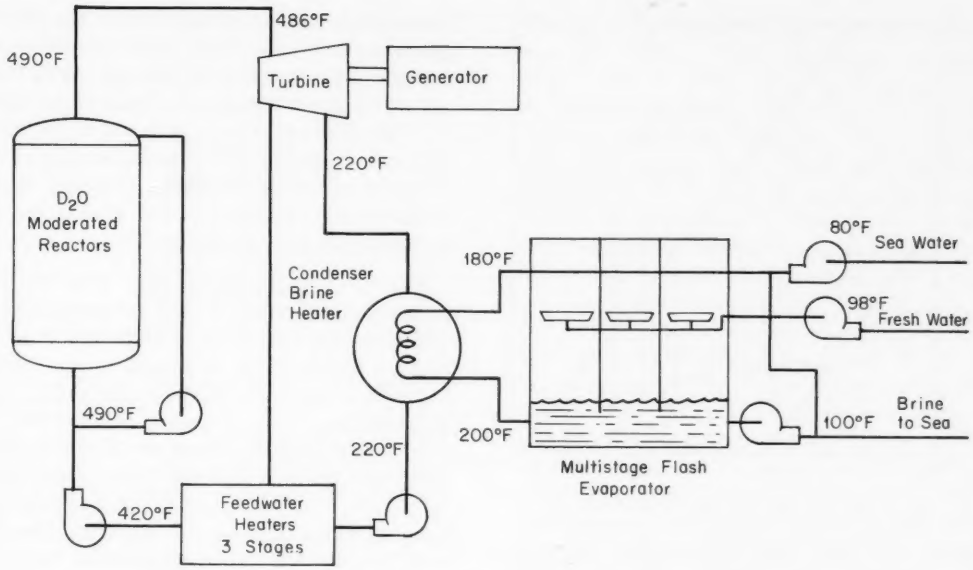

Fig. I-3 Schematic of dual-purpose plant.[3]

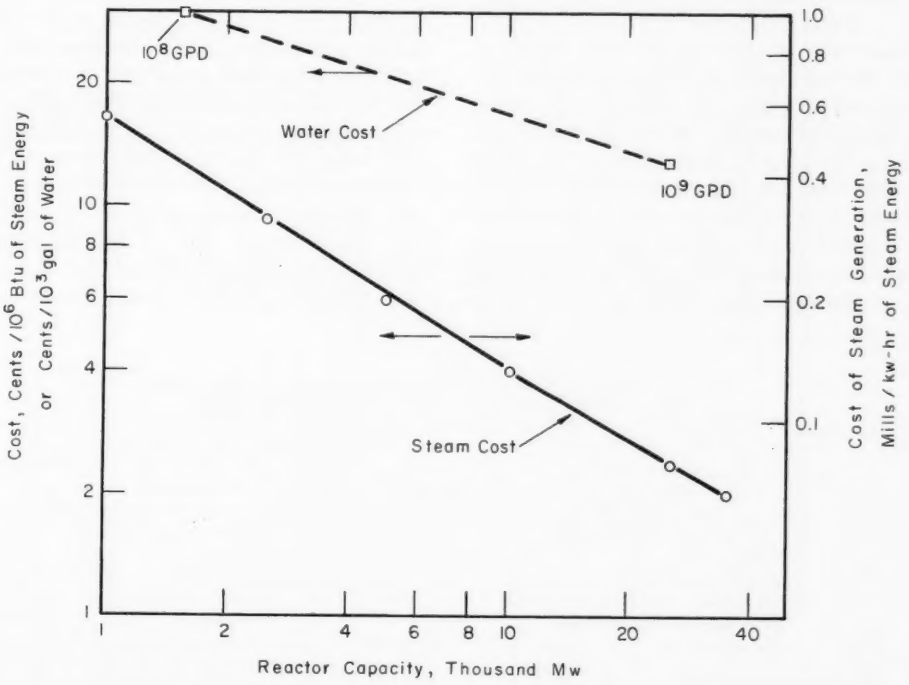

Fig. I-4 Estimated costs of steam production by fast-breeder reactors and corresponding costs of desalinizing seawater.[2] Single-purpose operation; 90% plant factor; municipal financing: 7.75% on depreciating capital, 5.5% on working capital, 3.75% on fuel inventories.

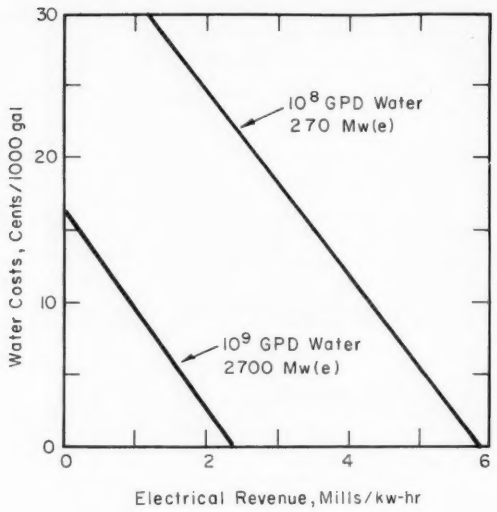

Fig. I-5 Effect of electrical revenue on water production costs.[2] Reactors and ground rules are the same as for Fig. I-4.

When one considers the possibilities of very large desalinization plants, along with the possibilities of concurrent electric power production under the various conceivable financing schemes, the situation becomes so complex and so far removed from past nuclear experience that a casual assessment of the proposals has little value. It is at least possible, however, to gain some understanding of the goals and requirements of the application by examining selected results from the studies mentioned above.

Figure I-4, constructed from the results of Ref. 2, shows estimated steam and fresh water costs for single-purpose plants in the 10^8 to 10^9 gal/day range, for plants utilizing fast-breeder reactors. Regardless of how one views the accuracy of the estimates, it seems clear that, for very low desalinization costs, one is speaking of the nuclear generation of steam energy at costs of about 10 cents per million Btu or less, corresponding to thermal-power generation costs of about 0.35 mill/kw-hr or less.

For current desalinization technology, high steam temperatures are not required, since the use of temperatures above about 300°F leads to scaling problems in the evaporators. If the reactor type used for steam production is capable of producing steam at considerably higher temperature, it seems obvious that the use of backpressure turbines for the production of electricity in conjunction with the desalinization process would be economically attractive in any case where there is a market for the power. Since the thermal energy in the exhaust steam from the backpressure turbines is still usable in the desalinization process, the economics of power generation are particularly favorable if the electricity can be considered as a by-product; for the use of energy in the power cycle is effectively 100% efficient, and only a fraction of the total plant cost is attributable to the electrical generation. The estimated improvement in economics is illustrated in Fig. I-5, from Ref. 2, which shows the 10^8 gal/day plant producing fresh water at about 18 cents per thousand gallons if electric power is sold at 3 mills/kw-hr. The 10^9 gal/day plant is estimated to produce fresh water at about 7 cents per thousand gallons if electricity is sold at

Table I-3 ESTIMATED STEAM, ELECTRICITY, AND WATER COSTS FOR 25,000-Mw(t) STATION* USING THREE H_2O-COOLED, D_2O-MODERATED REACTORS[3]

Steam cost (600 psi), cents/10^6 Btu		Electricity cost, mills/kw-hr		Water cost, cents/10^3 gal	
Capital	3.8	1.16		Heat	1.4
D_2O inventory	0.8	0.10		Electricity	1.8
Fuel cycle	0.9	0.11		Capital	6.0
Operation and maintenance, insurance	1.0	0.18		Operation and maintenance	0.8
				Chemicals	1.0
Totals	6.5	1.55			11.0

*Economic ground rules: plant investment at 7.7%/year; fuel and D_2O at 5.5%/year; natural U_3O_8 at $5/lb; Pu as nitrate at $6.7/g; D_2O at $20/lb; load factor = 90%; size of fueling industry = 10 tons/day; fuel owned by plant operator.

1.5 mills/kw-hr. These numbers are somewhat lower, but not drastically so, than those estimated in Ref. 3 for a station of comparable size utilizing the heavy-water-moderated reactors (Table I-3).

The results of Ref. 7 can be used, conceptually, to examine a transition from reactors of currently contemplated sizes to the very large reactors such as those considered in Refs. 2 and 3 and to throw some light on the effects of the dual-purpose (vs. power only) application and methods of financing. The nine reactor types considered in the study are described in Table I-4. The uncertainties in estimating the very large plants may be inferred from the lack of specificity in their descriptions. In Table I-5 the estimated costs of producing steam energy for water desalinization are given for the nine types in a way that compares dual-purpose operation with power-only operation. For each of the plant types, Ref. 7 gives curves similar to that of Fig. I-6, which applies to the plant utilizing fast-breeder reactors (Case 9). The reference also gives for each case the estimated cost of electric power generation if the plant is designed for that purpose only. In Table I-5 the costs of steam production listed are those for the dual-purpose plant which correspond to the sale of electricity at a price equal to its production cost in the single-purpose plant. This is illustrated in Fig. I-6. The estimates for the very large plants (Cases 7-9) are not greatly different than those given in Table I-3.

Since the costs of steam production in the large plants of Table I-5 do not appear to be substantially less than the costs necessary for the economic large-scale desalinization of water, one might conclude, at least tentatively, that revenue from the sale of steam for de-

Table I-4 REACTOR TYPES USED IN STUDIES OF NINE DIFFERENT ELECTRIC GENERATION-DESALINIZATION CASES IN REF. 7

1. One 1500-Mw(t) light-water reactor of current technology.
2. Three 1500-Mw(t) light-water reactors in a single plant, current technology.
3. One 3220-Mw(t) light-water reactor, current technology.
4. One 3500-Mw(t) heavy-water-moderated organic-cooled reactor, current technology.
5. One 3500-Mw(t) graphite-moderated light-water-cooled reactor, current technology.
6. One 8300-Mw(t) heavy-water-moderated organic-cooled reactor; 1975 technology.
7. A multiunit 25,000-Mw(t) station with high-conversion-ratio reactors, such as: heavy-water-moderated organic-, light-water-, or heavy-water-cooled reactors; graphite-moderated organic-, or light-water-cooled reactors; or graphite-moderated gas-cooled thorium-cycle reactors; 1980 technology.
8. A 25,000-Mw(t) station utilizing an unspecified number of slightly enriched reactors such as: light-water-moderated in combination with graphite-moderated steam-cooled reactors, graphite-moderated sodium-cooled reactors, or graphite-moderated gas-cooled reactors; 1980 technology.
9. An unspecified number of fast-breeder reactors of 25,000 Mw(t) total capacity; 1980 technology.

Table I-5 ESTIMATED COSTS OF PRODUCING ELECTRICITY AND HEAT IN THE FORM OF STEAM FOR SEAWATER DISTILLATION[7]

Case (see Table I-4)	Cost of electricity from plant designed for power only, mills/kw(e)-hr		Cost of heat in steam from dual-purpose plant if electricity is sold at the cost of its production in the power-only plant, cents/10^6 Btu		Net electrical output of power-only plant, Mw(t)	Net electrical output of dual-purpose plant, Mw(e)
	7% to 5% financing	14% to 12.5% financing	7% to 5% financing	14% to 12.5% financing		
1	3.97	6.16	20	30	470	240
2	3.67	5.65	18.5	27	1410	720
3	3.45	5.28	18	26	1002	510
4	3.01	4.88	13	20	1110	620
5	3.03	4.89	15	22	1140	600
6	2.18	3.53	10	16	2770	1600
7*	1.87 to 1.67	3.20 to 3.01	9 to 8	14 to 6	8300	4800
8*	2.20 to 2.14	3.61 to 3.46	8 to 7.5	12 to 12	9000	6350
9*	1.78 to 1.57	3.30 to 3.07	6 to 5	11 to 10	9000	6350

*The range of the estimates results from a range of assumptions as to natural-uranium cost, plutonium value, and capacity of fuel reprocessing plant.

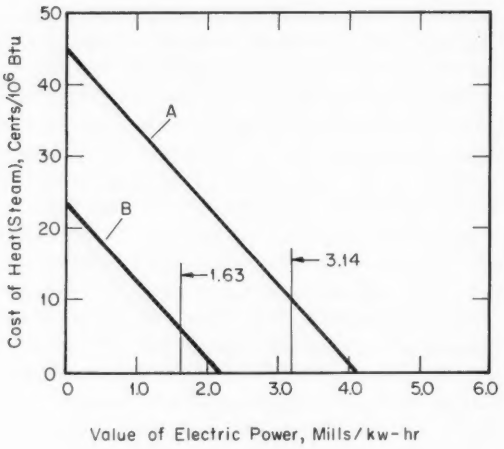

Fig. I-6 Effect of electrical revenue on cost of producing steam heat for desalinization by fast-breeder reactors, from Ref. 7 (Case 9). Curve A is for annual fixed charge rates of 14% and 12.5% for depreciating and nondepreciating capital, respectively; curve B is for rates of 7% and 5%. Plant factor is 80%. The vertical lines show the estimated electric power costs if the plant is designed for power only.

salinization is unlikely to make possible large reductions in the cost of electrical generation from a reactor of given thermal capacity. The more important aspect of the dual-purpose application may be that it increases the opportunities for utilizing plants of very large energy output.

References

1. R. P. Hammond, Large Reactors May Distill Sea Water Economically, *Nucleonics*, 20(12): 45 (December 1962).
2. A. Sesonske and R. P. Hammond, A Preliminary Evaluation of Fast Oxide Breeder Reactors for Sea Water Conversion, USAEC Report LA-2733, Los Alamos Scientific Laboratory of the University of California, August 1962.
3. I. Spiewak, A Large Desalinization Reactor Based on Current Technology, *Nucleonics*, 21(7): 64 (July 1963).
4. Sargent and Lundy, Saline Water Conversion Power Reactor Plants, USAEC Report SL-1998, Jan. 11, 1963.
5. Edging Toward Desalination, *The Forum Memo to Members*, Atomic Industrial Forum, Inc., 10(10): 8 (October 1963).
6. Nuclear Desalter Called Too Costly, *Engineering News-Record*, 17(19): 23 (Nov. 7, 1963).
7. Bechtel Corp., Large Reactor Study for Sea Water Distillation, Final Report for Office of Program Evaluation, Division of Reactor Development, U. S. Atomic Energy Commission, July 1963.
8. R. Revelle, Water-Resources Research in the Federal Government, *Science*, 142(3595): 1027 (Nov. 22, 1963).
9. D. G. Stephan, Water Renovation ... What It Means to You, *Chem. Eng. Progr.*, 59(11): 19 (November 1963).

Section

II

Power Reactor Technology

Physics

Thermal-Neutron Diffusion Parameters

The good agreement between the measurement and calculation of neutron diffusion parameters, which was indicated several years ago, has been found to be somewhat premature with the advent of more advanced experimental techniques and more sophisticated methods of analysis. The purpose of this article is to review some of the recent papers pertaining to the measurement and calculation of diffusion parameters and to present the current status. Many of the papers reviewed were presented at the Neutron Thermalization Conference held at the Brookhaven National Laboratory in the spring of 1962.

The various aspects of the thermal diffusion problem are best seen by examining the space-time-energy-dependent diffusion equation in a nonmultiplying scattering medium:

$$1/v\,\frac{\partial\phi(E,r,t)}{\partial t} = -\Sigma_a(E,r)\,\phi(E,r,t) + D(E,r)\,\nabla^2\,\phi(E,r,t) + H(E,r)\,\phi(E,r,t) + S(E,r,t) \quad (1)$$

where

$$H(E,r)\,\phi(E,r,t) = \int_r\int_E \phi(E',r',t)\,\Sigma_s(E',r' \rightarrow E,r)\,dE'dr' - \phi(E,r,t)\,\Sigma_s(E)$$

and

v = neutron velocity corresponding to the energy E

ϕ = neutron flux

D = diffusion coefficient

∇^2 = thermalization operator

Σ_a = absorption cross section

S = source term

$\Sigma_s(E',r' \rightarrow E,r)$ = differential cross section for scattering

$\Sigma_s(E)$ = total cross section for scattering

In a pulsed medium at large times after the injection of the neutron burst, the asymptotic solutions of Eq. 1 can be written as:

$$\phi(r,E,t) = R(r)\,\phi_\alpha(E)e^{-\alpha t} \quad (2)$$

where α is the lowest eigenvalue of the equation

$$\left(-\frac{\alpha}{v} + \Sigma_a + DB^2\right)\phi(E) = H\phi(E) \quad (3)$$

and $\phi_\alpha(E)$ is the eigenfunction.

Integrating Eq. 3 over all energies, and considering only $1/v$ absorbers, gives

$$B^2\,\overline{Dv} + \alpha_0 - \alpha = 0 \quad (4)$$

where $\overline{Dv} = \dfrac{\int n(v)v\,Ddv}{\int n(v)\,dv}$

$$\alpha_0 = v(kT)\,\Sigma_a(kT) = v_0\Sigma_a(kT)$$

k = the Boltzmann constant

T = the absolute temperature

For $B^2 = 0$ (pulsed infinite medium), the solution to Eq. 3 is a Maxwellian flux distribution and $\alpha = \alpha_0$. When $B^2 > 0$, the spectrum $n(v)$ is displaced to lower energies, and diffusion cooling results. If $B^2 < 0$, the spectrum is shifted to higher energies, and diffusion hardening is the result. Therefore $\overline{Dv}$ is a continuous function of B^2 and can be expanded in the power series:

$$\overline{Dv}(B^2) = D_0 - CB^2 + FB^4 \ldots \quad (5)$$

where C is known as the diffusion cooling constant. If Eq. 4 is substituted in Eq. 5, the relation between α and B^2 is found as

$$\alpha = \alpha_0 + D_0B^2 - CB^4 + FB^6 + \ldots \quad (6)$$

Here B^2 is the geometrical buckling and is given as the lowest eigenvalue of the equation

$$\nabla^2 R + B^2 R = 0 \qquad (7)$$

In the stationary or time-independent case, there may be asymptotic solutions of Eq. 1 at large distances from the source of the form

$$\phi(r,E) = e^{-\kappa z}\ \phi_\kappa(E) \qquad (8)$$

where κ is the smallest eigenvalue of

$$(\Sigma_a - D\kappa^2)\ \phi(E) = H\phi(E) \qquad (9)$$

and ϕ_κ is the eigenfunction. The term κ^2 can be expressed as

$$\kappa^2 = a_1\Sigma_a(kT) + a_2\Sigma_a^2(kT) + a_3\Sigma_a^3(kT) + \ldots \qquad (10)$$

and κ^{-1} can be defined as the thermal diffusion length when it is the eigenvalue corresponding to a positive eigenfunction $e^{-\kappa x}\ \phi_\kappa(E)$ describing the exponential decay of the thermal flux in an infinite source-free region, with no variation in the transverse y or z directions. For very weak absorption and at a large distance from the source, $n(v) = \phi(E)/v$ has a Maxwellian distribution at room temperature and deviates progressively and becomes hardened as the absorption in the medium is increased.

Equations 3 and 9 are of the form

$$\left(Dk_1 - \frac{k_2}{v_0}\right)\phi(E) = H\phi(E) \qquad (11)$$

where

Pulsed-source experiment $k_1 = B^2$,

$$k_2 = \alpha - \alpha_0;\ \alpha_0 = v_0\Sigma_a(kT) \qquad (12a)$$

Diffusion-length experiment $k_1 = -\kappa^2$,

$$k_2 = -v_0\Sigma_a(kT) \qquad (12b)$$

A schematic of these functions is shown in Fig. II-1. Here α_0 is v_0 times the cross section in pure moderator at the temperature T, and κ_0^2 is the inverse diffusion length in the pure moderator. The uniform addition of a $1/v$ poison $\Delta\Sigma_a(kT)$ shifts the curve a distance $v_0\Delta\Sigma_a(kT)$ in the direction of positive α without changing the shape of the curve. Thus a larger value of κ^2, namely κ_1^2, is obtained on the abscissa. The dotted curve in the pulsed-neutron experiment region in Fig. II-1 relates the value of the decay constant α to the geometrical buckling of a medium that has an intrinsic $1/v$ absorption cross section $\Sigma_{a_0}(kT) = \alpha_0/v_0$ and to which a uniform $1/v$ poison cross section $\Delta\Sigma_a(kT)$ has been added. The solid curve in the diffusion-length experiment region relates κ^2, or the inverse length $1/L^2$, to the added poison $\Delta\Sigma_a(kT)$ in an infinite medium having an intrinsic $1/v$ cross section

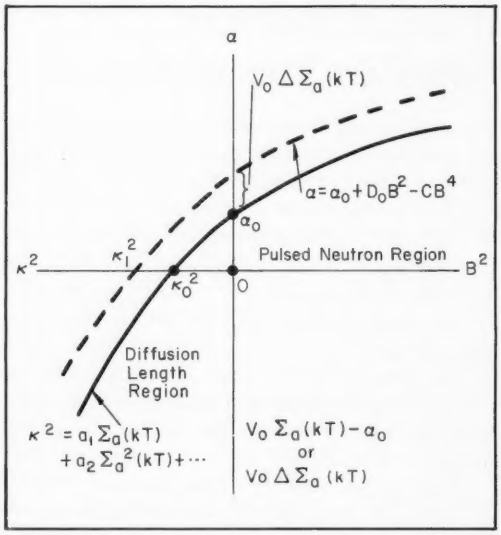

Fig. II-1 Schematic[12] of the functions $\alpha\ (B^2)$ and $\kappa^2[v_0\ \Sigma_a(kT)]$.

$\Sigma_{a_0}(kT) = \alpha_0/v_0$. Only the small segment between the intercepts cannot be measured by either of the techniques.

The nonasymptotic solutions of Eq. 1 describe the neutron flux and spectral distribution near discontinuities in the time-independent form of Eq. 1 and the flux and spectrum during the thermalization process in the time-dependent form.

Diffusion-Length Measurements in H_2O

Three techniques have been used to measure the thermal diffusion length in water, differentiated by the source of thermal neutrons as follows: (1) thermal neutrons from a thermal column; (2) a point source of low-energy neutrons; and (3) a pulsed neutron source. One of the recent measurements is that made by Bal-

lowe et al.,[1,2] at the Vallecitos Atomic Laboratory of the General Electric Company. In this measurement the thermal column of the General Electric Nuclear Test Reactor (NTR) was used as a source of thermal neutrons. The experimental arrangement consisted of a cylindrical cadmium-lined water tank, 23.75 in. in diameter, containing a close-fitting piston that was faced with cadmium except for a thin aluminum window at its center. The neutron detector, a thin B^{10}-ZnS(Ag) scintillator, was mounted behind the window. Varying the position of the piston permitted the length of the column of water between the end of the tank and the piston to be varied as desired. The end of the cylindrical water tank abutted the transition region to the graphite thermal column of the NTR, which served as the neutron source. The relaxation length of the thermal neutrons emanating from the thermal column was evaluated by measuring the thermal-neutron flux as a function of the length of the water column between the piston and the end of the water tank.

Because of the cadmium facing, the logarithmic shape of the curve of flux vs. distance remained the same regardless of the length of the water column, and the slope of this curve was the same as that measured in a medium of infinite length. The slope determined the relaxation length and hence the diffusion length in the medium when corrections were made for geometry and background.

The measurements were made at temperatures ranging from 25 to 93°C in pure water. Measurements were also made over essentially the same range in H_3BO_3, $CdSO_4$, and $Gd(NO_3)_3$ solutions. The water result at room temperature is one of those listed in Table II-1.

Starr and Koppel[3] have measured the diffusion lengths, using thermal neutrons from a thermal column in H_2O poisoned by various concentrations of H_3BO_3. The measurements were made in a cylindrical water tank situated atop the Brookhaven Research Reactor, using small, bare indium foils spaced at intervals of 0.375 in. (or for heavily poisoned water, 0.250 in.) along a direction perpendicular to the thermal column. The value obtained for pure water at 21°C is also listed in Table II-1.

Table II-1 DIFFUSION-LENGTH MEASUREMENTS ON THERMAL NEUTRONS IN WATER

Authors	Year	Reference	Method	Temp. at which measurement was made, °C	Diffusion length L, cm	Diffusion length L (at 22°C),* cm
J. L. Russell et al.	1962	1,2	Thermal column	24.55	2.873 ± 0.008	2.858 ± 0.012
Starr and Koppel	1961	3	Thermal column	21	2.754 ± 0.008	2.760 ± 0.008
Reier and DeJuren	1961	4	Sb-Be	23	2.781 ± 0.006	2.775 ± 0.006
Rockey and Skolnik	1961	5	Sb-Be	25.9	2.859 ± 0.018	2.835 ± 0.018
Rohr	1962	7	Sb-Be	16	2.742 ± 0.011	2.778 ± 0.011
Lopez and Beyster	1962	6	Pulsed source	26.7	2.828 ± 0.016	2.803 ± 0.016
Küchle	1960	8	Pulsed source	22	2.744 ± 0.080	2.744 ± 0.080
Dio	1958	9	Pulsed source	22	2.739 ± 0.06	2.739 ± 0.06

*Conversion to 22°C made using $dL/dT = 0.006$ cm/°C.

M. Reier and J. A. DeJuren[4] made diffusion measurements in pure water over the range from 23 to 244.4°C. They also made diffusion measurements at 23°C with various amounts of boron poison in the water and with one cadmium solution, using an Sb^{124}-Be photoneutron source. They used the inhomogeneous form of the diffusion equation (which contains a source term) to determine corrections to the measured relaxation length because of the significant thermalization of the 24-kev neutrons, even at considerable distances from the source where the cadmium ratios were greater than 100. The solution to the inhomogeneous equation, on the assumption of spherical symmetry, consisted of the solution $n = Ge^{-r/L}/r$, the source-free diffusion equation multiplied by a slowly varying correction term involving exponential integrals. The details of the source correction are given in Ref. 4. The measured diffusion length corrected for source effects at 23°C and the corrected value inferred for 22°C are listed in Table II-1. The source corrections at 23°C and 49°C reduced the uncorrected values of L by 0.8%. At 70 and 90°C the correction was 0.6%.

The diffusion length was measured in water over the range from 25.9 to 295.3°C in the pres-

sure vessel of the Knolls Atomic Power Laboratory high-temperature critical assembly by K. S. Rockey and W. Skolnik.[5] They used 5- and 10-mil foils made of P metal, an alloy of manganese (71%), copper (18%), and nickel (10%). The room-temperature result is listed in Table II-1. It is possible that the somewhat high value measured can be attributed to the neglect of source-neutron corrections.

The third technique for measurement of the thermal diffusion length consists in injecting pulses of fast neutrons into moderator regions of different sizes and measuring the decay constant of the leakage neutrons distributed in the fundamental spatial mode. The asymptotic decay constant α is generally fitted to the series expansion given in Eq. 6:

$$\alpha = \alpha_0 + D_0 B^2 - CB^4 + \ldots$$

where α_0 = thermal-neutron density absorption probability of the unpoisoned medium, $v_0\Sigma_{a_0}(kT)$, at the ambient temperature, T
D_0 = thermal-neutron density coefficient*
C = diffusion cooling coefficient
B^2 = geometrical buckling

The expression for the diffusion length may be found by using the prescription in Eqs. 12a and 12b to obtain stationary diffusion parameters from pulsed diffusion parameters. Substituting $-1/L^2 = \kappa^2$ for B^2 in Eq. 6 gives the relation

$$L^2 = \frac{D_0}{v_0\Sigma_a(kT)}\left[1 + \frac{v_0 C\,\Sigma_a(kT)}{D_0^2}\right] \qquad (13)$$

when $4\Sigma_a(kT)v_0C \ll D_0^2$. This equation should yield values of L that are directly comparable to values measured by stationary methods.

Lopez and Beyster[6] measured the thermal-neutron diffusion length in water at 26.7°C by the pulsed-source technique. The measured value of the diffusion length lies between values measured by Rohr[7] and Rockey and Skolnik (Table II-1). Küchle and Dio,[8,9] who earlier used the pulsed-source technique to measure the diffusion length, obtained values that were somewhat low, as are shown in Table II-1. These lower values may have been the result of underestimation of the effects of higher harmonic modes or to a container reflection phenomenon. Both of these sources of error are discussed in Ref. 6.

*The value D_0 cm^2/sec is related to the more familiar average diffusion coefficient for neutron flux $\overline{D}$ having the dimension (cm^2) by the average neutron velocity $\overline{v}_0$, namely $D_0 = \overline{v}_0\overline{D}$, where the averages are over the ambient temperature Maxwellian spectrum.

Other Neutron-Diffusion Parameters in H_2O

The close relation between the equations governing pulsed-source experiments and diffusion-length measurements in poisoned water permits the evaluation of the characteristic pulsed-source diffusion parameters α_0, D_0, and C from stationary measurements. Although this has been known for many years, the measurements of Starr and Koppel[3] are the first to yield data of sufficient accuracy to yield a determination of the diffusion cooling C term (see Eq. 6). Thus the stationary and pulsed experimental results may be compared directly by comparing the diffusion parameters.

In evaluating the diffusion parameters, Starr and Koppel[3] made a least-squares fit of the experimental data $[\kappa_i^2, \Sigma_{a_i}(kT)]$ to Eq. 6 and to Eq. 10, substituting $-\kappa^2$ for B^2 and $-v_0\Sigma_a(kT)$ for $\alpha - \alpha_0$ as prescribed in relations 12a and 12b, to obtain for Eq. 6

$$\frac{\Sigma_a(kT)}{\kappa^2} = \frac{D_0}{v_0} + \frac{C}{v_0}\,\kappa^2 \qquad (14)$$

and to obtain for Eq. 10

$$\frac{\kappa^2}{\Sigma_a(kT)} = a_1 + a_2\Sigma_a(kT) \qquad (15)$$

The coefficients a_1 and a_2 of Eq. 15 may be evaluated in terms of the diffusion parameters by recognizing the inverse series expansion of Eq. 6 to be

$$B^2 = \frac{\alpha - \alpha_0}{D_0} + \frac{C}{D_0}\left(\frac{\alpha - \alpha_0}{D_0}\right)^2 + \ldots \qquad (16)$$

and making the substitutions prescribed in relations 12a and 12b for B^2 and $\alpha - \alpha_0$ to obtain

$$\frac{\kappa^2}{\Sigma_a(kT)} = \frac{v_0}{D_0} - \frac{C}{D_0^3}\,v_0^2\,\Sigma_a(kT) \qquad (17)$$

for Eq. 15. In this equation κ is the inverse diffusion length measured in the poisoned medium, having the total macroscopic cross section $\Sigma_a(kT) = \Sigma_H + \Sigma_B$. The value of the hydrogen

cross section was found by varying the value of Σ_H in the expression

$$\sum_n \left[\frac{K^2}{\Sigma_a} - \frac{K^2}{\Sigma_a}(\text{calc})\right]$$

until the variance from the least squares fit to the coefficients in Eq. 17 was a minimum. Using the linear functions, Eqs. 14 and 17, the diffusion parameters can then be obtained from the intercept and slope of these functions evaluated at the zero values of κ^2 or $\Sigma_a(kT)$. The results that were obtained from each equation are:

Equation No.	D_0	C/D_0
14	35,506 cm²/sec	0.11045 cm²
17	35,852	0.07648

Although the values of D_0 are in good agreement, the values of C/D_0 are not. This is the result of the neglect of the higher order terms and is not surprising in the light of the 20% spectral shift in the most heavily poisoned medium.

For a particular experimental error on the experimental points, there is apparently an optimum range of poison concentration beyond which no further accuracy would be obtained in the determination of the diffusion parameters, D_0 and C Actually, if higher order terms were included in Eqs. 14 and 17 in order to fit the large poison concentrations better, the uncertainty in the first two terms would remain roughly constant. Thus a fit over a small range of poison concentration seems to be as good as a fit over a wider range, so far as the determination of D_0 and C is concerned. Therefore, to obtain an estimate of the error in the value of the diffusion parameters resulting from truncating the series, Starr and Koppel[3] repeatedly fitted Eqs. 14 and 17 with progressively fewer points, dropping those corresponding to the highest poison concentrations and, at the same time, obviously increasing the uncertainty in both D_0 and C. Since the values of C as evaluated using Eqs. 14 and 17 would tend toward the same limit, and the ends of the error bars would tend to approach one another as the equations are fitted over a range of progressively lighter poison concentrations, the fitting of the equations with fewer points was continued until the upper end of the error bar corresponding to the lesser value of C just touched the lower end of the error bar corresponding to the greater value of C. At this point a minimum total uncertainty could be assigned to the diffusion cooling coefficient C. The results obtained using this method of analysis are listed in Table II-2. When C/D_0 was determined from Eq. 17, the dropping of points caused much less shift in the values than when Eq. 14 was used; this indicates that the data are described better by Eq. 17.

The thermal-column measurements of D_0 reported by Reier[10] are also listed in Table II-2.

The Beyster and Lopez neutron diffusion parameter data, listed in Table II-2, were measured, using a high-intensity pulsed neutron source obtained by bombarding a water-cooled lead or tungsten alloy target with 23- to 25-Mev

Table II-2 MEASURED AND CALCULATED DIFFUSION PARAMETERS IN WATER

Author	Year	Reference	Method	Temp. at which measurement was made, °C	D_0, cm²/sec	D_0 (at 21°C) cm²/sec	C	σ_{aH_2O}, mb	F
Starr and Koppel	1961	3	Thermal column	21	35,850 ± 100	35,850 ± 100	2,900 ± 350	326.9 ± 1.6	
Reier	1960	10	Thermal column	22	37,618 ± 205	37,488 ± 205*		328 ± 6	
Beyster and Lopez	1961	6,11	Pulsed source	26.7	37,426 ± 368†	36,685 ± 368	4,852 ± 763	325.3 ± 1.6	
					37,630 ± 404‡	36,889 ± 404*	4,153 ± 852	324.8 ± 1.6	
Küchle	1960	8	Pulsed source	22	35,400 ± 700	35,300 ± 700*	4,200 ± 800	326 ± 6	
Honeck		12	Calculation			37,460	2,878		180

*D_0 was corrected to 21°C, using $dD_0/dT = 130$ cm²/(sec)(°C). No attempt was made to correct C, since this would shift C by a fraction of the error limits.

†Extrapolation length = 0.32 cm.

‡Extrapolation length = $f(B^2)$.

electron pulses to produce bursts of 2×10^{10} neutrons each by the (γ,n) process. Neutron lifetime measurements were performed on small and large water samples that ranged in geometrical buckling from 0.014 to 0.59 cm^{-2}. Reference 11 lists additional data obtained over the buckling range 0.6 to 1.5 cm^{-2}. The effects of harmonic modes in the large water geometries were determined by measurements of the time-dependent spatial flux. It was found that these flux distributions were also adequately described by simple diffusion-theory calculations.

A three-parameter fit was made to the data, using Eq. 6. The extrapolation distance was calculated in two different ways. In case 1 the extrapolation distance was taken to be a constant $d = 2.131\ D_0/\bar{v}$ with $\bar{v} = 2/\sqrt{\pi}\ 2.2 \times 10^5$ cm/sec. In case 2, d was assumed to vary with B^2. The method of treatment of the extrapolation length did not greatly affect the results. The results of Küchle[8] are also listed in Table II-2. These results were obtained by a three-parameter analysis in the buckling range $B^2 = 0$ to 0.7 cm^{-2}.

Comparison of Experimental and Calculated Diffusion Parameters

Extensive calculations of diffusion parameters in H_2O, D_2O, and graphite have been made by Honeck.[12] He solved the eigenvalue equation, Eq. 3, using the transport formulation for different amounts of poison and employing the Nelkin bound-proton scattering kernel with oxygen included. The calculated eigenvalues were then expanded into a power series to obtain values of D_0, C, and F (Eq. 6). These values are listed in Table II-2.

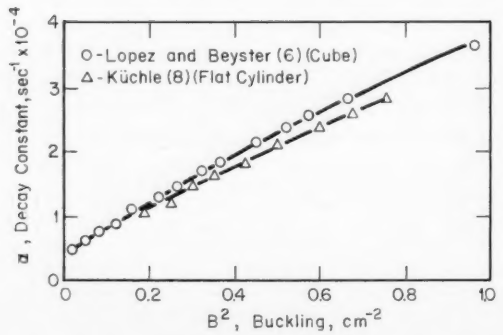

Fig. II-2 α vs. B^2 for H_2O at 26.7°C.[13]

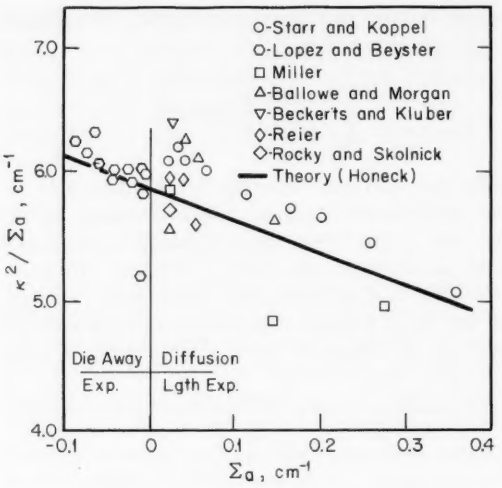

Fig. II-3 Computed and measured diffusion parameters in water.[12]

A comparison of the α vs. B^2 curves for H_2O from the pulsed-source results of Lopez and Beyster and those of Küchle[8] are given in Fig. II-2. Since the shape of Küchle's curve is very similar to that found by earlier investigators, Beckurts[13] concludes that background, backscattering, and even higher spatial modes cannot be the reason for the discrepancy. According to Buckurts the discrepancy must arise from the fact that Küchle and the other investigators made the measurements in flat cylindrical assemblies, whereas Lopez and Beyster used cubical assemblies. This contention is supported by the very strong effect of the extrapolation length in small water geometries found by Hall et al.,[14] who did pulsed measurements on square and flat systems with quite different results. Since there are problems in connection with specifying the buckling in small water systems, Beckurts[13] is of the opinion that there are, at present, doubts as to the accuracy of pulsed measurements in water and that more confidence should be placed in the poisoning experiments. Although both the pulsed-source and poisoning techniques are suitable methods for measuring D_0 and $\sigma_{a\,H_2O}$, there is uncertainty in determining the higher order coefficients in the power series Eqs. 6 and 10. Therefore it is preferable to compare the different measurements point by point rather than by the coefficients of a least-squares fit. Some of the measured and computed diffusion parameters

discussed above are compared in this way in Fig. II-3.

Neutron-Diffusion Coefficient in D_2O

Brown and Hennelly[15] measured the thermal-neutron diffusion coefficient as a function of temperature in D_2O lattices. These measurements were made over the temperature range from 20 to 220°C by measuring the relaxation length of thermal neutrons in D_2O containing known amounts of heterogeneous poison in the form of thin-walled copper tubes spaced on a variety of square lattice pitches. The measurements were corrected for the volume displacement and scattering of the copper as well as for the thermal-expansion coefficients. The measured values of $D = D_0/v_0$ are plotted in Fig. II-4.

The value of D obtained from pulsed source measurements in D_2O by Ganguly and Waltner[16] are also plotted in Fig. II-4. These experiments gave a value of $C = 37{,}200 \pm 5000$ for the diffusion cooling coefficient, which compares favorably with Sjöstrand's[17] preliminary value of preliminary value of 35,000 ± 8000 cm^4/sec.

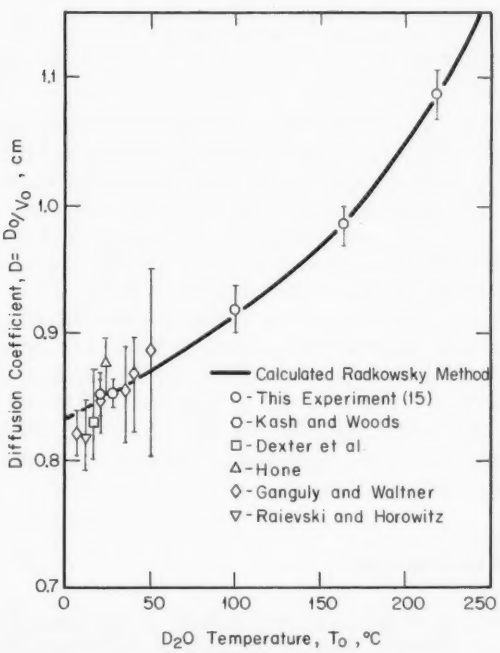

Fig. II-4 Diffusion coefficient of D_2O as a function of temperature.[15]

The experimental values of the neutron diffusion coefficient D obtained by boron poisoning, measurement of extrapolation distance, and pile oscillation are also indicated. The agreement among all the measurements is good. The temperature dependence of the thermal diffusion coefficient was calculated using Radkowsky's method in Ref. 15. This result is plotted in Fig. II-4; the variation of D with temperature is well described by this simple calculational model.

Diffusion Parameters in Graphite

Early pulsed-source measurements in graphite systems resulted in a value of C, the diffusion cooling coefficient, in the range of 12 to 16×10^5 cm^4/sec at a graphite density of 1.6 g/cm^3. These values are in good agreement with the theoretical value of $C = 14 \times 10^5$ calculated by Nelkin.[18] Later French and German measurements have indicated a C value about twice as large, as well as discrepancies in other parameters. Therefore careful remeasurements have been made by Klose, et al.,[19] Starr and Price,[21] and Starr and de Villiers.[20]

Klose made pulsed-source measurements on 45 graphite piles that ranged in buckling from 7×10^{-4} cm^{-2} to 240×10^{-4} cm^{-2}. A three-parameter least-squares fit of the decay constants to the B^2 power series for α (Eq. 6) was obtained with the α values weighted according to their relative accuracy. The fitting procedure was repeated, dropping all measured points with B^2 larger than a fixed B^2_{max}, in order to investigate the dependence of the diffusion parameters on the buckling range used. By this analytical procedure it was concluded that, if the B^2 ranged included in the fitting procedure is small (i.e., only a few points are used), low values for D_0 and C are obtained, whereas, when B^2 exceeds about 60×10^{-4} cm^{-2}, D_0 and C increase continuously, indicating that the three-parameter fit is no longer adequate. With a four-parameter fit, no definite tendencies were noted, but the D_0 and C values were somewhat lower over the entire range of B^2_{max}. These values are listed in Table II-3. It was surprising that a large negative value was obtained for the F parameter, since previous theoretical estimations have predicted a small positive value. However, recent calculations by Honeck[12] confirm the negative sign and the order of magnitude of this coefficient. The calculated results are listed in Table II-3. The large size and the negative sign of

F may arise because the thermalization power of graphite decreases strongly with the decreasing neutron "temperature" or spectral softening (diffusion cooling) that occurs with increasing buckling.

Starr and de Villiers[20] have determined the diffusion cooling parameter C in graphite by measurement of the average neutron velocity in graphite. The asymptotic neutron decay of a neutron burst in a series of graphite piles of differing bucklings was measured, using simultaneously a detector in which every incident neutron was counted and a detector which had a $1/v$ response sensitivity. Thus, at long times after the pulsed-source neutron burst, the ratio of the counting rate of the thermally black detector to that of the $1/v$ response detector is proportional to the density-weighted average velocity $\bar{v}$. The detectors used were two physically identical BF_3 proportional counters. The black detector contained 96% enriched B^{10} and the gray detector contained 11% B^{10}. The diffusion cooling constant C was determined by assuming that D is a constant in the expression $\overline{Dv}$ in Eq. 5. Since D_0 equals $\bar{v}_0\bar{D}$, D can be written as $D_0/\bar{v}_0$, and Eq. 5 can be rearranged as follows:

$$\bar{v} = \bar{v}_0\left(1-\frac{C}{D_0}B + \ldots\right)$$

Therefore a direct measurement of the average velocity as a function of buckling will yield the diffusion cooling coefficient C in terms of the more precisely known D_0. The results of this measurement are listed in Table II-3.

Starr and Price[21] measured the diffusion length in graphite and various graphite-bismuth assemblies by exponential measurements in connection with an investigation of liquid-metal-fueled reactor systems. The diffusion parameters of these systems were subsequently measured by pulsed-source methods, and the results were compared. The results were then combined to obtain a more accurate set of parameters. In all cases the diffusion length determined from pulsed-source experiments agreed within statistical error with the diffusion length determined by exponential experiments.

Table II-3 MEASURED AND CALCULATED DIFFUSION PARAMETERS IN GRAPHITE

Author	Year	Ref.	Method	Fitting	Density	D cm²/sec	C, cm⁴/sec	F, cm⁶/sec	σ_a^c, mb
Klose, Küchle, and Reichardt	1962	19	Pulsed source	3-parameter	ρ = 1.6 g/cm³	$2.13 \pm 0.02 \times 10^5$	$26 \pm 5 \times 10^5$	$-20 \pm 10 \times 10^7$	4.77 ± 0.07
				4-parameter	ρ = 1.6 g/cm³	$2.11 \pm 0.02 \times 10^5$	$16 \pm 5 \times 10^5$		4.80 ± 0.07
Honeck	1962	12	Calculation	4-parameter		2.178×10^5	24.57×10^5	-8.31×10^7	
Starr and de Villiers	1962	20	Pulsed source (average velocity measurements)						
Starr and Price	1962	21	Pulsed source		AA graphite, ρ = 1.674 g/cm³	$2.09 \pm 0.03 \times 10^5$	$41 \pm 4 \times 10^5$		3.83 ± 0.06
Starr and Price	1962	21	Pulsed source		GBF graphite, ρ = 1.697 g/cm³	$2.02 \pm 0.01 \times 10^5$	$34 \pm 3 \times 10^5$		
Starr and Price	1962	21	Exponential measurements		AA graphite	Diffusion-length average 54.5 ± 0.5 cm			
					GBF graphite	Diffusion-length average 50.7 ± 0.3 cm			

Since the pulsed-source experiments yield an accurate value of the diffusion constant, and the exponential experiments yield an accurate value of the diffusion length, the combined data should result in a more accurate determination of the thermal absorption cross sections. The experimental results are listed in Table II-3.

The disparity of the values for the diffusion cooling parameter, C, listed in Table II-3, may result from variations in density and from anisotropy effects in the graphite. However, the experiments indicate that the diffusion cooling parameter is substantially greater than was previously estimated.

References

1. W. C. Ballowe, Measurement of the Diffusion Length of Thermal Neutrons in Light Water, in Proceedings of the Brookhaven Conference on Neutron Thermalization, April 30 to May 2, 1962, Vol. III, Experimental Aspects of Tran-

sient and Asymptotic Phenomena, USAEC Report BNL-719, pp. 799-804, Brookhaven National Laboratory, November 1962.

2. J. L. Russell, Jr., W. C. Ballowe, W. R. Morgan, and M. V. Mosgovoy, Thermal Neutron Diffusion Length Measurements in Light Water from 20°C to 90°C, USAEC Report GEAP-4018, Vallecitos Atomic Laboratory, April 1962.
3. E. Starr and J. Koppel, Determination of Diffusion Hardening in Water, *Nucl. Sci. Eng.*, 14(3): 224 (November 1962); also in USAEC Report BNL-719, pp. 1012-1033, Vol. III.
4. M. Reier and J. A. DeJuren, Diffusion Length Measurements of Thermal Neutrons in Water from 23°C to 244°C, *J. Nucl. Energy: Pt. A & B*, 14(1): 18 (April 1961); also in USAEC Report BNL-719, pp. 977-980, Vol. III.
5. K. S. Rockey and W. Skolnik, Measurements on the Diffusion Length of Thermal Neutrons in Water from 25 to 296°C, *Nucl. Sci. Eng.*, 8(1): 62 (July 1960).
6. W. M. Lopez and J. R. Beyster, Measurement of Neutron Diffusion Parameters in Water by the Pulsed Neutron Method, *Nucl. Sci. Eng.*, 12(2): 190 (February 1962).
7. Personal communication between K. H. Beckurts, Kernforschungszentrum Karlsruhe, Germany, and G. Rohr, Brookhaven National Laboratory, 1962 (referenced in BNL-719, Vol. III).
8. M. Küchle, *Nukleonik*, 2: 131 (1960) (as referenced in BNL-719, Vol. III, p. RE-60.
9. W. H. Dio, *Nukleonik*, 1: 13 (1958) (as referenced in BNL-719, Vol. III, p. RE-71).
10. M. Reier, WAPD-T-1140, 1960. [As referenced in USAEC Report BNL-719 (Vol. IV), p. 1202, Brookhaven National Laboratory.]
11. J. R. Beyster, J. R. Brown, H. C. Honeck, D. H. Houston, J. U. Koppel, W. M. Lopez, Y. D. Naliboff, D. E. Parks, G. D. Trimble, F. Wikner, and J. C. Young, Integral Neutron Thermalization, Annual Summary Report, October 1, 1961 – September 30, 1962, USAEC Report GA-3542, p. 187, General Dynamics Corp., General Atomic Division, Mar. 15, 1963.
12. H. C. Honeck, On the Calculation of Thermal Neutron Diffusion Parameters, in Proceedings of the Brookhaven Conference on Neutron Thermalization April 30 to May 2, 1962, Vol. IV, Theoretical Aspects of Transient and Asymptotic Phenomena, USAEC Report BNL-719, pp. 1186-1210, Brookhaven National Laboratory, December 1962.
13. K. H. Beckurts, Transient Effects in Space, Time, and Energy, in Proceedings of the Brookhaven Conference on Neutron Thermalization April 30 to May 2, 1962, Vol. III, Experimental Aspects of Transient and Asymptotic Phenomena, USAEC Report BNL-719, pp. RE1-62, Brookhaven National Laboratory, November 1962.
14. R. S. Hall, S. A. Scott, and J. Walker, *Proc. Phys. Soc. (London)*, 79: 257 (1962) (as referenced in BNL-719, Vol. III, p. RE-60).
15. H. D. Brown and E. J. Hennelly, Neutron Thermalization Studies at Savannah River, in Proceedings of the Brookhaven Conference on Neutron Thermalization April 30 to May 2, 1962, Vol. III, Experimental Aspects of Transient and Asymptotic Phenomena, USAEC Report BNL-719, pp, 879-894, Brookhaven National Laboratory, November 1962.
16. N. K. Ganguly and A. W. Waltner, Measurement of Neutron Diffusion Parameters of Heavy Water at Different Temperatures by Pulsed Source Method, *Trans. Am. Nucl. Soc.*, 4(2): 282 (November 1961).
17. N. G. Sjöstrand, *Arkiv Fysik*, 15: 145 (1958) (as referenced in BNL-719, Vol. III, p. RE-61).
18. M. Nelkin, The Diffusion Cooling of Neutrons in a Finite Moderator, *J. Nucl. Energy: Pt. A&B*, 8 (1-3): 48 (November 1958).
19. H. Klose, M. Küchle, and W. Reichardt, Pulsed Neutron Measurements on Graphite, in Proceedings of the Brookhaven Conference on Neutron Thermalization, April 30 to May 2, 1962, Vol. III, Experimental Aspects of Transient and Asymptotic Phenomena, USAEC Report BNL-719, pp. 935-945, Brookhaven National Laboratory, November 1962.
20. E. Starr and J. W. L. de Villiers, Determination of Diffusion Cooling in Graphite by Measurement of the Average Neutron Velocity, in Proceedings of the Brookhaven Conference on Neutron Thermalization April 30 to May 2, 1962, Vol. III, Experimental Aspects of Transient and Asymptotic Phenomena, USAEC Report BNL-719, pp. 997-1011, Brookhaven National Laboratory, November 1962.
21. E. Starr and G. A. Price, Measurement of the Diffusion Parameters of Graphite and Graphite-Bismuth by Pulsed Neutron Methods, in Proceedings of the Brookhaven Conference on Neutron Thermalization April 30 to May 2, 1962, Vol. III, Experimental Aspects of Transient and Asymptotic Phenomena, USAEC Report BNL-719, pp. 1034-1073, Brookhaven National Laboratory, November 1962.

Section

III

Power Reactor Technology

Fluid and Thermal Technology

Burnout in Multirod Geometry

By John S. Wiley

Introduction

An article in the last issue of *Power Reactor Technology* compared two burnout heat-flux correlations[1,2] with data taken using channels of relatively simple cross section. The purpose of this article is to extend consideration to more complex geometries, namely, those involving a bundle of heated rods. Instead of considering the correlations themselves, this article compares the multirod data, where possible, with data taken in the simpler test sections. The annular test-section data are from Refs. 3 and 10, and the rectangular-channel data and circular test-section data are from Ref. 4.

A basic difficulty in understanding flow phenomena in multirod bundles is illustrated by looking at a cross section of a typical bundle, Fig. III-1. The various flow subchannels, which are numbered in Fig. III-1, offer ample opportunity for mixing of their contents. One of the points made in Fig. III-14 of the last issue was that the test section's equivalent diameter was an important variable.* Consideration of Fig. III-1 reveals that there are a number of equivalent diameters, and some of the flow channels are bounded by unheated surfaces. The varying equivalent diameters give rise to mixing, of course, and thus any diameter effect is inseparably tied to the amount of mixing between subchannels.

Presentation of Data

The first multirod data to be considered are found in Ref. 5. A total of five test sections

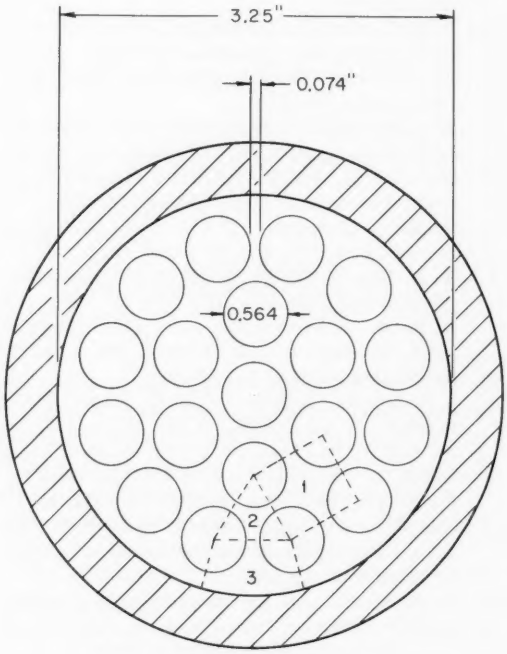

$$\bar{D}_e = \frac{4(\text{Total Flow Area})}{(\text{Total Wetted Perimeter})} = 0.32"$$

$D_{e_1} = 0.36"$

$D_{e_2} = 0.23"$

$D_{e_3} = 0.35"$

Fig. III-1 Cross section of one of the multirod test sections used for burnout studies at Hanford Atomic Products Operation (HAPO).

*The diameter effect shown on that figure can be approximated by $(0.18/D)^{0.4}$. This approximation will be used to extrapolate data to different equivalent diameters.

Table III-1 DESCRIPTION OF EXPERIMENTAL TEST SECTIONS[5]

Test-section designation	Spacing between rods within bundle, in.	Spacing between outer rod and pressure tube, in.		Heater rod outside diameter, in.	Heater length, in.	Radial heat-flux variation, outer/inner/center rod	Wire wraps					Type of thermocouple
		Nominal	Minimum				Test-section orientation	Diameter, in.	Pitch, in.	Material	Heat generated in wire wrap	
I	0.074	0.112	0.074	0.564 ±0.001	18.5	1/0.83/0.83	Vertical	0.074	10	Ceramic beads on 0.028 wire	No	Single-point contact, no water thermocouples
II	0.015	0.060	0.050	0.629 ±0.001	19.5	1/1/1	Horizontal	0.015	10	Inconel wire	Yes, ~1/3 of rod flux or ~2% of total power	Single-point contact, no water thermocouples
III	0.050	0.101	0.074	0.587 ±0.001	19.5	1/1/1	Horizontal	0.050	9	Ceramic beads on 0.024 wire	No	Copper plug, no water thermocouples
IV	0.050	0.101	0.074	0.587 ±0.001	19.5	1/1/1	Horizontal	0.050	9	MgO-filled tubing	Yes, ~1/3 rod flux or ~2% of total power	Copper plug, 5 water thermocouples
V	0.050	0.101	0.085	0.587 ±0.001	76.0	1/1/1	Horizontal	0.050	9	MgO-filled tubing	Yes, ~1/10 rod flux or ~0.5% of total power	Copper plug, 10 water thermocouples

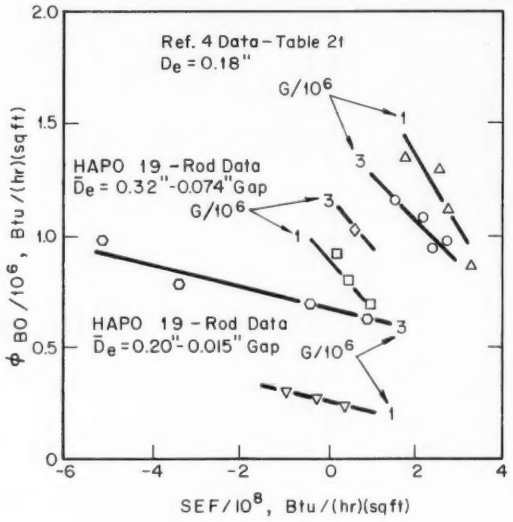

Fig. III-2 Comparison of Hanford multirod test-section data[5] with rectangular-channel data given in Ref. 4. Pressure = 1200 psi.

were utilized in the study, and the description of each is given in Table III-1. The cross section of test section I is shown in Fig. III-1, and the various equivalent diameters are given on the figure. Burnout data taken with test sections I* and II are shown in Fig. III-2, and burnout data taken with test sections III and V are shown in Fig. III-3. Also plotted on Fig. III-3 are burnout data taken with test sections of annular and rectangular cross section. The annular-channel data were interpolated from the data given in Fig. III-4. The rectangular-channel data at an equivalent diameter of 0.28 in. were extrapolated from the data taken with a channel having an equivalent diameter of 0.19 in., using the following relation:

$$\phi_{BO_{D=D_0}} = \phi_{BO_{D=0.18}} (0.18/D_0)^{0.4} \quad (1)$$

where $\phi_{BO_{D=D_0}}$ is the burnout heat flux at diameter D_0, Btu/(hr)(sq ft); $\phi_{BO_{D=0.18}}$ is the burnout heat flux at a diameter of 0.18 in., Btu/(hr)(sq ft); and D_0 is the equivalent diameter, in.

Consideration of Fig. III-2 reveals that increasing the average equivalent diameter, $\overline{D_e}$, increases the burnout heat flux, which is opposite to the trend observed for the simpler channels, and is expressed in Eq. 1. This probably is caused by improved mixing as the rod-to-rod spacing is increased, although it is not possible to establish this quantitatively. Some mixing data for test section V have been reported.[6] These data were obtained[7] by measuring local water temperatures just downstream of the heated section, and the data were taken employing single-phase flow. A total of 10 thermocouples were utilized. The data were treated as though the rod bundle consisted of two regions, one being within the bundle and the other being a region between the bundle and the pressure tube. This is shown schematically in Fig. III-5. The results of the mixing study are quoted as follows:[6]

> ... The data show that, over the 6.3-foot length, the average increase in the enthalpy of the coolant in sub-channels within the bundle is about 1.4 times the enthalpy increase of the coolant in the sub-channels between the bundle and the pressure tube wall. If no interchannel mixing had occurred, the enthalpy increase ratio should be about 3.0 ...

If mass and energy balances are written for the bundle and wall regions, it is possible to solve for m_1, m_2, H_1, and H_2 if the relation between m_1 and m_2 or H_1 and H_2 are known. The equations are as follows:

$$m_t = \phi\left(\frac{A_1}{H_1 - H_{in}} + \frac{A_2}{H_2 - H_{in}}\right) \quad (2)$$

$$H_1 = H_{in} + \frac{\phi A_1}{m_1} \quad (3)$$

$$H_2 = H_{in} + \frac{\phi A_2}{m_2} \quad (4)$$

$$(H_1 - H_{in}) = k(H_2 - H_{in}) \quad (5)$$

where $m_{1,2}$ = steam-water flow rate in bundle and wall regions, lb/hr
m_t = total steam-water flow rate, lb/hr
ϕ = heat flux, Btu/(hr)(sq ft)
$A_{1,2}$ = heat-transfer areas in bundle and wall regions, sq ft
$H_{1,2}$ = outlet enthalpy of steam-water mixture from bundle and wall regions, Btu/lb
H_{in} = inlet enthalpy, Btu/lb
k = constant expressing relation between H_1 and H_2

*The heat fluxes plotted in Fig. III-2 correspond to the average burnout heat fluxes for test section I.

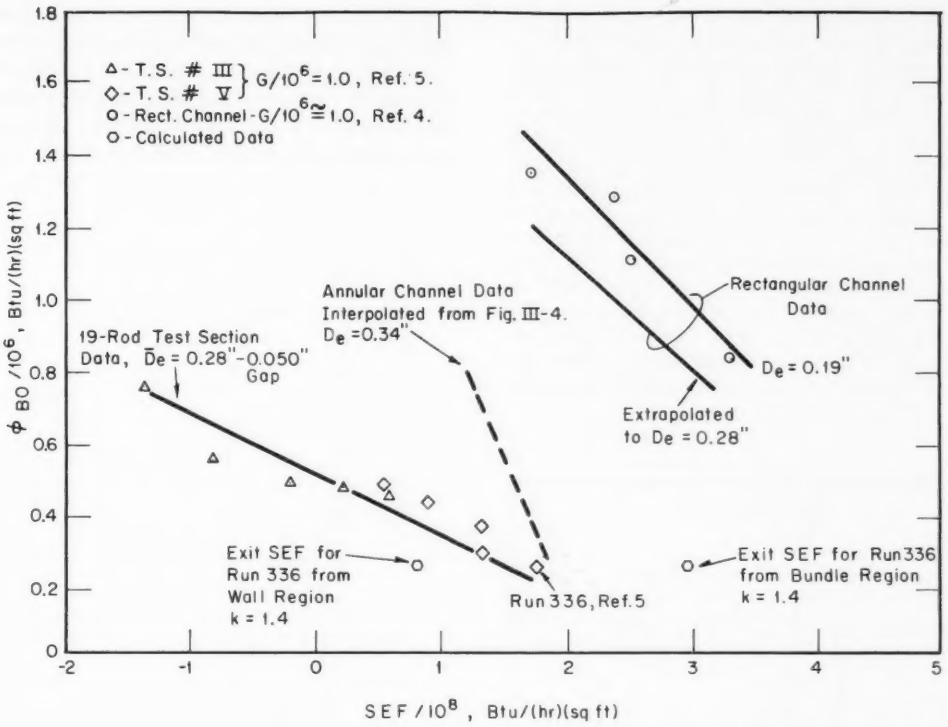

Fig. III-3 Comparison of Hanford multirod test-section (T.S.) data[5] with data given in Refs. 3 and 4. Pressure = 1200 psi.

With $k = 1.4$, solving Eqs. 2 to 4 for run 336 (Ref. 5) results in the data shown in Table III-2. The calculations shown in Table III-2 are approximate, since the division of flow area and heat-transfer area between the bundle region and the wall region was arbitrarily set and the area of the wire wraps was neglected. It was also assumed that mixing as measured with single-phase flow is representative of the behavior of two-phase flow. The outlet steam energy flows for the bundle, and wall regions are plotted on Fig. III-3; however, the agreement with rectangular-channel data is still lacking. Although agreement with the annular-channel data is not good either, the figure illustrates that local conditions may be quite different from average conditions in a bundle with interconnected flow passages.

The Westinghouse multirod burnout data are contained in Ref. 8. The cross section of the bundle is shown in Fig. III-6, and the test pressure was 2000 psia. The Westinghouse multirod data correlate well with the rectangular-channel data given in Tables 21 and 15 of Ref. 4, and this is shown in Fig. III-7. The figure illustrates one burnout point and several scanning points. The Westinghouse nine-rod test section was instrumented to measure wall-temperature increases at the exit of the center tube. These thermocouples did not function satisfactorily; hence the protection afforded by these thermocouples was lacking. The burnout run resulted in physical destruction of the test section, whereas the scanning runs were designed to approach the rectangular-channel correlation but with a heat flux about 15 to 20% lower. That this procedure was satisfactory is illustrated by Fig. III-7. The circular-channel data, illustrated in Fig. III-8, appear to be conservative compared with the multirod burnout points. The test section was equipped with pressure taps located within the rod bundle as well as within the shroud (the area between the rod bundle and the walls defining the flow channel). An approximate analysis of the data resulted in the following conclusion:[8]

... (a) At the entrance, the velocity in the rod area is lower because the entrance pressure-loss coefficient is larger; (b) in the center region, where boiling has not yet started, the velocity in the rod area is greater because the equivalent diameter in this area is larger; (c) near the end of the rod bundle, the velocity in the rod area decreases because of the increased flow resistance caused by boiling and because the exit-loss coefficient is higher in the rod area. Since these flow patterns are only qualitative, their effect on DNB is not known, and depends upon many factors such as radial flux gradient, rod length and pitch, flow rates, entrance and exit losses and two-phase densities. In the present tests, axial-flow redistribution apparently had little effect upon axial pressure drop and burnout.

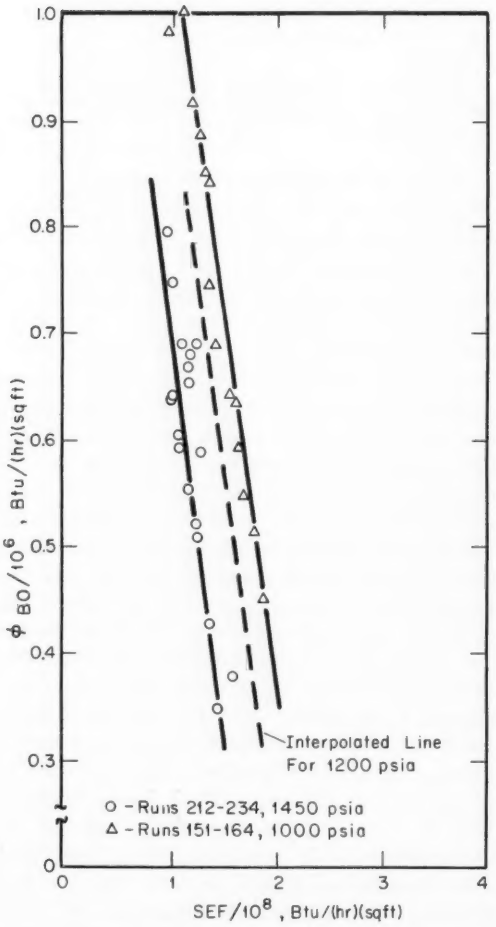

Fig. III-4 Burnout heat-flux data from Ref. 3. Annular-channel geometry: equivalent diameter = 0.34 in.; mass flow = 1.1×10^6 lb/(hr)(sq ft).

Additional data that will be discussed can be found in Ref. 9. The test section used employed nine heated rods and is shown in Fig. III-9. It is quite similar to the Westinghouse nine-rod test section except that the rod-to-rod spacing was quite a bit larger, about 0.19 in., as was

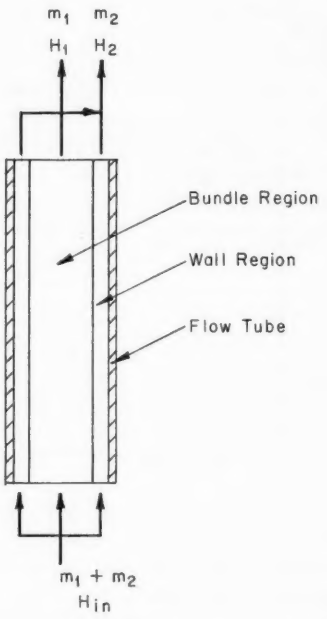

Fig. III-5 Schematic of pressure tube and rod bundle. Here m = flow rate in pounds per hour; H = enthalpy in Btu's per pound.

the rod-to-shroud spacing, 0.17 in. The actual values for these spacings are given in the reference. The above quoted numbers, as well as the equivalent diameters shown on Fig. III-9, are only approximate. Four test sections were constructed with a cross section as given in Fig. III-9 and a heated length of 18 in. The relative heater-rod powers were as follows:

Test-section No.	Relative heater-rod power			
	Rod A	Rod B	Rod C	All others
1, 3, 4	1.00	1.00	1.00	0.80
2	1.22	1.00	1.00	0.80

Assemblies 3 and 4 were destroyed because rod A bowed at midspan and caused an electrical short to the shroud. The spacers for electrical insulation shown on Fig. III-9 were made

of Rulon. One set of spacers was positioned about 10 in. upstream of the heated end of the test section, and a second set was positioned about 1 in. downstream of the end of the test section.

Data were taken at nominal pressures of 1000 and 1400 psia, and the 1000-psia data are illustrated in Fig. III-10. Also plotted in Fig. III-10 are rectangular-channel data from Ref. 10. It is evident that the kind of agreement between rectangular-channel data and nine-rod test-section data shown in Fig. III-7 is not present. The combination of an unknown amount of bowing of rod A and the presence of the spacers as shown in Fig. III-9, however, make detailed analyses difficult. Although the upstream spacer was about 20 hydraulic diameters upstream of the burnout point, the downstream spacer was only about two hydraulic diameters downstream of the burnout point, and it seems likely that any flow redistribution caused by the downstream spacer would be evident only several equivalent diameters upstream.

The steam-energy flows plotted on Fig. III-10 were computed using the bulk exit qualities given in Table 4 of Ref. 9. Of particular interest are the five points taken with test section No. 2, where the relative power of rod A was 22% higher than in the data taken with test section No. 1. In all but three of the points plotted on Fig. III-10 for the nine-rod section, burnout was detected as occurring on rod A, and the authors of the reference conclude that "... turbulent cross flow is sufficient to maintain a distributed quality pattern regardless of the distribution of quality generation for the clear-

Table III-2 RESULTS OF MIXING CALCULATIONS WITH $k = 1.4$, RUN 336 OF REF. 5

[H_{in} = 503 Btu/lb, m_t = 22,120 lb/hr, ϕ = 284,000 Btu/(hr)(sq ft)]

Outlet enthalpies, Btu/lb	
Bundle	769 (32.2)*
Wall region	693 (19.8)*
Average	746 (28.3)*
Outlet mass flow, lb/(hr)(sq ft)	
Bundle region	1.49×10^6 (13,430)†
Wall region	0.67×10^6 (8,690)†
Average	1.01×10^6
Outlet steam energy flow, Btu/(hr)(sq ft)	
Bundle region	2.94×10^8
Wall region	0.81×10^8
Average	1.74×10^8

*Number in parentheses is outlet quality in percent.

†Number in parentheses is outlet mass flow in pounds per hour.

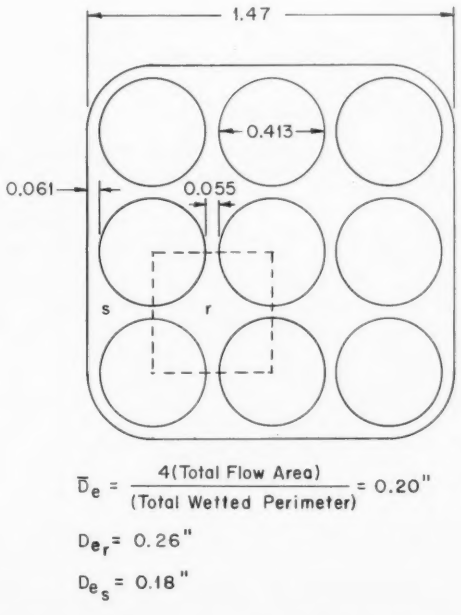

Fig. III-6 Cross section of multirod test section used for burnout studies at Bettis Atomic Power Laboratory.

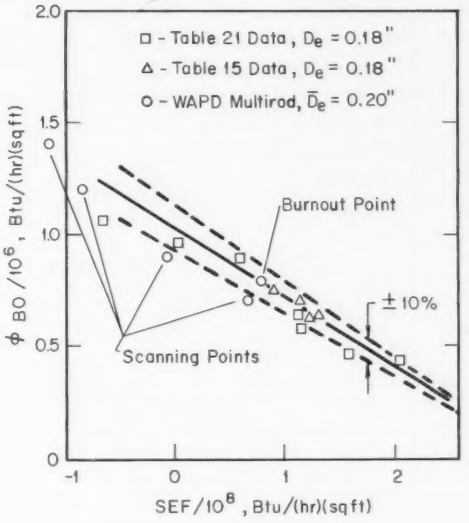

Fig. III-7 Comparison of nine-rod test-section data[8] with rectangular-channel data appearing in Tables 15 and 21 of Ref. 4. Pressure = 2000 psia; mass flow = 1.0×10^6 lb/(hr)(sq ft).

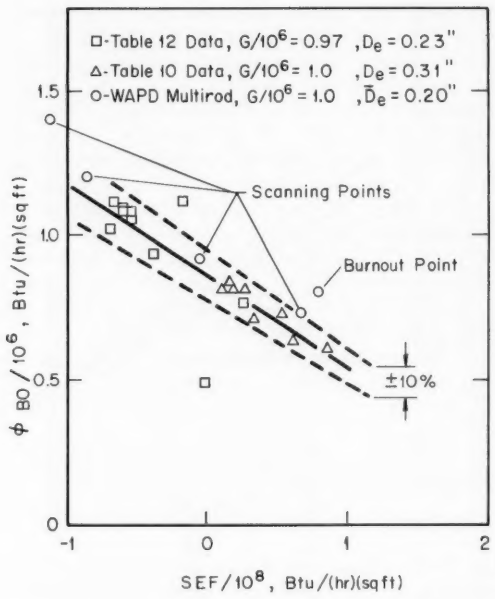

Fig. III-8 Comparison of nine-rod test-section data[8] with circular-channel data appearing in Tables 10 and 12 of Ref. 4. Pressure = 2000 psia.

ances of this test section." Although this may be true, there is almost a 22% spread in the data about the appropriate line drawn on Fig. III-10.

Figure III-11 compares the multirod data appearing in Fig. III-10 with annular-channel data taken from Ref. 3. Although the comparison is not exact, it appears that the annular-channel data are a better representation of the burnout behavior of the multirod geometry than are the data taken in the rectangular test section. The two curves at a G of 1.1×10^6 lb/(hr)(sq ft) show good agreement. Unfortunately it is difficult to tell whether this is accidental or not since, as shown in Fig. III-9, the multirod test section had a variety of equivalent diameters.

The test section used to obtain the data given in Ref. 11* was similar in cross section to Fig. III-1 and was called the "high-heat-flux" test section. The shroud inside diameter was 3.195 in., and the rods had an outside diameter of 0.550 in. Twelve of the rods were wrapped with stainless-steel spirals, and the test section was equipped with a burnout detector. The rod-to-rod spacing was 0.083 in. (the diameter of the spacer wires), whereas the rod-to-shroud spacing was about 0.1 in. minimum. The system pressure was a nominal 1000 psia; the data are shown in Fig. III-12. The particular values plotted are those termed "good validity of the burnout point" in the reference. Other data having low or questionable validity are not shown. The heater tube material was Inconel X, having a heated length of 36 in. The relative heat fluxes were:

Outer rod	1.0
Inner rod	0.854
Center rod	0.807

The burnout heat fluxes plotted on Fig. III-12 are those corresponding to the power dissipated via the outer ring of rods.

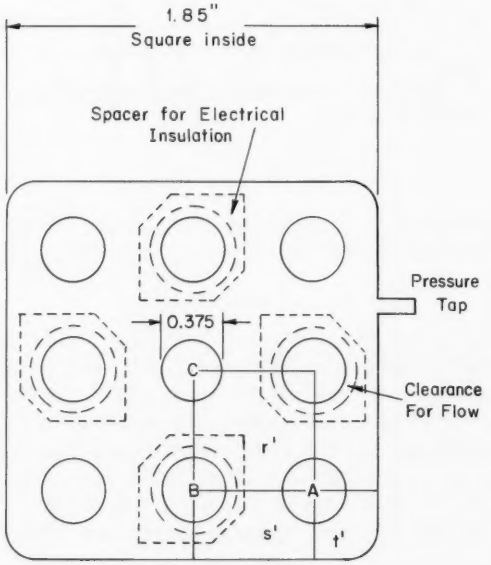

$$\bar{D}_e = \frac{4(\text{Total Flow Area})}{(\text{Total Wetted Perimeter})} = 0.52"$$

$$D_{e_{r'}} = 0.67"$$

$$D_{e_{s'}} = 0.48"$$

$$D_{e_{t'}} = 0.33"$$

Fig. III-9 Cross section of multirod test section used for burnout studies at General Electric's Atomic Power Equipment Department (GE-APED).

*The results of the Columbia program have been summarized and published as Ref. 14, which will be discussed shortly.

If Fig. III-12 were superimposed on Fig. III-11, it would be found that the data for the multirod test sections were very close together for a mass flow of 0.5 and 1.0×10^6 Btu/(hr)(sq ft). Thus the burnout behavior of the two-rod bundles appears to be reasonably well approximated by the annular test-section data.

Other multirod burnout data to be discussed will be found in Ref. 12. A cross section of the four-rod test section is shown in Fig. III-13, and a summary of the parameters of importance is shown in Table III-3. The spacers were designed to present as little restriction to flow as possible. They consisted of small cylindrical pins, oriented as shown in Fig. III-13. The spacers were located in planes 2 in. above the upper end and 9 in. below the upper end of the heated section. The spacers are quite different than the ones shown in Fig. III-9 and do appear to present little flow restriction. As shown in Table III-3, one rod had a slightly thicker wall to increase the heat flux, and the critical heat-flux detection thermocouples were welded to the hot rod. Some data were taken with all rods having an identical wall thickness; "... the data obtained with one rod hotter were compared with the data with all rods the same, and there was no difference in critical heat flux values, when the hot rod heat flux and average bulk steam qualities were used ..."[12]

Results obtained with the four-rod test section are shown in Fig. III-14. Presumably these data were taken with one rod slightly hotter, although no distinction was given in Ref. 12 as to which data were which. In Fig. III-14 a hysteresis effect was noted in plotting the $G = 0.2 \times 10^6$ lb/(hr)(sq ft) data. This is noted in Fig. III-14 by two straight, dotted lines running through the appropriate points. Although the differences in the locations of the two dotted lines are of minor importance, it would be of interest to know why there is a difference. Comparative annular-channel data are shown in Fig. III-15. Although the annular-channel data do not exactly reproduce the four-rod data, there is a good correspondence at mass velocities in excess of 0.5×10^6 lb/(hr)(sq ft).

Table III-3 TEST-SECTION PARAMETERS: FOUR-ROD GEOMETRY[12]

Heated length	3 and 4 ft
Hydraulic diameter	0.419 in.
Heater tube wall thickness	0.020 and 0.022 in.
Heater tube material	Inconel X, heat-treated to 1300°F for 20 hr, air cooled
Rod-to-rod spacing	0.187 in.
Rod-to-wall spacing	0.135 in.
L/D ratio	86 for 3-ft heated length; 104 for 4-ft heated length
Flow direction	Vertical, upward
Electric power	Single-phase, alternating current
Distance between spacers	11 in.

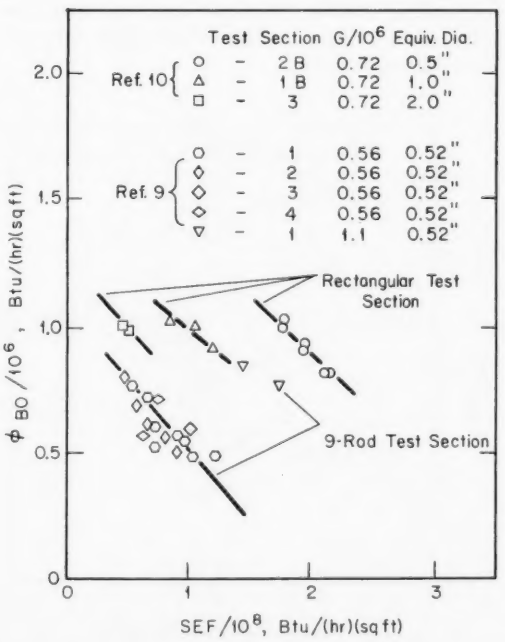

Fig. III-10 Comparison of nine-rod test-section data[9] with rectangular-channel data appearing in Ref. 10. Pressure = 1000 psia.

Discussion

The use of rectangular cross-section test-section burnout data may not be conservative in the thermal design of power reactors employing bundles of fuel rods. The Westinghouse data suggest that it is possible to design a multirod test section to yield good agreement between rectangular-channel and multirod burnout data, although not many experimental points are reported in Ref. 8. Lack of mixing might be blamed for the relatively poor multirod burnout performance shown in Figs. III-2, III-10, and III-12 (compared to rectangular test-section data), but it is difficult to make quantitative

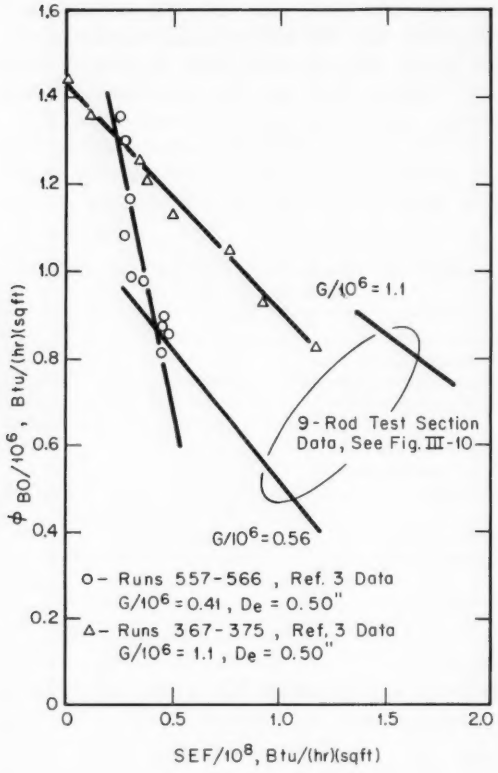

Fig. III-11 Comparison of nine-rod test-section data[9] with annular-channel data appearing in Ref. 3. Pressure = 1000 psia.

statements since few analytical or experimental mixing data are available for comparison. Reference 13 contains results of mixing experiments done with the fuel element for the Carolinas-Virginia Tube Reactor (CVTR). The CVTR bundle is similar to the bundle shown in Fig. III-1 except that the outer ring of rods is on a hexagonal geometry instead of a circle, and a hexagonal flow liner surrounds the bundle. Boiling did not take place. Mixing was evaluated by injecting lithium nitrate into various subchannels at the test-section inlet and measuring its concentration in various subchannels at positions along the length of the test section. The results will not be discussed herein; however, this type of experiment may represent a method of obtaining two-phase mixing and burnout data in a single test setup.

The applicability of the annular-channel data to the prediction of rod-bundle burnout can best be considered by looking at the individual plots and comparing the two. Figure III-11 shows good agreement at a $G/10^6$ of 1.1 between GE-APED nine-rod-bundle data and annular test-section data, although only two runs were reported for the nine-rod bundle at this value of mass flow. At a mass flow of about 0.5×10^6, the DNB-1 lines for annular and rod-bundle geometries have different slopes. Figure III-15 illustrates good correlation between GE-APED four-rod and annular-geometry data at mass flows from 1.0 to 1.5×10^6 and fair agreement at a mass flow of 0.5×10^6.

The Hanford and Columbia University experiments with 19-rod test sections are compared in Fig. III-16. The data originating at Columbia plotted therein were taken with the "six-foot-long" test section; this was similar to the "high-heat-flux" test section discussed earlier but had a heated length of 6.0 ft and the relative heat fluxes were as follows:

Outer rod	1.0
Inner rod	0.806
Center rod	0.766

The values of ϕ_{BO} plotted on Fig. III-16 for the "six-foot-long" test section are those corresponding to the heat flux impressed on the outer rods. The Columbia University data are available in Ref. 14.

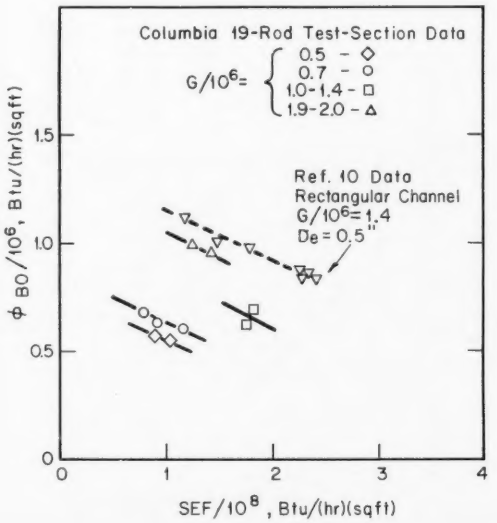

Fig. III-12 Comparison of Columbia 19-rod test-section data[11] with rectangular-channel data appearing in Ref. 10. Pressure = 1000 psia.

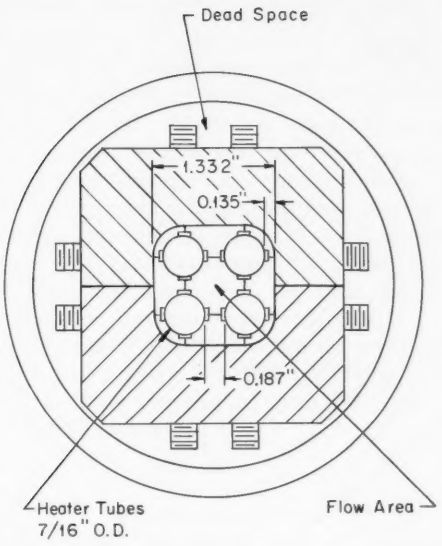

Fig. III-13 Cross section of four-rod test section used for burnout studies at GE-APED.

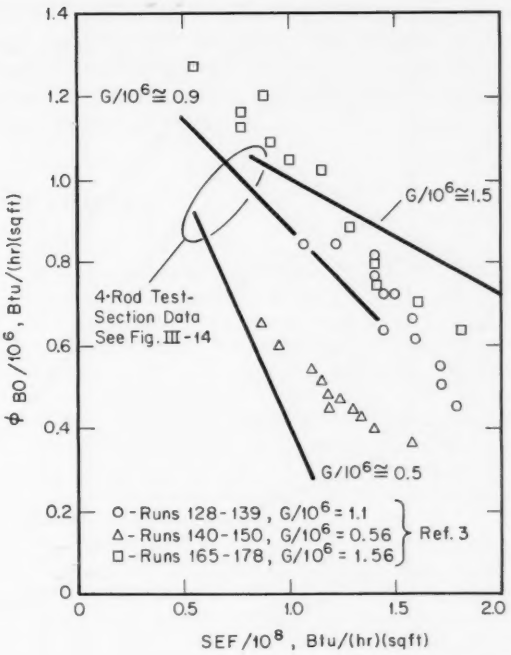

Fig. III-15 Comparison of four-rod test-section data[12] with annular-channel data appearing in Ref. 3. Pressure = 1000 psia.

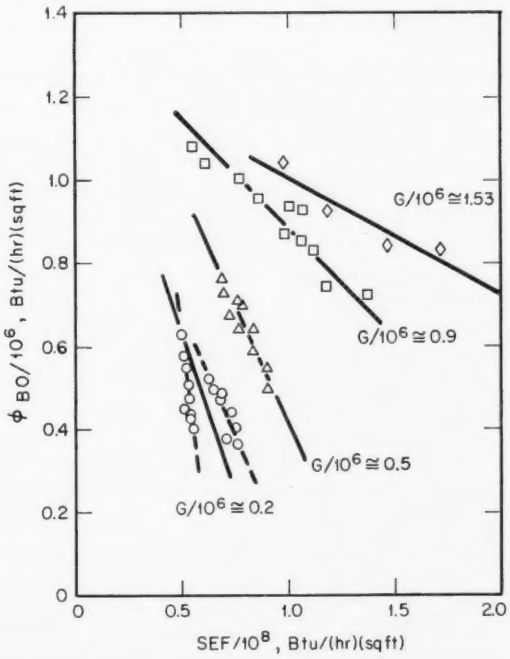

Fig. III-14 Steam-energy flow plot of burnout data taken with 4-rod test section and reported in Ref. 12. Pressure = 1000 psia.

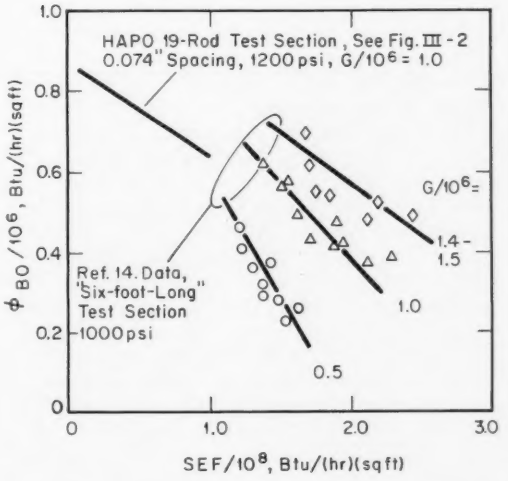

Fig. III-16 Comparison of Hanford[5] and Columbia[14] University 19-rod test-section burnout data.

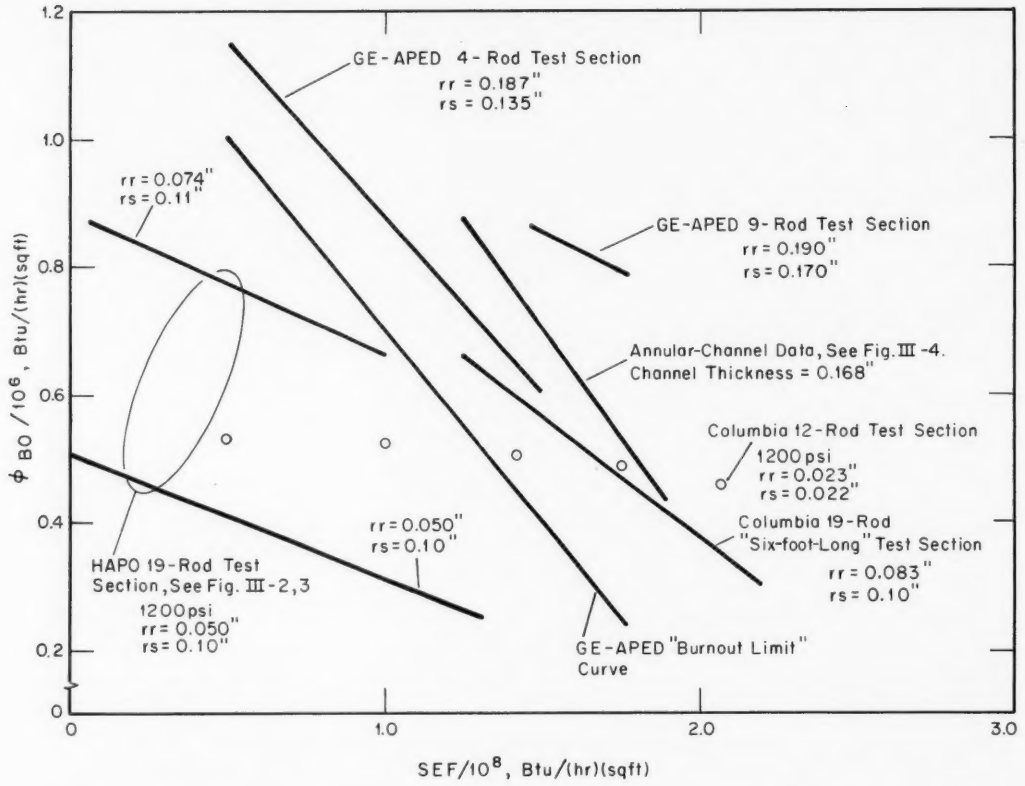

Fig. III-17 Summary of burnout data. Pressure = 1000 psia except where noted. Here rr = rod-to-rod spacing in inches; rs = rod-to-shroud spacing in inches; $G/10^6 \cong 1.0$ lb/(hr)(sq ft).

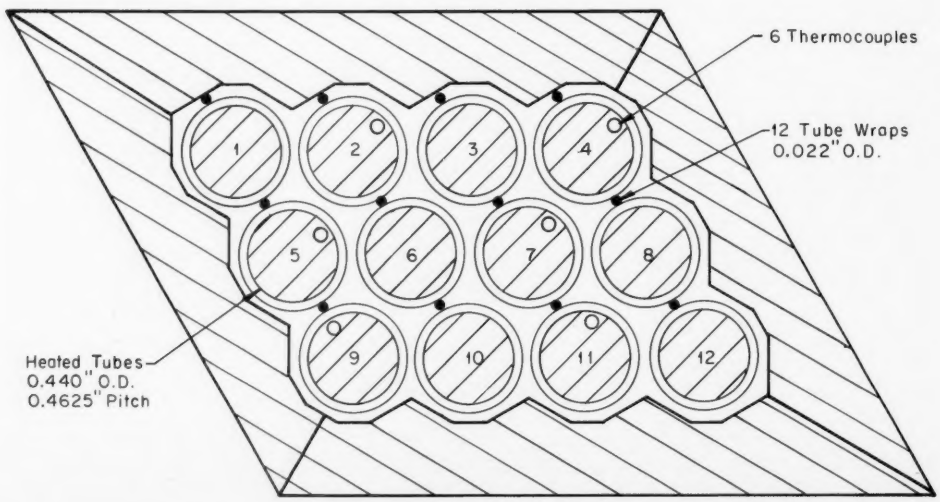

Fig. III-18 Cross section of Columbia 12-rod test section at ½ in. from exit end of heated length.

The Hanford and Columbia data show fairly good agreement provided the rod-to-rod spacing of the Hanford 19-rod test section is at least 0.074 in. Consideration of Figs. III-2 and III-16 suggests that the rod-to-rod spacing is an important parameter and that ϕ_{BO} increases with an increase in this spacing, other variables remaining constant. The Hanford data fall under the (extrapolated) Columbia data at a mass flow of 1.0×10^6. This is reasonable, however, since the average heat flux across the Hanford bundle is plotted as a comparison to the heat flux for the outer ring of rods of the Columbia University test section, and the Hanford test section operated at 1200 psi compared to 1000 psi for the Columbia test section.

Conclusions

Figure III-17 is offered as a conclusion to this article. In this figure are plotted rod-bundle data, annular test-section data, and the GE-APED burnout limit curve of Ref. 2. The only previously unpresented data appearing in Fig. III-17 are those taken with the Columbia 12-rod test section, shown in Fig. III-18. The test pressure was 1200 psia, and the heated length was 12 in. The burnout limit curve appears to adequately represent the rod-bundle data from the standpoint of safety except for the Hanford and the Columbia 12-rod test-section data. Although the Hanford runs were at a different pressure, there is no other evidence for such a large effect of pressure, and therefore the reason for the low burnout behavior of the Hanford 19-rod test section must be due to another variable. This could possibly be the relatively close rod-to-rod spacing, but the Hanford experiments on test sections II to V were done with the section horizontal, and this also might have had an effect on the results. The rod-to-rod spacing is noted on Fig. III-17, and it can be noted that ϕ_{BO} does improve, in general, as the spacing is increased. The Columbia 12-rod test section is, of course, the exception. It is possible that ϕ_{BO} is not a simple function of rod-to-rod and rod-to-shroud spacing, and ϕ_{BO} goes through a minimum corresponding to the values of rr and rs of the Hanford test section with the 50-mil rod-to-rod spacing. On the other hand, the data from the Columbia 12-rod section are the first report for an entirely triangular pitch; the GE-APED test sections had square pitch, and the 19-rod test sections had a mixture of triangular and square flow channels. The relative confusion present in Fig. III-17 will probably continue until mixing data are available on these several test sections.

References

1. L. S. Tong, H. B. Currin, and A. G. Thorp II, New Correlations Predict DNB Conditions, *Nucleonics*, 21(5): 43 (May 1963).
2. E. Janssen and S. Levy, Burnout Limit Curves for Boiling Water Reactors, Report APED-3892, General Electric Company, Atomic Power Equipment Department, Apr. 1, 1962.
3. E. Janssen and J. A. Kervinen, Burnout Conditions for Single Rod in Annular Geometry, Water at 600 to 1400 psia, USAEC Report GEAP-3899, General Electric Company, Atomic Power Equipment Department, February 1963.
4. R. A. DeBortoli, S. J. Green, B. W. LeTourneau, M. Troy, and A. Weiss, Forced-Convection Heat Transfer Burnout Studies for Water in Rectangular Channels and Round Tubes at Pressures Above 500 psia, USAEC Report WAPD-188, Westinghouse Electric Corp., Bettis Plant, October 1958.
5. E. D. Waters, G. M. Hesson, D. E. Fitzsimmons, and J. M. Batch, Boiling Burnout Experiments with 19-Rod Bundles in Axial Flow, USAEC Report HW-77303, Hanford Atomic Products Operation, August 1963.
6. J. K. Green and J. E. Brown, Hanford Atomic Products Operation, Mar. 26, 1963. (Unpublished)
7. Hanford Atomic Products Operation, Jan. 17, 1963. (Unpublished)
8. S. J. Green, G. W. Mauer, and A. Weiss, Burnout and Pressure-Drop Studies for Forced-Convection Flow of Water Parallel to Rod Bundles, ASME Paper No. 62-HT-43, presented at the ASME-AIChE Heat Transfer Conference and Exhibit, Houston, Texas, August 5–8, 1962.
9. E. E. Polomik and E. P. Quinn, Multi-Rod Burnout at High Pressure, USAEC Report GEAP-3940, General Electric Company, Atomic Power Equipment Department, September 1962.
10. F. E. Tippets, Critical Heat Flux and Flow Pattern Characteristics of High Pressure Boiling Water in Forced Convection, USAEC Report GEAP-3766, General Electric Company, Atomic Power Equipment Department, April 1962.
11. B. Matzner, Basic Experimental Studies on Boiling Fluid Flow and Heat Transfer at Elevated Pressures. Monthly Progress Report, April 1962, USAEC Report TID-15637, Columbia University, Engineering Research Laboratories, April 1962.
12. J. E. Hench, Multirod (Four-Rod) Critical Heat Flux at 1000 psia, USAEC Report GEAP-4358, General Electric Company, Atomic Power Equipment Department, September 1963.

13. A. A. Bishop, P. A. Nelson, and E. A. McCabe, Jr., Thermal and Hydraulic Design of the CVTR Fuel Assemblies, USAEC Report CVNA-115, Westinghouse Electric Corp., Atomic Power Division, June 1962.
14. B. Matzner and J. S. Neill, Forced-Flow Boiling in Rod Bundles at High Pressure, USAEC Report DP-857, Savannah River Laboratory, September 1963.
15. B. Matzner, Heat Transfer and Hydraulic Studies for SNAP-4 Fuel Element Geometries, Topical Report No. 2, USAEC Report TID-19563, Columbia University, Engineering Research Laboratories, September 1963.

Section

IV

Power Reactor Technology

Fuel Elements

Plutonium-Bearing Fuels

The potential use of plutonium for recycle in power reactors has been discussed in several previous issues of *Power Reactor Technology*. The development of satisfactory plutonium-bearing elements is of vital significance to the fast-breeder reactor, but development is under way for both fast and thermal reactor applications. The purpose of this review is to give a reasonably comprehensive picture of the present status of plutonium-bearing fuel-element development. The importance accorded plutonium as a fuel can be judged from the number of laboratories in the United States that are working on plutonium-bearing fuel development; these include Argonne National Laboratory, Hanford Atomic Products Operation, Los Alamos Scientific Laboratory, Mound Laboratory, General Electric's Atomic Power Equipment Department (GE-APED), Battelle Memorial Institute, Nuclear Materials & Equipment Corporation, and United Nuclear Corporation. In addition, most other countries supporting power-reactor programs are conducting developmental work on plutonium fuels.

This review includes discussions of the fabrication, properties, and irradiation behavior of plutonium compounds and their use in plutonium-bearing fuel elements. Basic metallurgical and physical property information is not included, in general, since another Technical Progress Review, *Reactor Materials*, has a section devoted to this type of information. Reference 47 contains a quite detailed account of the history of the discovery of the element plutonium and some recent developments.

Oxides: PuO_2 and PuO_2-UO_2

The applicability of PuO_2 is suggested by the widespread success that UO_2 has achieved as a fuel for power reactors. The French fast reactor Rapsodie may employ UO_2-PuO_2 as a fuel,[1] and the Plutonium Recycle Test Reactor (PRTR) has operated principally with fuel rods[2] containing UO_2 and PuO_2. The latter reactor is of the pressure-tube heavy-water-moderated type. These two programs are of particular interest since the fabrication processes for producing the elements are quite different. The French technique produces the basic fuel rod shown in Fig. IV-1 via a pelletizing process. The fuel-pin dimensions are shown in Table IV-1, which also includes the dimensions of a pin fabricated of an alternate fuel material, U-Pu-Mo alloy. The oxide process is based on the fabrication of pellets of the mixed oxides entirely in a glove-box line. The raw materials are ammonium diuranate precipitated UO_2 (ADU) and calcined plutonium oxalate for the PuO_2. The materials are ball-milled and mixed to a paste after the addition of alcohol, camphor, and stearine. The paste is granulated and fed to a pellet-forming machine. The pellets are baked under vacuum and sintered at 1700°C under hydrogen. The final pellets contain 25 wt.% UO_2 and are loaded into the stainless-steel jacket tubes that are closed by electron welded end plugs. As of the writing of Ref. 1, the production line had been tested with UO_2.

The production of fuel elements containing PuO_2 at Hanford Atomic Products Operation (HAPO) has been the subject of a considerable amount of research.[4] The various methods considered are summarized in Fig. IV-2, and a number of different shapes have been produced. This discussion will concentrate on the fabrication methods used for those elements irradiated in the PRTR. The first core of the PRTR consisted of 52 natural UO_2 assemblies and 33 enriched spike assemblies of 1.8 wt.% plutonium (low exposure) alloyed with aluminum.[2,5] Both types of elements employed 19-rod clusters of

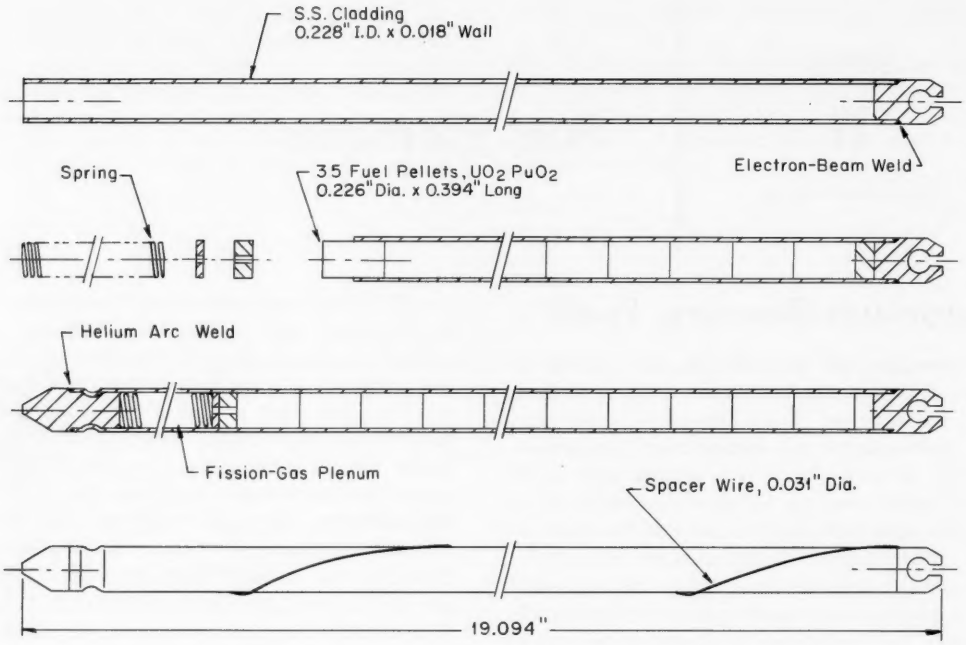

Fig. IV-1 Ceramic fuel rod for the French fast reactor Rapsodie.[1]

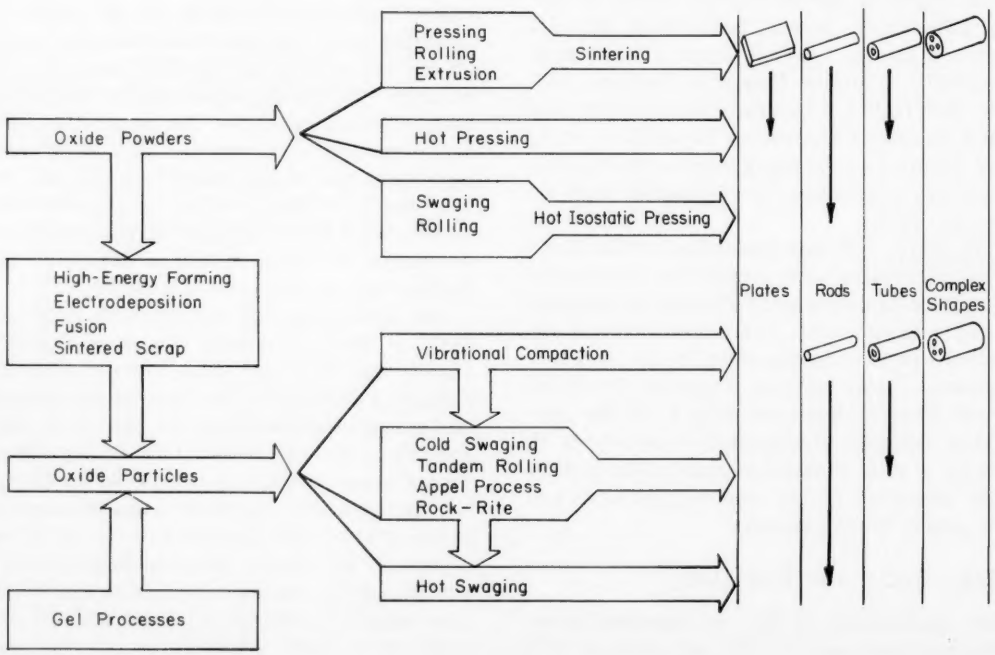

Fig. IV-2 Oxide fabrication methods under study at Hanford Atomic Products Operation.[4]

Table IV-1 FUEL-PIN DIMENSIONS[3] IN INCHES AT 20°C

	Alloy fuel	Oxide fuel
Rod length	15.75	13.39
Rod diameter	0.216	0.226
Niobium cladding outside diameter	0.232	
Niobium cladding thickness	0.008	
Stainless-steel cladding outside diameter	0.264	0.264
Stainless-steel cladding thickness	0.0157	0.019
Expansion space height	1.968	4.685

$^{9}/_{16}$-in.-diameter rods that had a length of 8 ft and employed Zircaloy cladding. The natural UO_2 elements were prepared by cold swaging.

The histories of the PRTR fuel elements and the development work connected with the plutonium program at HAPO have been reported in a variety of Hanford publications. Prior to October of 1962, the results of the plutonium programs at Hanford were reported in the quarterly progress reports of the Fuels Development Operation[6–9] and the Plutonium Metallurgy Operation.[10–13] With the quarter starting October 1962, the information appeared in the quarterly progress report of the Ceramics Research and Development Operation.[14–16] The power operation[17] of the PRTR commenced in May 1961, and during the next year the reactor output was 7261 Mwd(t). The following quotation[12] summarizes the status of the fuel-element program early in 1962:

> In the early part of 1962 the Plutonium Recycle Program (PRP) was advanced almost a year by a change in the core loading schedule for the Plutonium Recycle Test Reactor (PRTR). This was accomplished by eliminating the spike core loading of thirty high exposure aluminum-plutonium fuel elements and by advancing the charging date and charging rate of uniformly enriched Urania-Plutonia (UO_2-PuO_2) fuel elements. The new schedule resulted in a concerted fabrication effort and thirty UO_2-PuO_2 19-rod cluster fuel elements were produced from March through June, 1962. Eighteen of these elements were produced by a cold swage compaction process and twelve by a vibratory compaction process. In addition, during this period three high exposure aluminum-plutonium, four low exposure aluminum-plutonium, and one swaged MgO-PuO_2 spike fuel element were assembled and transferred to the PRTR for irradiation.

In September 1962 the several special fuel elements had been inserted into the PRTR (see Table IV-2), and as of March 1963 the PRTR core contained 44 UO_2-PuO_2, 22 Al-Pu, and 19 UO_2 elements, of which four UO_2-PuO_2, one Al-Pu, and seven UO_2 elements were considered as test elements.[18] The composition of the PRTR core as a function of irradiation history is shown in Fig. IV-3. The fabrication of the Pu-Al spike elements is summarized in Refs. 19 and 20, and Ref. 21 gives details on swageable end-cap design for the UO_2-PuO_2 elements. Reference 22 contains details on vibratory-compaction fabrication techniques.

The MgO-PuO_2 fuel element mentioned in Table IV-2 proved to be a particularly interesting one. In August of 1962 high coolant activity led to the examination of that fuel bundle, with the following results:[14]

> Postirradiation examination revealed a longitudinal split ($1^{1}/_{2}$-inches long and $^{1}/_{4}$-inch wide) in the cladding of one rod, and washout of approximately 9 inches of fuel material. There is no nonuniform discoloration of the cladding that would indicate overheating.

Table IV-2 SPECIAL TEST FUEL ELEMENTS[2]

Fuel type	Fabrication method	Fuel geometry	No. of elements	Average exposure (Sept. 1, 1962)
UO_2	Vipac	Tubular	1	1338 Mwd/ton of U
UO_2	Vipac	19-rod	1	1129 Mwd/ton of U
UO_2	Hot swage	19-rod	1	1010 Mwd/ton of U
Pu-Al (HX)*	Extrusion	19-rod	3	34.8 Mwd
UO_2-PuO_2 (HX)	Cold swage	19-rod	2	16.6 Mwd
UO_2-PuO_2 (HX)	Vipac	19-rod	2	17.0 Mwd
MgO-PuO_2 (HX)	Cold swage	19-rod	1	7.5 Mwd

Maximum exposure to date for the UO_2 element, 2650 Mwd/ton of U
Total reactor exposure to date, 8550 Mwd

* (HX) = high-exposure plutonium, 10 to 17 at.% Pu^{240}.

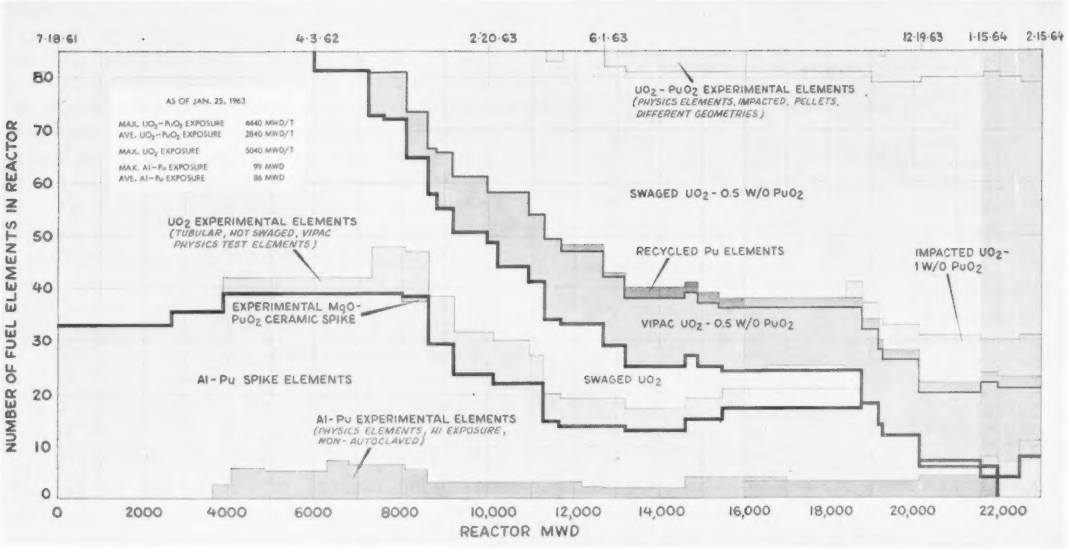

Fig. IV-3 PRTR fuel-element history.

The causes of the failure have been postulated as follows:[23]

A combination of three factors probably caused the PuO_2-MgO rod failure in the PRTR last August according to a tentative mechanism based on post-irradiation analyses: High localized temperatures were generated at several points of unexplained higher-than-normal plutonium concentration distributed at six-inch intervals along the rods; autoradiographs of some of the rods, including the failed one, revealed the high localized plutonium concentrations. Moisture released by the MgO at excessive operating temperatures attacked the inside of the Zircaloy cladding. A trace of impurity, possibly fluoride from an etchant trapped in an internal cladding defect, caused the water to react much more rapidly than otherwise; severe pitting corrosion, not normally associated with water corrosion of Zircaloy, was found on the inside of the cladding around the failure. The hypothesis goes on to state that corrosion-generated hydrogen dissolved in the cladding and migrated to the cooler outside surface where it precipitated to form a massive hydride layer, since observed metallographically. The weakened cladding failed in a brittle manner, producing a "leaker". Continued irradiation permitted waterlogging and/or hydration of the MgO to cause further splitting of the cladding in a ductile manner. This resulted in exposure of a section of the core to the heavy water coolant and a significant amount of core washout.

Specifications for the $MgO-PuO_2$ are given in Table IV-3 along with another developmental element containing ZrO_2-PuO_2.

Preirradiation autoclave tests of deliberately defected (drilled holes) rods containing samples of the fuel used in the test elements were conducted. No evidence indicated that swelling of

Table IV-3 SPECIFICATIONS FOR $MgO-PuO_2$ AND ZrO_2-PuO_2 19-ROD PRTR ELEMENTS[12]

	Swage-compacted ZrO_2-PuO_2	Swage-compacted $MgO-PuO_2$
Rod outside diameter, in.	0.565 to 0.570	0.565 to 0.570
Core outside diameter, in.	0.503 ± 0.002	0.503 ± 0.002
Cladding thickness, in.	0.032	0.032
Core length, in.	88	88
Fuel core volume, cm^3/element	5449	5449
Core density, % of theoretical	90	90
Weight of core material, kg/element	27.217	17.928
Weight of PuO_2, g/element	371	371
Percentage of PuO, wt.%	1.3	2.1
Maximum core temperature, °F	2923 (1606°C)	1652 (900°C)

the high-fired magnesia would occur under PRTR operating conditions. However, additional tests after the failure of the PRTR element showed that swelling behavior was sensitive to the shape of the defect. As before, capsules defected with drilled holes did not swell, but those having splits milled in the cladding to simulate longitudinal cladding splits did swell.

The PuO_2-MgO fuel rods, made by the incremental loading technique, provided an interesting evaluation of the effect of fissionable fuel distribution on postfailure washout behavior. Nonfissionable magnesia was readily washed from regions of low plutonium concentration, but further loss of fuel was prevented where plutonium concentration was high. In general, where fissionable materials are uniformly distributed, experience has shown that in-reactor sintering of particle fuels effectively prevents loss of significant quantities through cladding defects.

Following the failure of the MgO-PuO_2 element all the PRTR fuel elements were ultrasonically decontaminated, inspected, and recharged into the reactor. No significant damage was discovered, although several bundles had missing or broken spacers. The reactor itself, and primary loop components, were also decontaminated. The details are given in Ref. 22. A total time of 15 weeks was used for this cleanup, and the residual contamination was estimated to be less than 10 mg of Pu, out of an original washout of about 1.8 g. Reference 16 reports on two additional bundles with failed fuel rods. One bundle (5113) contained a rod with a $^3/_{16}$-in. by $^3/_{32}$-in. hole about a yard down from the top of the rod. The second bundle (5174) contained three failed rods, with the holes adjacent to the top end cap weld.

In extensive postirradiation examination and analysis, the failures were shown to be related to specific, small batches of fuel. Evidence points to three separate types of fuel contamination suffered during the summer and fall of 1963. These were: (1) fluoride and chloride impurities introduced as contaminants in plutonium metal that was to be oxidized; (2) high moisture content sorbed from glove-box atmospheres during periods of high outdoor humidity; and (3) traces of hydrocarbon introduced by failure of a bearing seal. The halide concentration of plutonium was experienced when a change was made in the source of supply. Purification processes were developed to adequately remove these halides. Diffusion of water vapor through rubber gloves and plastic glove-box bags raised the moisture content of glove-box atmospheres to an undesirably high level (PuO_2-containing fuel appears to sorb and hold moisture more tenaciously than does UO_2 alone). Failure of mechanical processing equipment is an obvious possibility that must be considered by any fuel fabricator. The unsuspected introduction of traces of oil from such mechanical failures points out the necessity for careful examination and possible redesign of commercially available equipment that may cause trouble in semiremote operations.

Table IV-4 DESIGN DATA FOR EBWR PLUTONIUM-BEARING CORE[14]

Reactor loading	
Central core region	Plutonium fuel, 36 fuel assemblies in 6 by 6 array
Outer core region	UO_2 fuel, 148 assemblies
Total number of plutonium assemblies	42 (6 spares)
Number of rods per assembly	36 (6 by 6 geometry)
Core composition	UO_2–1.5 wt.% PuO_2 (depleted UO_2, 0.2% U^{235}; high-exposure PuO_2, 8% Pu^{240})
Core length, in.	48.5
Core weight, g	830
Core density, % of theoretical density	86 to 89
Cladding	Zircaloy-2 tubing
Inside diameter, in.	0.372
Wall thickness, in.	0.025

The use of mixed oxides in the form of powder in the loading of fuel rods has one advantage in that it is possible to vary the concentration of plutonium along the length of the rods to shape the axial power profile. This is accomplished by simultaneously loading small increments of PuO_2, mixed with fine UO_2, along with increments of a coarse UO_2 fraction. The incremental loading can be done either during vibratory compaction or prior to a swaged-compaction step. One of the Hanford research programs reported[24] involved the fabrication of a variable enrichment element for irradiation in the Engineering Test Reactor (ETR), and other programs[14] have involved incrementally loading rods with the increments varying from 80 to 150 increments of PuO_2-UO_2 per rod. In general, the results have indicated that this incremental loading may produce segregation of the

plutonium-bearing material, and in one PRTR incrementally loaded rod the PuO_2 segregation made temperatures sufficiently high to cause center void formation and columnar grain growth[16,25] in a limited region.

Another common way of loading the PuO_2-UO_2 mixtures is called "bottle loading." In this procedure all the fuel materials for one rod are preblended by mixing for a given period of time. This method produces a blend with a constant PuO_2 distribution to within ±0.1 wt.% when finally loaded into a fuel rod.[16]

A plutonium-bearing core for the Experimental Boiling-Water Reactor (EBWR) is being fabricated at Hanford. Table IV-4 shows design data for the fuel loading. The fabrication technique consists of blending PuO_2 with depleted UO_2 that has been pulverized and air roasted.

Table IV-5 DETAILS OF EBWR-ETR CAPSULES[16]
GEH-14-421, -422, -423, AND -424

Fuel composition	UO_2–2.5 wt.% PuO_2
UO_2	Arc-fused; depleted U contains 0.22 wt.% U^{235}
PuO_2	Pu contains 7.8 wt.% Pu^{240}
GEH-14-421, -422	Impacted physical mixture
GEH-14-423, -424	Physical mixture
Dimensions, in.	
Fuel, outside diameter/length	0.383/3.00
Zircaloy-2 outside diameter/thickness/length	0.420/0.019/3.70
Aluminum outside diameter/inside diameter/length	1.125/0.420/4.38
Complete assembly with bail, length	5.00
Requested irradiation conditions	
Thermal-neutron flux, neutrons/(cm^2)(sec)	0.62×10^{14}
Rod power, kw/ft	16.2
Heat flux, Btu/(hr)(sq ft)	500,000
Exposure, Mwd/ton of fuel	1430

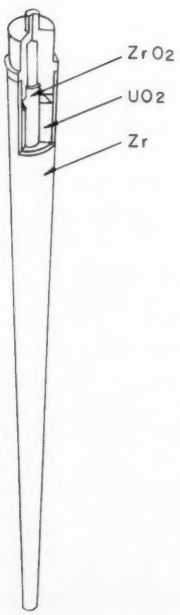

Fig. IV-4 Rod for fuel-element rejuvenation studies.[14]

This material is then put through the Dynapak process, which is described in Ref. 15. This process involves pneumatic impaction of the oxides at a temperature of 1200°C and an impact pressure of about 250,000 psi. Following the Dynapak operation the mixed oxides are loaded via vibrational compaction to 86 to 89% of theoretical density. Irradiations in the ETR of PuO_2-UO_2 fuel rods have been accomplished, and details are given in Table IV-5.

Another project under way at Hanford is one pertaining to fuel-element rejuvenation.[14] Fuel rejuvenation is defined as reenrichment of the fuel without total reprocessing and is being studied with the help of the fuel rod shown in Fig. IV-4. The element is designed to be reenriched after irradiation by opening the rod and inserting PuO_2, or enriched UO_2, into the concentric $\frac{1}{8}$-in.-ID ZrO_2 tube. One irradiation cycle had been accomplished at the time of writing of Ref. 16. The ZrO_2 tube was filled with vibratory-compacted enriched UO_2, resealed, and returned to the Materials Testing Reactor (MTR) for irradiation. Another concept involves the fast reactor to thermal re-

actor exchange element. This concept consists of "...enriching depleted uranium fuel elements in the blanket of a fast reactor and then irradiating them in the core of a thermal reactor without intervening separation and refabrication processes ..."[16] This element was designed to be irradiated in an existing fast reactor and the PRTR. Details of the element are given in Table IV-6.

A number of capsule irradiations have been conducted to study various aspects of the mixed-oxide fuel elements. Table IV-7, for example, gives data on a series of irradiation tests with the following purposes:[14]

> (a) determining the effect of PuO_2 content on the irradiation stability of the fuel, (b) comparing the in-reactor performance of fuel pellets prepared from mixtures of UO_2 and PuO_2 and from mixtures of UO_2 and (U, Pu)O_2 (from calcination of $Pu(OH)_4$ and $(NH_4)_2U_2O_7$ coprecipitated from hot ammonium hydroxide), and (c) investigating the in-reactor sintering of low density (63–65% TD) uranium-plutonium oxide pellets.

The high-density oxide capsules were designed to operate with a surface heat flux of 440,000 Btu/(hr)(sq ft), whereas the low-density capsules were designed to operate with a surface heat flux of 275,000 Btu/(hr)(sq ft). After irradiation to an exposure of 166×10^{18} fissions/cm^3, capsule GEH-14-86 was cross sectioned and samples were taken, with the aid of a diamond-tipped microdrill, from various radial locations within the pellet.* These samples were analyzed radiochemically, with the results as shown in Table IV-8. These data show that Pu, Ce^{144}-Pr^{144}, Zr^{95}-Nb^{95}, and Sr^{90} were relatively fixed within the capsule (little relocation), but the concentrations of the more volatile Cs^{137} and Ru^{106} were greater by orders of magnitude near the periphery of the pellet.

Table IV-6 FAST-THERMAL REACTOR EXCHANGE ELEMENT[16]

Fuel rods	
Cladding material	Zircaloy-2
Fuel	Depleted UO_2
Fuel density	86 to 89% of theoretical density
Rod outside diameter	0.563 in.
Rod inside diameter	0.505 in.
Overall length	71 3/8 in.
Fuel length	68 5/8 in.
Wire wrap material	Zircaloy-2
Wire wrap diameter	0.35 in.
Wire wrap pitch	10 in.
Assembly	
No. of rods	16
Array	Square, 4 by 4
Rod centerline spacing	0.598 in.
Can material	304L stainless steel
End hanger material	304L stainless steel
Overall length	96 1/2 in.

Table IV-7 CAPSULE IRRADIATION TESTS[14] OF UO_2-PuO_2

Capsule data	
UO_2-PuO_2 pellet size	1/2 in. in diameter
Diametral gap	0.001 to 0.003 in.
Cladding	Zircaloy-2, 0.031 in. thick
Atmosphere	Helium
Size of capsule	9/16 in. in outside diameter by 2 1/2 in. in length
High-density pellet capsules (6 pairs)	
Identity number	GEH-14-19, -20, -85 to -91
PuO_2 content	0.0259 to 5.67 mole %
PuO_2 type	4 MCO,* 8 MM†
Sintering conditions	1600°C in H_2, to 11 hr
Density	90 to 93% of theoretical density
Low-density pellet capsules (6 pairs)	
Identity number	GEH-14-21, -22, -65 to -74
PuO_2 content	0.0259 to 7.45 mole %
PuO_2 type	2 MCO, 10 MM
Heating conditions	1000°C in H_2
Density	63 to 65% of theoretical density

* MCO, mixed crystal oxide; ratio of UO_2 to PuO_2 is 5 to 1.
† MM, mechanical mixture of UO_2 (natural) and PuO_2.

GE-APED has conducted a series of irradiation experiments with PuO_2-UO_2 fuel. These experiments were done in the General Electric Test Reactor (GETR), the irradiations taking place during part of the year 1960. The results of the experiments are reported in Ref. 26. References 27 and 28 describe studies done to compare oxide and carbide fuels for use in a fast reactor; they use the results obtained in Ref. 26.

A total of 40 stainless-steel-clad specimens were fabricated[29] and irradiated to burnups from 5000 to 99,000 Mwd/ton at heat fluxes ranging from 0.5×10^6 to 1.6×10^6 Btu/(hr)(sq ft). Following irradiations the specimens were given gamma scans, dimensional measurements were taken, and the fission-gas re-

* This burnup corresponds to approximately 5600 Mwd/ton of UO_2 and PuO_2.

Table IV-8 FISSION-PRODUCT DISTRIBUTION IN IRRADIATED[16] UO_2–4.13 MOLE % PuO_2 CAPSULE (GEH-14-86)

Sample	Radius, cm	Radius, in.	Plutonium, dis/(min)(μg U)	Uranium, μg/sample	Ru^{106}, dis/(min)(μg U)	$Ce^{144}Pr^{144}$, dis/(min)(μg U)	$Zr^{95}Nb^{95}$, dis/(min)(μg U)	Ce^{137}, dis/(min)(μg U)
1	0.378	0.147	8.6×10^3	1.8×10^2	7.7×10^5	1.3×10^6	5.3×10^6	2.5×10^3
2	0.142	0.056	1.1×10^4	1.5×10^2	1.9×10^3	1.3×10^6	5.3×10^6	4.0×10^3
3	0.262	0.103	7.6×10^3	1.4×10^2	3.7×10^2	1.1×10^6	4.1×10^6	1.7×10^3
4	0.373	0.147	8.9×10^3	1.6×10^2	5.6×10^5	1.1×10^6	4.5×10^6	2.9×10^3
5	0.462	0.182	7.7×10^3	1.1×10^2	2.2×10^5	1.1×10^6	4.5×10^6	5.0×10^3
6	0.538	0.212	9.6×10^3	1.6×10^2	7.8×10^5	1.6×10^6	5.7×10^6	2.1×10^4
7	0.599	0.236	7.0×10^3	1.3×10^2	5.3×10^5	1.2×10^6	4.1×10^6	6.4×10^4

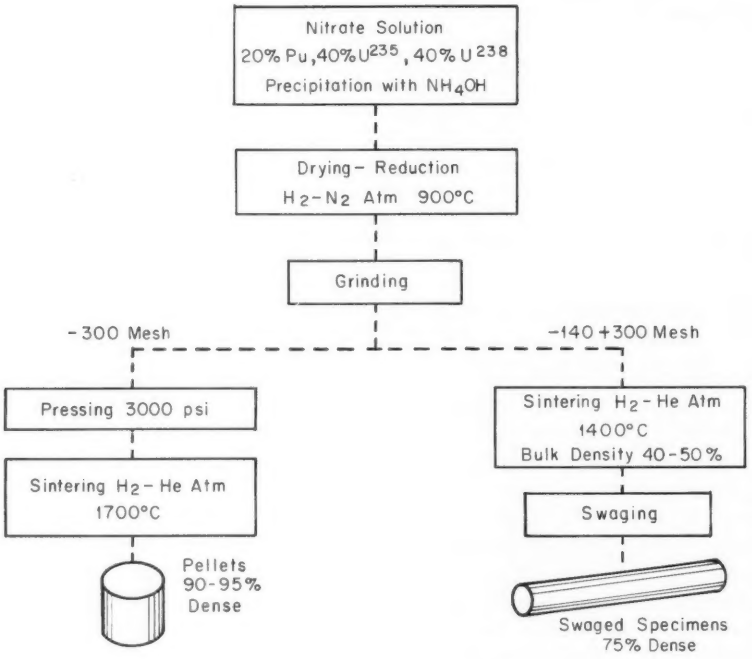

Fig. IV-5 Fuel preparation and fabrication flow sheet.[26]

lease was determined. Central voids were measured, and some metallographic examinations were made. The fuel preparation is shown in Fig. IV-5, and the test specimens are shown in Fig. IV-6. The actual composition of the fuel is shown in Table IV-9. A total of 10 irradiation capsules were fabricated, each containing four of the fuel specimens. These capsules were placed in the GETR, which is cooled by water. Details of the irradiation conditions are shown in Table IV-10. The results of the fuel-element measurements are shown in Table IV-11. The fission-gas release data are given in parts *a* and *b* of Fig. IV-7. Assumptions used to compute the data shown in the figure can be found in Ref. 26.

Possibly the most interesting result is the presence of the void formed during irradiation. As indicated in Table IV-11, only 4 out of the 40 specimens went through the experiment without forming a central void. In the case of the swaged specimens, it was possible to ascertain an approximate correlation between void size and heat flux, and this relation is shown in part *a* of Fig. IV-8. It can be seen that no void formed in the swaged specimens for heat fluxes

below about 500,000 Btu/(hr)(sq ft). Part *b* of Fig. IV-8 shows similar data for the pelleted specimens. The voids are smaller for the pelleted than for the swaged specimens at a given value of heat flux, and the void size is not so strongly correlated with heat flux. In a comment on the void formation in the pelleted specimens, the reference[26] states: "... since the pelleted specimens were fabricated with a 6–8 mil diametral gap between the fuel and the cladding, and it is not known whether or not this gap closed during irradiation, this might explain the anomalies in the void formation in the pelleted specimens ..." The mechanism of the formation of the central void is postulated to be[26] grain growth brought about by sintering and/or vaporization and redeposition rather than melting. Two of the specimens had off-center "central" voids, and these same samples also had fuel-to-cladding gaps that may have allowed the fuel to contact the cladding at an isolated spot. Interestingly, a fuel-to-cladding gap in a swaged specimen during operation is postulated.

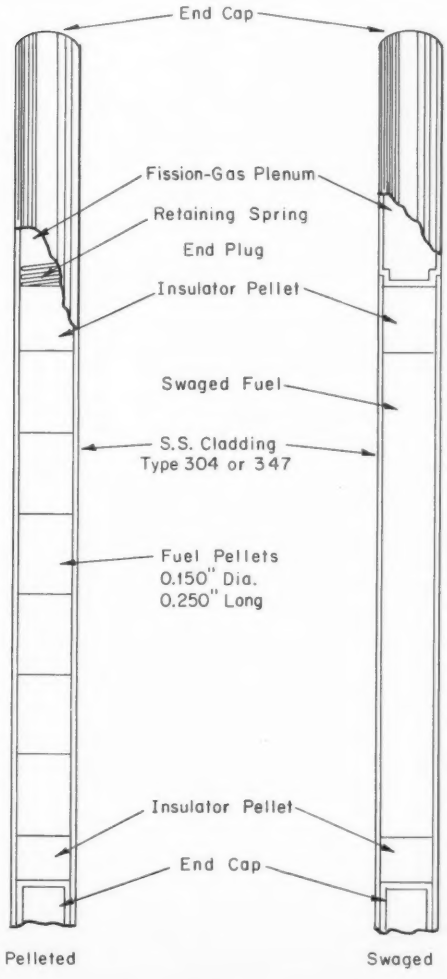

Fig. IV-6 Typical test specimens.[26]

Table IV-9 FUEL COMPOSITION[26] OF GE-APED TEST SPECIMENS

Isotope	Wt.%
Pu^{239}	18.81
Pu^{240}	1.20
U^{235}	37.86
U^{238}	42.13

Two unidentified phases were found in the fuel, and additional results of the metallographic observations are given in Table IV-12. The two phases are called "silver" and "gray" in Table IV-12, and Ref. 26 gives some information on their behavior. In 1961 a paper was presented[30] at a symposium on Radiation Effects in Refractory Fuel Compounds that is, substantially, Ref. 26. The paper is discussed in Ref. 30, and this discussion would be of interest to the specialist.

Information on PuO_2 properties is given in the Battelle Memorial Institute reports listed as Refs. 31 to 33. The first of these references lists, in tabular form, information on composition; physical, mechanical, thermal, electrical, and chemical properties; and irradiation properties for a number of fuel materials, among which is PuO_2. Unfortunately the most common entry for this latter fuel material is "no data available." References 32 to 34 deal with the stability of PuO_2 under various conditions.

Carbides

The carbides are receiving considerable attention as potential plutonium-bearing fuels because their thermal conductivity is high compared to that of the plutonium-bearing oxides. In this country the Argonne National Laboratory (ANL) and the United Nuclear Corporation appear to have done the most development of (PuU)C.[35] In general, the fabrication method enjoying greatest popularity involves reacting

UO_2 and PuO_2 with carbon to produce the carbides. The mixed carbides can then be pelleted by cold pressing and sintering; densities up to 95% of theoretical density have been achieved by the use of nickel as a sintering aid. Los Alamos Scientific Laboratory (LASL) has prepared various UC-PuC compounds by the direct comelting of uranium and plutonium metal with carbon in an arc furnace.[36]

The results of ANL irradiations of UC-PuC fuel rods have been reported in the 1961 and 1962 annual reports of the Metallurgy Division

Table IV-10 EXPERIMENTAL PARAMETERS FOR GETR IRRADIATIONS[26]

Specimen No.	Burnup, Mwd/ton*	Heat flux, Btu/(hr)(sq ft) × 10^6		$\int k\,d\theta$,† Btu/(hr)(ft)		Surface temperature, °F‡	
		Maximum	Average	Maximum	Average	Maximum	Average
I-1-P§	16,600	1.41	1.30	5,600	5,200	1,040	970
I-2-P	13,600	1.36	1.10	5,400	4,400	1,010	830
I-3-P	8,700	1.03	0.75	4,100	3,000	1,040	750
I-4-P	4,700	0.62	0.40	2,500	1,600	1,010	650
II-1-S§	19,400	1.33	1.28	5,300	5,100	1,080	1,050
II-2-S	16,100	1.34	1.09	5,400	4,400	1,120	940
II-3-S	10,700	1.06	0.73	4,300	2,900	1,160	830
II-4-S	6,600	0.72	0.45	2,900	1,800	1,130	750
III-1-S	26,000	1.14	1.06	4,600	4,200	810	760
III-2-P	18,800	1.10	0.96	4,300	3,800	790	730
III-3-P	15,100	1.02	0.77	4,000	3,000	820	670
III-4-S	11,700	0.75	0.48	3,000	1,900	710	500
IV-1-S	19,100	0.91	0.78	3,600	3,100	890	820
IV-2-P	14,000	0.82	0.71	3,200	2,800	1,030	910
IV-3-P	10,900	0.69	0.55	2,700	2,100	990	820
IV-4-S	9,000	0.53	0.37	2,100	1,500	880	660
V-1-S	99,000	1.52	1.27	6,000	5,100	1,260	1,060
V-2-P	77,400	1.58	1.30	6,200	5,100	1,180	1,020
V-3-P	54,400	1.28	0.92	5,000	3,600	1,130	880
V-4-S	42,700	0.86	0.55	3,400	2,200	930	650
VI-1-S	69,100	1.00	0.89	4,000	3,500	1,140	1,030
VI-2-P	41,600	0.79	0.68	3,100	2,700	1,060	950
VI-3-P	34,900	0.76	0.57	3,000	2,200	1,210	950
VI-4-S	30,900	0.62	0.40	2,400	1,600	980	680
VII-1-S	70,300	1.44	1.31	5,700	5,200	1,220	990
VII-2-P	49,900	1.50	1.32	5,900	5,200	1,170	950
VII-3-P	38,900	1.24	0.92	4,800	3,600	1,080	790
VII-4-S	29,600	0.86	0.55	3,400	2,200	950	630
VIII-1-S	45,200	1.07	0.83	4,200	3,300	1,180	930
VIII-2-P	28,300	0.85	0.66	3,300	2,600	1,220	920
VIII-3-P	23,100	0.75	0.54	2,900	2,100	1,150	840
VIII-4-S	19,300	0.50	0.36	2,000	1,400	820	590
IX-1-P	47,600	1.40	1.36	5,460	5,270	1,060	930
IX-2-P¶	38,300	1.36	1.19	5,300	4,700	**	**
IX-3-P	34,500	1.21	0.95	4,850	3,200	990	740
IX-4-P¶	17,600	0.86	0.56	3,350	2,160	**	**
X-1-S††	36,300	0.91	0.88	3,600	3,500	**	**
X-2-P	23,700	0.85	0.75	3,400	3,000	**	**
X-3-P	16,800	0.71	0.54	2,800	2,200	**	**
X-4-S	15,000	0.57	0.37	2,300	1,500	**	**

* Tons of plutonium and uranium (2000 lb/ton).
† Linear power generation = $4\pi \int k\,d\theta$.
‡ Temperature at inner surface of cladding.
§ P, pelleted specimen; S, swaged specimen.
¶ These specimens had no gas plenum.
** Cladding thermocouple failed.
†† Estimated data; majority of thermocouples failed during irradiation.

of ANL.[37] Arc-melted PuC and PuC-UC, and pressed and sintered pellets of PuC-UC, were irradiated in the EBR-I. The burnups achieved were all the order of 1000 Mwd/metric ton. The arc-melted material was very friable and fractured into large numbers of pieces on removal from the stainless-steel cladding or during subsequent handling. Minor dimensional changes were measured, with the densities, in general, decreasing on the order of 1%. The pressed and sintered material was stated to be "very durable" with minor dimensional changes. The

Table IV-11 POSTIRRADIATION FUEL MEASUREMENTS[26]

Specimen No.	Preirradiation density, % of theoretical	Active fuel length, in.			Central void data			
		Pre-irradiation	Post-irradiation	Postirradiation/ preirradiation	Diameter, in.	% of cross-sectional area	Length, in.	% of post-irradiation length
I-1-P*	93.5	1.605	†		0.034 to 0.044	5.0 to 9.7	1.60	100
I-2-P	92.5	1.605	†		0.019 to 0.041	1.7 to 7.5	1.60	100
I-3-P	93.3	1.605	†		†		†	
I-4-P	92.7	1.600	†		No void			
II-1-S	75	1.825	†		0.051 to 0.071	11.7 to 21.3	1.67	90
II-2-S	75	1.825	†		†		†	
II-3-S	75	1.825	†		†		†	
II-4-S	75	1.825	†		0.017 to 0.021	1.4 to 2.0	1.18	63
III-1-S	75	1.825	1.91	1.05	0.056 to 0.057	12.5	1.30	68
III-2-P	93.3	1.544	1.65	1.07	0.014 to 0.018	1.0 to 1.1	0.50	30
III-3-P	92.3	1.553	1.63	1.05	0.020 to 0.023	2.0 to 2.3	1.32	81
III-4-S	75	1.825	1.91	1.05	0.014 to 0.050	1.0 to 11.0	1.33	70
IV-1-S	75	1.825	2.07	1.13	0.036	5.7		
IV-2-P	90.7	1.552	1.65	1.06	0.034 to 0.035	5.1 to 5.4	1.55	94
IV-3-P	89.0	1.564	1.63	1.04	0.031 to 0.035	4.0 to 5.4	0.70	43
IV-4-S	75	1.835	2.04	1.13	No void			
V-1-S	75	1.825	1.99	1.09	0.047 to 0.067	9.8 to 19.5	1.50	75
V-2-P	95.8	1.495	1.58	1.06	0.022 to 0.031	2.0 to 4.0	0.81	51
V-3-P	94.5	1.473	1.53	1.04	0.005 to 0.009	0.2 to 0.4	0.86	56
V-4-S	75	1.825	1.89	1.03	0.031 to 0.045	4.0 to 9.1	1.78	94
VI-1-S	75	1.825	1.96	1.07	0.042 to 0.054	7.8 to 13.0	1.26	664
VI-2-P	96	1.527	1.59	1.04	0.029 to 0.031	3.5 to 4.0	0.62	39
VI-3-P	95.3	1.531	1.58	1.03	0.013 to 0.031	0.7 to 4.0	0.75	47
VI-4-S	75	1.825	1.96	1.07	0.026 to 0.034	3.0 to 5.1	0.75	38
VII-1-S	75	1.825	1.90	1.04	0.051 to 0.060	11.6 to 16.0	1.61	84
VII-2-P	94.7	1.520	1.63	1.07	0.028 to 0.036	3.2 to 5.3	0.88	55
VII-3-P	96	1.516	1.58	1.04	0.033 to 0.038	4.5 to 5.9	0.57	36
VII-4-S	75	1.825	1.98	1.08	0.022 to 0.036	2.2 to 5.8	1.32	67
VIII-1-S	75	1.825	1.82	1.00	0.040 to 0.049	7.1 to 10.8	1.44	79
VIII-2-P	94.2	1.530	1.57	1.03	0.013 to 0.013	0.7	1.17	74
VIII-3-P	94.3	1.529	1.59	1.04	No void			
VIII-4-S	75	1.825	1.82	1.00	0.027 to 0.027	3.0	0.28	15
IX-1-P	86.5	1.333	1.36	1.02	0.026 to 0.040	2.8 to 6.6	0.95	70
IX-2-P‡	94.8	1.521	1.58	1.04	0.022 to 0.031	2.2 to 4.2	1.10	70
IX-3-P	83.7	1.348	1.36	1.01	0.027 to 0.036	3.2 to 5.7	1.36	100
IX-4-P‡	95.8	1.774	1.83	1.03	No void			
X-1-S§	75	1.825	1.85	1.01	0.040 to 0.054	7.1 to 13.0	1.72	93
X-2-P	96	1.517	1.52	1.00	0.009 to 0.018	0.3 to 1.3	0.61	41
X-3-P	96.5	1.514	1.57	1.04	0.013 to 0.027	0.7 to 3.0	0.42	27
X-4-S	75	1.825	1.84	1.01	0.008	0.3		

* P, pelletized specimen; S, swaged specimen.

† No measurements taken.

‡ These specimens had no gas plenum.

§ Estimated data; majority of thermocouples failed during irradiation.

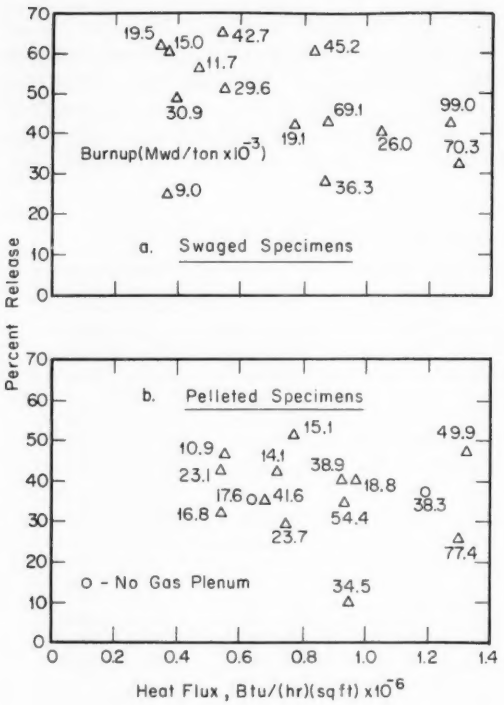

Fig. IV-7 Fission-gas release data.[26]

pressed and sintered pellets released 12% of the theoretical fission-gas release, and this was attributed[38] to the low density of the pellets, about 55%. LASL has reported data on a number of the properties of (UPu)C.[36,39]

The UKAEA has been studying mixed carbides for fast reactor applications.[40] Specimens of (UPu)C have been prepared by arc-melting uranium, plutonium, and carbon and casting in massive copper molds. Pellets have been prepared by cold pressing and sintering to greater than 95% of theoretical density. Data are shown in Table IV-13. Thermal conductivity of the carbides is given in Table IV-14. These data indicate that the addition of PuC to UC has the effect of reducing the thermal conductivity of the latter substance to about 70% of its former value.

Additional information on the preparation of PuC and (UPu)C can be found in Ref. 41, and Ref. 42 reports on the examination of irradiated (PuU)C fuel pellets. Irradiation data on (UPu)C pellets contained in Ref. 40 apparently came from the same experiments described in Ref. 42, and since the latter reference was issued later, the irradiation data contained therein will be cited. The reference[42] reports on the irradiation of nine stainless-steel-clad carbide fuel elements in the PLUTO reactor. Four of the elements contained arc-cast $(U_{90}Pu_{10})C$ pellets fabricated by direct arc-melting U-Pu metal with graphite. The pellets had a diameter of 0.1 in. They were ground to size and were incorporated in 20 Cr–20 Ni titanium-stabilized double-vacuum-melted stainless-steel tubing. Fission-gas space was allowed at one end of the assembly. Details on the sizes of the elements and conditions during irradiation are given in Table IV-15. Following irradiation, dimensional measurements were taken and no significant changes in dimensions were recorded. As stated in Ref. 42: "... it was concluded that no noticeable distortion of the sheathing had occurred during irradiation ..." Gas-release data are given in Table IV-16. It is evident that sample 8024 exhibited considerably more gas release than a comparable sample, 8025. No reasons for this difference are given in the reference, although metallographic examinations were done to see if an explanation could be found. The

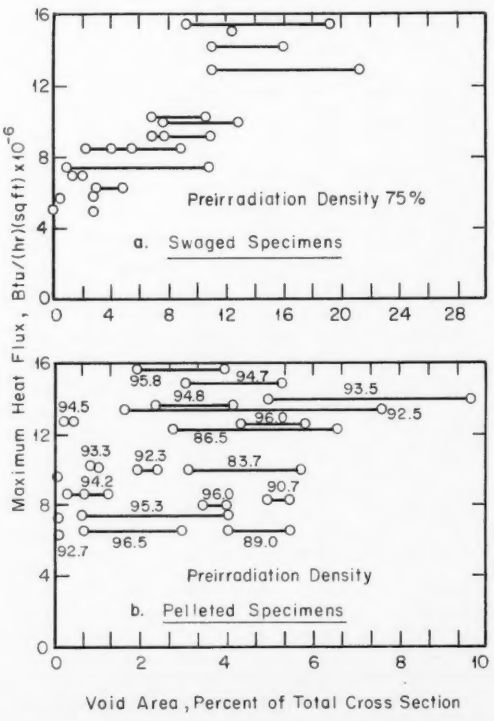

Fig. IV-8 Central void data, heat flux vs. void area.[26]

Table IV-12 SUMMARY OF METALLOGRAPHIC OBSERVATIONS[26]

Specimen	Burnup, Mwd/ton	Average heat flux, Btu/(hr)(sq ft)	Preirradiation density, % of theoretical	Approx. diameter of central void, in.	Fuel cracking	Structure	Other phases and constituents	Fuel-to-cladding gap
V-1-S	99,000	1.27×10^6	~75	0.060	Mainly radial with some circumferential	Small grains at OD; long columnar grains extending out from central void, porous band along OD of fuel, little or no grain growth at OD	Silver phase present throughout fuel	Fuel in contact with cladding
VI-1-S	69,100	0.89×10^6	~75	0.055	Mainly radial with some circumferential	Equiaxed grains at OD; long columnar grains extending out from central void; some grain growth at OD	Silver phase present throughout fuel. Gray phase present along OD of fuel	Fuel-to-cladding gap with particles of fuel adhering to cladding
V-4-S	42,700	0.55×10^6	~75	0.050	Radial	Equiaxed grains at OD; columnar grains extending out from central void; grain growth at OD	Silver phase present throughout fuel	Fuel-to-cladding gap exists
IV-4-S	9,000	0.37×10^6	~75	Small irregular shape	Radial	Unsintered or partially sintered fuel at OD; small columnar grains at central void	Large deposits of silver phase throughout fuel	Fuel-to-cladding gap exists
V-2-P	77,400	1.30×10^6	95.8	0.030	Mainly radial with some circumferential	Small grains at OD; long columnar grains extending out from central void; porous band along OD of fuel, little or no grain growth at OD	Silver phase present throughout fuel. Polygon-shaped crystals within columnar grains	Fuel in contact with cladding
V-3-P	54,400	0.92×10^6	94.5	Very small irregular shape	Mainly circumferential, some radial	Small grains at OD; equiaxed grains in mid-radius region, short columnar grains around central void	Silver phase present throughout fuel	Fuel in contact with cladding
IX-3-P	34,500	0.84×10^6	83.7	0.070	Mainly radial with some wide circumferential cracks near OD	Equiaxed grains at OD; long columnar grains extending out from central void; grain growth at OD	Silver phase present throughout fuel. Gray phase present along OD	Fuel-to-cladding gap exists
IV-3-P	10,900	0.55×10^6	89.0	0.035	Radial and wide circumferential cracks	Equiaxed grains at OD; long columnar grains extending out from central void; grain growth at OD	Silver phase present throughout fuel. Gray phase present along OD	Fuel-to-cladding gap exists
Unirradiated pellet			93.7		None	Uniform cross section	Two small deposits of silver phase	

reference notes that the lack of fuel swelling can possibly be explained by the fact that the 0.020-in.-thick cladding effectively restrains the fuel material.

The plutonium fuel programs at the United Nuclear Corporation (UNC) are described in Ref. 43. The fabrication technique involves the reaction of a pelletized mechanical mixture of UO_2, PuO_2, and carbon. The resulting material, called a clinker, is ground, cold pressed, and sintered. The advantage of using the nickel sintering aid can be seen in Table IV-17.

Table IV-13 EFFECT OF SOME SINTERING VARIABLES ON THE DENSITY OF UC AND $(U_{85}Pu_{15})C$ PELLETS[40]

Pellet	Carbon content, wt.%	Sintering time, hr	Sintering temp., °C	Bulk density, g/cm³
(UPu)C	4.69	4	1585	13.11
(UPu)C	4.89	4	1585	13.11
(UPu)C	5.25	4	1550	13.12
UC	4.70	5	1550	12.99
UC	4.70	12	1550	12.94

Table IV-14 THERMAL CONDUCTIVITIES OF UC AND $(U_{85}Pu_{15})C$ CYLINDERS[40]

Fabrication method	Density, g/cm³	Carbon content, wt.%	Thermal conductivity,* cal/(sec)(cm)(°C)
Uranium carbide			
Arc cast	13.87	4.40	0.052
Arc cast	13.64	3.77	0.052
Arc cast	13.40	5.06	0.058
Hot pressed	13.08	4.91	0.041
Uranium plutonium carbide			
Arc cast	13.67	4.55	0.031
Arc cast	13.55	4.71	0.036
Arc cast	13.24	4.84	0.041
Hot pressed	13.21	4.92	0.030
Arc cast		5.03	0.040
Hot pressed	12.90	~5.2	0.030
Hot pressed	13.04	5.41	0.030

* Uncorrected for porosity.

Metallic Fuels: Alloys

These fuels are of particular interest since a plutonium-containing alloy is proposed for use in the EBR-II for core 2. This alloy has the composition shown in Table IV-18. The goal mentioned in Ref. 44 for design of the plutonium-bearing element is a burnup of 5% (about 45,000 Mwd/metric ton) with central metal temperatures up to about 700°C. Unfortunately the reference alloy (Table IV-18) undergoes serious swelling at lower burnups and lower temperatures. One suggested method of attacking the problem has been the use of a strong jacket to restrain the fuel material mechanically. The strong-jacket concept was discussed in *Power Reactor Technology*, 4(4): 86, and Ref. 55 is a more recent publication dealing, in part, with the subject. Another suggested solution has been reduction of the plutonium content to 10 to 15%, which also improves radiation stability.[44] Results of irradiation of prototype EBR-II core 2 fuel elements were reported at a recent meeting of the American Nuclear Society.[45] This reference states that the minimum desired fuel burnup is 1.5 to 2 at.% and gives results of irradiations conducted in capsules in the CP-5 reactor. The cladding had a wall thickness of 0.009 in. and was separated from the fuel material by a sodium-filled gap with a (radial) dimension of 0.0006 in. Results are quoted as follows:

> The initial irradiations were conducted primarily with commercially obtained Nb/1 wt% cladding. The cladding had an internal void volume amounting to

Table IV-15 IRRADIATION DETAILS OF CARBIDE FUELS[42]

(Specimen Composition in Each Case Is 10 Wt.% PuC–90 Wt.% Natural UC)

Specimen No.	Carbon content, wt.%	Specimen size, in.		Specimen density, g/cm³	Capsule total heat output, watts	Calculated specimen rating, watts/g	Measured mean burnup, provisional Mwd/metric ton of fuel	Gas bond	Measured can surface temp., °C	Estimated specimen temp., °C	
		Diameter	Length							Surface	Center
8024	4.53 to 4.64	0.10	0.963	13.40 to 13.54	140	38	5,650	Ar	545	980	1010
8025	No analysis	0.10	1.00	10.22 to 13.42		38	6,550	Ar	545	980	1010
8013	4.54 to 4.61	0.10	1.94	13.35 to 13.59	252*	76.5†	12,500	He	420	462	480
8014	4.52 to 4.65	0.10	1.34	13.24 to 13.59	196	91.5‡	16,500	Ar	520	752	777

* Estimated heat output.
† Actually 54 watts/g.
‡ Actually 21 watts/g.

13 per cent of the fuel volume. Other cladding materials were also evaluated as they became available. Among these were niobium, Nb/1 wt% V alloy, Nb/33 wt% Ta/1 wt% Zr alloy, vanadium, molybdenum, and Ta/0.1 wt% W alloy. Cladding failures during irradiation could not be correlated with reported rupture strengths of the materials, and were generally traced to defects in the tubing materials. The failures occurred at burnups in the range of 1.0 to 1.5 atom per cent and were characterized by fracture or splitting of the cladding, originating at the hottest portion of the specimen and extending along the length of the specimen. Once a fissure had been established, the fuel generally extruded through the opening. The majority of cladding failures were by brittle fracture of the material. Vanadium cladding in the fully annealed condition failed in a ductile manner.

By improving the quality of the jacketing material and increasing the void volume within the cladding, the attainable burnup of the fuel prior to clad failure was extended from 1.3 atom per cent to 1.9 atom per cent. The attainable burnup was further extended to 2.1 atom per cent by venting the cladding to permit escape of entrapped fission gas or bond sodium.

Duplex tubing consisting of austenitic nickel alloys coated on the inside surface with 0.002-in. of tungsten is also under evaluation. The tungsten barrier is used to isolate the plutonium alloy from the austenitic nickel, thereby preventing formation of a molten eutectic. With this configuration it has been possible to achieve a 2.6 atom per cent burnup without failure.

A tertiary alloy is being considered for the French fast reactor Rapsodie.[3] The philosophy of canning the alloy, U-Mo-Pu, in a strong can is also being followed by the French, and a schematic of the Rapsodie fuel pin, using the alloy fuel, is shown in Fig. IV-9. The alloy will be injection cast into the niobium tube and capped with a resistance-welded niobium capsule. The niobium rod is then placed inside a stainless-steel can, using sodium as a thermal bonding material. Apparently a whole fuel pin such as is shown in Fig. IV-9 had not been fabricated when Ref. 3 was written, and the authors express concern as to the success of the double canning operation. Irradiation of U-Mo-Pu has also been done for the United Kingdom reactor program with the following quoted results: "... the avoidance of severe swelling at temperatures as high as 600°C presents a difficult problem..."[40]

There are, of course, potentially a large number of alloys with plutonium. The Pu-Al alloy was used as the spike enrichment elements for the PRTR, although these elements, as designed, had short reactivity lifetimes and high throughput rates.[2] The PRTR spike enrichment fuel elements are 8-ft-long 19-rod clusters. Additional data on the elements are given in Table IV-19. Irradiation of the Pu-Al elements in the PRTR has produced shortening

Table IV-16 FISSION-GAS RELEASE MEASUREMENTS[42]

(Composition of Each Fuel Specimen Is 10 Wt.% PuC–90 Wt.% Natural UC)

Specimen No.	Estimated volume of Xe produced, cm^3 at NTP	Recoil contribution, cm^3 at NTP	Measured volume of Xe on puncture, cm^3 at NTP	Percentage gas release [(measured/total produced) × 100]
8013	1.052	3.6×10^{-3}	3.4×10^{-4}	3.2×10^{-2}
8014	0.953	3.3×10^{-3}	1.3×10^{-5}	1.4×10^{-3}
8024	0.238	8.55×10^{-4}	4.7×10^{-3}	1.96
8025	0.279	9.9×10^{-4}	8.1×10^{-5}	2.9×10^{-3}

Table IV-17 DENSITIES OF (UPu)C OBTAINED WITH AND WITHOUT NICKEL SINTERING AID[43]

Material	Sintering temp. for 1 hr, °C	Approximate number of pellets made	Average density		Maximum density	
			g/cm^3	% of theoretical	g/cm^3	% of theoretical
$(U_{0.8}Pu_{0.2})C_{0.95}$	1965	200	12.54	92.4	12.83	94.4
$(U_{0.8}Pu_{0.2})C_{0.95}$ + 0.1 wt.% Ni	1590	200	13.15	96.8	13.30	97.8

of the fuel rods, which has been made apparent by the loosening of the spiral spacing wires around the rods.[11,15] Although the reason for the shortening of the rod apparently is not known in detail, Ref. 11 suggests that it is due to interaction between the Pu-Al core and the Zircaloy cladding. The shortening is a progressive phenomenon affected by the number of thermal cycles and/or fuel-element exposure. The lack of wear and/or fretting corrosion as a result of the loose wires suggests that at operating temperature the wires are tightened by the differential expansion between the core and the cladding.[11] The shortening has been noticed at an exposure of 54 Mwd, and one element with an average exposure of 74.2 Mwd exhibits a 0.28% shortening of a rod.[15]

Table IV-18 FUEL ALLOY FOR INITIAL CORE 2 LOADING: EBR-II[44]

Element	Wt.%
Zirconium	1.0
Molybdenum	2.9
Ruthenium	4.2
Rhodium	0.7
Palladium	2.2
U^{238}	Bal.
U^{235}	15 to 18
Plutonium	18 to 15

A number of intermetallic compounds such as U-Pu, Th-Pu, Bi-Pu, Co-Pu, and Fe-Pu have been prepared,[36] and some have been irradiated.[46] The irradiations were at maximum fuel temperatures of about 450°C, and burnups of about 2% were attained. Cast alloys of thorium containing 5 and 10 wt.% plutonium exhibited excellent dimensional stability, but cold-rolled zirconium that contained 5 and 7 wt.% plutonium exhibited poor dimensional stability.[46]

Metallic Plutonium, Cermets, and Miscellaneous Compounds

One application for nearly pure plutonium for power-reactor fuel is in the Los Alamos Molten-Plutonium Reactor Experiment I (LAMPRE-I). The fuel for this experiment is 90 at.% Pu–10 at.% Fe contained in a tantalum capsule. The nominal rod size[48] is 0.36 in. in inside diameter by $6\frac{1}{4}$ in. in length, with a wall thickness of 0.025 in. The alloys considered for LAMPRE-I are shown in Table IV-20. The addition of the alloying elements lowers the melting point of the fuel with respect to that of unalloyed plutonium (about 640°C). The tantalum capsule material suffers intergranular attack if the fuel is operated above 575°C. The Pu-Ce-Co alloy is of particular interest, since the plutonium content can be varied from 20 to 88 at.% with a corresponding reduction in the cerium concentration.

An alloy of Pu–1.25 wt.% Al was used in core IV of EBR-I.[38] The slugs of Pu-Al were 0.232 in. in diameter and 2.121 in. long. They were contained in a Zircaloy-2 jacket, and a NaK bond was provided for heat transfer purposes. A total of 420 fuel rods and 10 thermo-

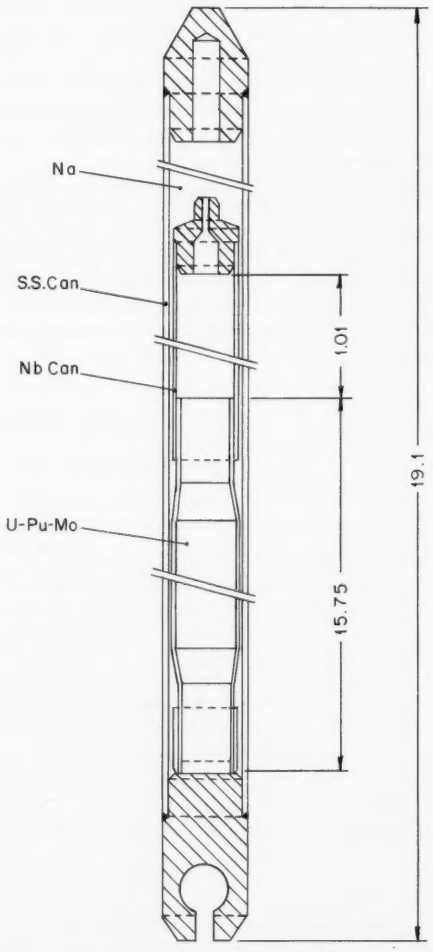

Fig. IV-9 The U-Pu-Mo fuel pin for the French fast reactor Rapsodie.[3]

couple rods containing the alloy were fabricated and successfully irradiated in the EBR-I.

Plutonium-bearing cermets have received considerable study. Researchers in the United Kingdom have prepared $(UPu)O_2$–stainless-steel and (UPu)C-Fe cermets.[40,41] The former material was fabricated by coating spheroids of $(UPu)O_2$ with stainless-steel powder and pressing into compacts. Plates were then formed by roll bonding. Some irradiations have been performed of 30, 40, and 50 vol.% oxide in stainless steel in the form of plates and pellets. The carbide-iron cermets were in a less advanced stage of study at the time of writing of Ref. 40. Oxide–stainless-steel cermets have been fabricated and irradiated in support of the Dounreay fast reactor program.[50] They are made by coating $(UPu)O_2$ granules with stainless-steel powder, pressing into pellets, and sintering in hydrogen. Preliminary irradiations have given mixed results, but the data given in Ref. 50 are of a preliminary nature. Cermets of PuO_2 and PuC in a zirconium-niobium base alloy are receiving study at the BelgoNucléaire Laboratories.[51] Hanford reports on properties of PuN-Pu, PuN-W, PuO_2-Zr, PuO_2-Mo, and PuO_2-W cermets in Refs. 14 and 16. LASL has prepared sintered pellets of PuO_2–stainless steel and PuO_2-Mo.[52,53]

Table IV-19 MARK I-G ALUMINUM-PLUTONIUM FUEL-ELEMENT DATA[20]

Core composition, wt.%	Pu, 1.81; Al, 95.40; Ni, 1.35; Si, 1.10; Fe, 0.33
Pu composition tolerance (standard deviation), wt.% Pu	0.04
Core density, g/cm^3	2.77
Average core weight (single rod), g	780
Average Pu weight per core (single rod), g	14.15
Average core weight per element, (19-rod cluster), g	14,820
Average Pu weight per element, (19-rod cluster), g	269.04
Core diameter, in.	0.500 ± 0.0002
Core length, in.	87.500 ± 0.020
Cladding material	Zircaloy-2
Cladding inside diameter, in.	0.505 ± 0.001
Cladding outside diameter (nominal), in.	0.565
Cladding thickness (nominal), in.	0.030
Cladding length, in.	89.115 ± 0.010
Rod length (overall), in.	
Regular rods	92.56
Center rod	93.11
Element length (overall), in.	97⅝
Rod weight (approximately), lb	3
Fuel-element weight, 19-rod cluster (approximately), lb	59
Wire wrap material	Zircaloy-2
Wrapping wire diameter, in.	0.072
Number of bands per element	4

Table IV-20 LOW-MELTING ALLOYS SUITABLE FOR MOLTEN-PLUTONIUM FUELS[49]

Alloy	Solidus point, °C
Pu–9.5 at.% Fe	409
Pu–12 at.% Co	405
Pu–12.5 at.% Ni	465
Pu–Ce–12 at.% Co	<450

In summary, metallic fuels face formidable swelling problems in a reactor designed to operate with high-temperature fuel irradiated to large burnups. Reference 54, in fact, concludes that "... the potential of metallic systems appears now to be very limited ..." On the other hand, the author of Ref. 55 favors a simple U-Pu metallic fuel element containing 25 to 30% internal void, and states that Nimonic-clad pins such as these have been successfully tested to 5% burnup (about 45,000 Mwd/metric ton) at 700°C temperature.

The mixed-oxides system has been irradiated to high burnup in the GETR. Although the results are encouraging, the irradiation of full-length fuel elements has only just started in the PRTR. It is concluded in Ref. 54 that PuO_2-UO_2 mixtures behave similarly to UO_2 alone but with somewhat higher fission-gas release for the mixed oxides. Of the remaining Pu-bearing fuels, the solid solution of PuC and UC has promise, but few basic data are presently available.

References

1. P. Bussy, The Plutonium-Based Fuel Production Programmes in France, in Proceedings Plutonium as a Power Reactor Fuel, American Nuclear Society Topical Meeting, Richland, Washington, September 13 and 14, 1962, USAEC Report HW-75007, p. 3.1, Hanford Laboratories, December 1962.
2. R. I. Smith and R. E. Peterson, Experience with the Plutonium Recycle Test Reactor, in Proceedings Plutonium as a Power Reactor Fuel, American Nuclear Society Topical Meeting, Richland, Washington, September 13 and 14, 1962, USAEC Report HW-75007, p. 11.1, Hanford Laboratories, December 1962.

3. F. Sebilleau and C. P. Zaleski, Plutonium as a Fuel for the Fast Reactor RAPSODIE, in Proceedings Plutonium as a Power Reactor Fuel, American Nuclear Society Topical Meeting, Richland, Washington, September 13 and 14, 1962, USAEC Report HW-75007, p. 15.1, Hanford Laboratories, December 1962.
4. E. A. Evans, Hanford Programs for Advanced Plutonium Fuel Designs and Fabrication Methods, in Proceedings Plutonium as a Power Reactor Fuel, American Nuclear Society Topical Meeting, Richland, Washington, September 13 and 14, 1962, USAEC Report HW-75007, p. 5.1, Hanford Laboratories, December 1962.
5. W. J. Bailey, Investigation of Plutonium-Bearing Fuel Elements for the Plutonium Recycle Test Reactor, Part 1, USAEC Report HW-70158 (Pt. 1) Hanford Atomic Products Operation, June 1961.
6. Hanford Atomic Products Operation, Fuels Development Operation Quarterly Progress Report, October–December 1961, USAEC Report HW-72346. (Classified)
7. Hanford Atomic Products Operation, Fuels Development Operation Quarterly Progress Report, January–March 1962, USAEC Report HW-72347, Apr. 16, 1962. (Classified)
8. Hanford Atomic Products Operation, Fuels Development Operation Quarterly Progress Report, April–June 1962, USAEC Report HW-74377, July 20, 1962. (Classified)
9. Hanford Atomic Products Operation, Fuels Development Operation Quarterly Progress Report, July–September 1962, USAEC Report HW-74378, Oct. 15, 1962. (Classified)
10. Hanford Atomic Products Operation, Plutonium Metallurgy Operation Quarterly Progress Report, October–December 1961, USAEC Report HW-72161, Jan. 15, 1962. (Classified)
11. Hanford Atomic Products Operation, Plutonium Metallurgy Operation Quarterly Progress Report, January–March 1962, USAEC Report HW-73318, Apr. 16, 1962.
12. Hanford Atomic Products Operation, Plutonium Metallurgy Operation Quarterly Progress Report, April–June 1962, USAEC Report HW-74162, July 16, 1962. (Classified)
13. Hanford Atomic Products Operation, Plutonium Metallurgy Operation Quarterly Progress Report, July–September 1962, USAEC Report HW-74718, Oct. 15, 1962. (Classified)
14. Hanford Atomic Products Operation, Ceramics Research and Development Operation Quarterly Progress Report, October–December 1962, USAEC Report HW-76300.
15. Hanford Atomic Products Operation, Ceramics Research and Development Operation Quarterly Progress Report, January–March 1963, USAEC Report HW-76301, Aug. 23, 1963.
16. Hanford Atomic Products Operation, Ceramics Research and Development Operation Quarterly Progress Report, April–June 1963, USAEC Report HW-76302, Nov. 4, 1963.
17. J. C. Fox, D. J. Foley, and J. F. Fletcher, Startup Experience with the Plutonium Recycle Test Reactor, Paper No. 62-WA-247 presented at Winter Annual Meeting of The American Society of Mechanical Engineers, Nov. 25–30, 1962.
18. Hanford Atomic Products Operation, Quarterly Progress Report, Research and Development Programs Executed for the Division of Reactor Development, January–March 1963, USAEC Report HW-78118, April 1963.
19. R. K. Koler, Pneumatic Injection Casting of Aluminum-Plutonium Fuel Elements, USAEC Report HW-69204, Hanford Atomic Products Operation, April 1961.
20. M. D. Freshley, Plutonium Spike Fuel Elements for the PRTR. Part I. The MARK I-G, USAEC Report HW-69200 (Pt. 1), Hanford Atomic Products Operation, March 1961.
21. L. C. Lemon and W. T. Ross, Head-Welded Swageable End Cap for UO_2-PuO_2 Fuel Elements, USAEC Report HW-74287, Hanford Atomic Products Operation, July 13, 1962.
22. H. E. Hanthorn, Calculated Costs of Fabrication of Plutonium-Enriched Fuel Elements, USAEC Report HW-74304, Hanford Atomic Products Operation, August 1962.
23. Hanford Laboratories, PuO_2-MgO Failure Mechanism Postulated, in Plutonium R&D Newsletter, Issue No. 2, January 1963.
24. I. D. Thomas, Plutonium Fuel Experience at Hanford, in Proceedings Plutonium as a Power Reactor Fuel, American Nuclear Society Topical Meeting, Richland, Washington, September 13 and 14, 1962, USAEC Report HW-75007, p. 6.1, Hanford Laboratories, December 1962.
25. Hanford Laboratories, Plutonium R&D Newsletter, Issue No. 3, April 1963.
26. J. M. Gerhart, The Post-Irradiation Examination of a PuO_2-UO_2 Fast Reactor Fuel, USAEC Report GEAP-3833, General Electric Company, Vallecitos Atomic Laboratory, November 1961.
27. K. M. Horst and B. A. Hutchins, Comparative Study of PuC-UC and PuO_2-UO_2 as Fast Reactor Fuel. Part I. Technical Considerations, USAEC Report GEAP-3880, General Electric Company, Atomic Power Equipment Department, Jan. 19, 1962.
28. G. D. Collins, Comparative Study of PuC-UC and PuO_2-UO_2 as Fast Reactor Fuel. Part II. Economic Considerations, USAEC Report GEAP-3880 (Pt. II), General Electric Company, Atomic Power Equipment Department, Nov. 15, 1962.
29. J. M. Cleveland, W. C. Cavannaugh, M. E. Snyder, and W. C. Cowden, Fast Oxide Breeder Project I—Fuel Fabrication. Part I. Plutonium-Uranium Dioxide Preparation and Pelletized Fuel Fabrication, Part II. Fabrication of Plutonium-Uranium Dioxide Specimens by Swaging, USAEC Report

GEAP-3486, General Electric Company, Vallecitos Atomic Laboratory, Aug. 15, 1960.

30. J. M. Gerhart, J. N. Siltanen, and J. S. Cochran, The Irradiation and Examination of a Plutonium-Uranium Oxide Fast Reactor Fuel, in Sixty-fourth Annual Meeting Papers: Symposium on Radiation Effects in Refractory Fuel Compounds, *Am. Soc. Testing Mater. Spec. Tech. Publ.*, No. 306, p. 154, American Society for Testing and Materials, Philadelphia.
31. Roy W. Endebrock (Ed.), Properties of Fuels for High-Temperature Reactor Concepts, USAEC Report BMI-1598, Battelle Memorial Institute, Nov. 1, 1962.
32. S. J. Paprocki, D. L. Keller, and W. M. Pardue, The Chemical Reactions of PuO_2 with Reactor Materials, USAEC Report BMI-1580, Battelle Memorial Institute, May 29, 1962.
33. S. J. Paprocki, D. L. Keller, C. A. Alexander, and W. M. Pardue, The Volatility of PuO_2 in Nonreducing Atmospheres, USAEC Report BMI-1591, Battelle Memorial Institute, Aug. 16, 1962.
34. E. E. Jackson and M. H. Rand, The Oxidation Behaviour of Plutonium Dioxide and Solid Solutions Containing Plutonium Dioxide, British Report AERE-R-3636, June 1963.
35. Nuclear Fuels and Materials Development, USAEC Report TID-11295(2nd ed.), September 1962.
36. J. A. Leary, W. J. Maraman, W. N. Miner, and F. W. Schonfeld, Quarterly Status Report on Solid Plutonium Fuels Program for Period Up to June 30, 1963, USAEC Report LAMS-2949, Los Alamos Scientific Laboratory, July 1963.
37. J. H. Kittel, L. A. Neimark, R. Carlander, O. L. Kruger, and R. C. Lied, Preliminary Irradiations of PuC and UC-PuC, USAEC Report ANL-6678, Argonne National Laboratory, September 1963.
38. W. R. Burt, Jr., A. G. Hins, R. M. Mayfield, and A. B. Shuck, Manufacture of EBR-I Core IV Fuel and Blanket Rods, Metallurgy Division Annual Report for 1962, USAEC Report ANL-6677, pp. 53-55, Argonne National Laboratory.
39. A. E. Ogard, C. C. Land, and J. A. Leary, The Thermal Expansion of PuC and PuC-UC Solid Solution, USAEC Report LA-2768, Los Alamos Scientific Laboratory, October 1962.
40. B. R. T. Frost, P. G. Mardon, and L. E. Russell, Research on the Fabrication, Properties, and Irradiation Behaviour of Plutonium Fuels for the U.K. Reactor Programme, in Proceedings Plutonium as a Power Reactor Fuel, American Nuclear Society Topical Meeting, Richland, Washington, September 13 and 14, 1962, USAEC Report HW-75007, p. 4.1, Hanford Laboratories, December 1962.
41. M. Palfreyman and G. A. Keig, Some Investigations on the Preparation and Properties of Plutonium Monocarbide, (UPu)C Solid Solutions and (UPu)C/Fe Cermets, British Report AERE-M-1106, September 1962.
42. B. T. Bradbury, J. E. Cole, B. R. T. Frost, and J. D. B. Lambert, Post Irradiation Examination of Stainless Steel Clad UC, UC-UFe_2 and PuC-UC Fuel Pellets, British Report AERE-R-4323, May 1963.
43. A. A. Strasser, Plutonium Fuel Programs of the United Nuclear Corporation, in Proceedings Plutonium as a Power Reactor Fuel, American Nuclear Society Topical Meeting, Richland, Washington, September 13 and 14, 1962, USAEC Report HW-75007, p. D3.1, Hanford Laboratories, December 1962.
44. F. G. Foote, Plutonium Fuel Programs at Argonne National Laboratory, in Proceedings Plutonium as a Power Reactor Fuel, American Nuclear Society Topical Meeting, Richland, Washington, September 13 and 14, 1962, USAEC Report HW-75007, p. 7.1, Hanford Laboratories, December 1962.
45. W. N. Beck, J. H. Kittel, and R. Carlander, Irradiation Behavior of Refractory-Alloy-Clad Plutonium Alloys, *Trans. Am. Nucl. Soc.*, 6(2): 375 (November 1963).
46. J. A. Horak, J. H. Kittel, and H. V. Rhude, The Effects of Irradiation on Some Binary Alloys of Thorium-Plutonium and Zirconium-Plutonium, USAEC Report ANL-6428, Argonne National Laboratory, July 1962.
47. A. S. Coffinberry and W. N. Miner (Eds.), *The Metal Plutonium*, University of Chicago Press, Chicago, 1961.
48. Los Alamos Scientific Laboratory, LAMPRE I Final Design Status Report, USAEC Report LA-2833, January 1962.
49. J. W. Anderson, W. D. McNeese, and J. A. Leary, Preparation and Fabrication of Plutonium Fuel Alloy for Los Alamos Molten Plutonium Reactor Experiment No. 1, USAEC Report LA-2439, Los Alamos Scientific Laboratory, Apr. 15, 1960.
50. P. Brock, L. H. Cope, and K. Q. Bagley, Fuel Elements for Fast Reactors, in Proceedings Plutonium as a Power Reactor Fuel, American Nuclear Society Topical Meeting, Richland, Washington, September 13 and 14, 1962, USAEC Report HW-75007, p. 18.1, Hanford Laboratories, December 1962.
51. E. Vanden Bemden, Description of the Belgonucleaire, in Proceedings Plutonium as a Power Reactor Fuel, American Nuclear Society Topical Meeting, Richland, Washington, September 13 and 14, 1962, USAEC Report HW-75007, p. 22.1, Hanford Laboratories, December 1962.
52. W. C. Pritchard, K. A. Johnson, J. A. Leary, and W. J. Maraman, Compaction and Sintering of PuO_2-Mo Powder Mixtures, USAEC Report LA-2621, Los Alamos Scientific Laboratory, Nov. 6, 1961.
53. W. C. Pritchard, K. A. Johnson, and J. A. Leary, Compaction and Sintering of PuO_2-Type 302B

Stainless Steel Powder Mixtures, USAEC Report LAMS-2898, Los Alamos Scientific Laboratory, Jan. 3, 1963.

54. A. A. Johnson, J. M. Hoffmann, J. E. Crawley, R. T. Huntoon, and D. A. Orth, Commercial Fabrication of Plutonium Fuel, USAEC Report DP-838, Savannah River Laboratory, June 1963.
55. L. R. Blake, Fast Reactor Design for Economic Power Production, *J. Nucl. Energy: Pt. A & B*, 16(11/12): 509 (November/December 1962).

Section

V

Power Reactor Technology

Materials

Neutron Irradiation of Type 347 Stainless Steel

Type 347 stainless steel is widely used in reactor core structures and fuel elements and in the construction of test loops for the in-pile testing of reactor materials and components. Information previously available in the literature[1–4] indicates that fast-neutron irradiation of stainless steels to exposures of about 3×10^{21} to 4×10^{21} nvt results in changes in mechanical properties such as increases of about 13% in ultimate tensile strength, increases of 60% in yield strength, and decreases of about 44% in total elongation. The study reported in Refs. 5 and 6 was undertaken to determine the effect of neutron exposures in excess of 4×10^{21} nvt. The study is of interest to designers, not only because it reports on the mechanical properties of encapsulated stainless-steel specimens after massive exposure to fast neutrons (1.1×10^{22} nvt), but also because it describes very interesting effects on test samples cut from sections of the operating J-10 pressure loop of the Engineering Test Reactor (ETR).

For the encapsulated sample tests, AISI type 347 stainless steel in the form of $\frac{5}{8}$-in.-diameter rod, annealed and cold finished, meeting the specifications of ASTM A-276-55 (with an additional specification that the yield strength should be in the 50,000- to 65,000-psi range) was purchased for the test material. The composition of the type 347 stainless steel employed in the test program is given in Table V-1. Table V-2 gives the results of tensile tests on the material.

Two of the 11 capsules included in the surveillance program contained full-size Charpy V-notch and modified subsize Izod specimens. The specimens were arranged in three clusters spaced over the 8-in. capsule length. Each cluster contained two Charpy and four Izod specimens held in place by stainless-steel clip holders.

The estimated fast-neutron flux exposures for capsules in the surveillance program, as of the end of ETR cycle 40 (Oct. 2, 1961), are given in Table V-3. The subsize tensile specimens contained in capsules BMI-24-6 and BMI-24-18 were examined and tested. It was noted visually that all specimens were in good condition. Those removed from the longer exposure capsule (capsule BMI-24-6) were more discolored with a deposit of light-reddish oxide than those removed from the shorter exposure capsule. Two specimens from each capsule were tested at room temperature (about 75°F), and two were tested at 600°F. The two remaining specimens of each capsule were annealed for a period of 1 hr at 1800°F and were then tested at room temperature or 600°F. The results of the mechanical tests are given in Table V-4.

Table V-1 MANUFACTURERS' ANALYSIS OF AISI TYPE 347 STAINLESS STEEL USED FOR IRRADIATION TEST SPECIMENS[5]

Chemical analysis, wt.%							
Carbon	Manganese	Phosphorus	Sulfur	Silicon	Nickel	Chromium	Tantalum and niobium
0.057	1.72	0.024	0.016	0.65	10.41	17.91	0.67

Table V-2 ROOM-TEMPERATURE MECHANICAL PROPERTIES OF AISI TYPE 347 STAINLESS STEEL USED FOR IRRADIATION TEST SPECIMENS[5]

Specimen	Tester	Tensile strength, psi	Yield strength, psi	Elongation, % in 1.1 in.	Reduction in area, %	Rockwell hardness
Standard (0.505 in. in diameter)	Manufacturer	88,000	53,000	43.0	65.0	B 92
	KAPL	91,300	56,000	63.0		B 84 to 87
Subsize (0.16 in. in diameter)	KAPL	92,600	38,800	64.3	75.6	A 48 to 52
	BMI	89,100	35,000	61.0	73.5	

Examination of the data in Table V-4 shows that irradiation increased the 0.2% offset yield strength about 190% at room temperature, increased the ultimate strength about 24%, and decreased the total elongation about 50%. Similar changes in these properties were also observed in tests at 600°F. The data indicated that the effects of increasing the neutron exposure from 6.5×10^{21} to 1.1×10^{22} nvt were minor at both test temperatures, being reflected chiefly in differences in yield strength and total elongation.

The properties of specimens irradiated to different levels of exposure and subsequently annealed for 1 hr at 1800°F before testing are also given in Table V-4. These results indicate that the annealing treatment was sufficient to remove nearly all effects of irradiation on the specimens. In particular, recovery of the yield and ultimate strengths of the stainless-steel specimens was facilitated, whereas recovery of preirradiation ductility was not quite so complete, especially in the specimens that received the higher irradiation exposure. A typical stress-strain curve of type 347 stainless steel, tested in the unirradiated condition at 75°F, after irradiation to an estimated exposure of 1.1×10^{22} nvt, and after irradiation and annealing, is shown in Fig. V-1. The slope of the stress-strain curve obtained from irradiated specimens after a 1-hr anneal at 1800°F is almost identical to that of an unirradiated specimen.

The results of impact and tensile tests on AISI type 347 stainless steel have been determined for exposures up to about 1.1×10^{22} nvt.

Table V-3 SUMMARY OF BMI-24 SURVEILLANCE-CAPSULE EXPOSURES[5] AS OF END OF CYCLE 40

Capsule	Type of specimens in capsule	Total exposure as of end of cycle 40 (10-2-61), $\times 10^{21}$ nvt		Remarks
		Top	Bottom	
BMI-24-2	Tensile and fatigue	8.7	10.3	In-pile since cycle 4
BMI-24-4	Tensile and fatigue	7.0	9.3	In-pile since cycle 4
BMI-24-6	Tensile and fatigue	11.0*	8.4*	In-pile since cycle 4
BMI-24-8	Tensile and fatigue	8.4	9.0	In-pile since cycle 4
BMI-24-10	Tensile and fatigue	9.1	7.4	In-pile since cycle 4
BMI-24-12	Tensile and fatigue	9.7	9.7	In-pile since cycle 4
BMI-24-14†	Impact	5.8	5.6	Discharged from reactor at end of cycle 28, and specimens tested
BMI-24-16†	Impact	9.7	8.4	In-pile since cycle 4
BMI-24-18	Tensile and fatigue	4.4*	6.4*	In-pile since cycle 19
BMI-24-20	Tensile and fatigue	4.4	6.4	In-pile since cycle 19
BMI-24-22	Tensile and fatigue	4.6	6.2	In-pile since cycle 19

*Capsules BMI-24-6 and BMI-24-18 were discharged from the reactor at the end of cycle 42 (about Jan. 15, 1962) with exposures of about 0.93×10^{22} to 1.1×10^{22} and 5.1×10^{21} to 7.4×10^{21} nvt, respectively.

†Capsules BMI-24-14 and BMI-24-16 contain 12 subsize modified Izod specimens and 6 regular-size Charpy V-notch specimens. All other capsules contain 6 each subsize tensile and cycle-strain fatigue specimens.

This exposure level is, to date, the highest for which tensile properties of type 347 stainless-steel specimens have been reported. At an exposure of about 6.5×10^{21} nvt, the impact strength was reduced by about 50% at room temperature and considerably more at liquid-nitrogen temperatures. The fracture produced at room temperature was generally of the ductile type. At liquid-nitrogen test temperatures, the fracture was a combination of cleavage and shear types, more indicative of brittle fracture.

Tensile tests performed on subsize specimens of type 347 stainless steel showed increases of nearly 200% in the 0.2% offset yield values and increases in the ultimate strength of about 25%, as results of irradiation to 1.1×10^{22} nvt. Conversely, very large decreases in total elongation were observed. The hardness of specimens irradiated to exposures of 6.5×10^{21} nvt increased approximately 15% over the hardness of similar unirradiated material. Little change in hardness occurred as the result of increasing the neutron exposure from 6.5×10^{21} to 1.1×10^{22} nvt. These data and the results of tensile tests indicate a trend to saturation of irradiation effects in type 347 stainless steel when irradiated at process-water temperature with neutron exposures near 6.5×10^{21} nvt.

The ability to remove most of the effects of neutron irradiation by postirradiation annealing was demonstrated. Annealing for 1 hr at 1800°F, in most cases, caused the recovery of the preirradiation properties, but complete recovery of ductility was not achieved, particularly in the specimens that received the higher neutron exposure.

In addition to the tests described above, Refs. 5 and 6 report the results of tests conducted on specimens cut from sections of the J-10

Table V-4 COMPARISON OF THE TENSILE PROPERTIES AT 75 AND 600°F OF UNIRRADIATED, IRRADIATED, AND IRRADIATED AND ANNEALED TYPE 347 STAINLESS STEEL[5]

Total integrated fast flux (>1 Mev), nvt	Capsule	Condition	Yield strength (0.2% offset), 10^3 psi	Ultimate tensile strength, 10^3 psi	Uniform elongation, %	Total elongation, % in 1.1 in.	Reduction of area, %
		Tested at 75°F					
0		Unirradiated	34.5	87.7	>40.0	61.8	75.0
0		Unirradiated	36.0	90.0	>40.0	62.6	73.5
0		Unirradiated	34.5	89.5	>40.0	66.3	72.0
0*		Unirradiated	38.3	92.5		63.4	75.0
0*		Unirradiated	38.7	92.8		64.7	76.0
0*		Unirradiated	39.3	92.4		64.7	75.6
7.6×10^{21}†	BMI-24-18	As irradiated	104.0	112.0	25.8	34.5	68.5
5.5×10^{21}‡	BMI-24-18	As irradiated	88.7	111.5	24.7	32.7	70.0
1.1×10^{22}‡	BMI-24-6	As irradiated	103.5	112.5	24.3	30.9	70.0
9.2×10^{21}†	BMI-24-6	As irradiated	109.0	113.0	25.4	30.9	78.0
1.1×10^{22}‡	BMI-24-18	Irradiated and annealed at 1800°F for 1 hr	33.0	87.1	52.1	55.5	75.0
6.6×10^{21}†	BMI-24-6	Irradiated and annealed at 1800°F for 1 hr	33.8	87.5	57.5	61.0	77.0
		Tested at 600°F					
0*		Unirradiated	26.9	63.8		36.4	71.0
0*		Unirradiated	28.5	66.5		34.9	71.6
0*		Unirradiated	28.0	65.9		34.9	69.4
7.2×10^{21}†	BMI-24-18	As irradiated	81.8	83.0	10.7	14.5	61.0
5.5×10^{21}‡	BMI-24-18	As irradiated	80.0	84.0	13.2	16.4	60.0
1.1×10^{22}‡	BMI-24-6	As irradiated	86.8	89.0	10.1	13.3	60.7
8.7×10^{21}†	BMI-24-6	As irradiated	85.3	87.5	9.0	11.9	60.7
1.0×10^{22}†	BMI-24-6	Irradiated and annealed at 1800°F for 1 hr	28.2	64.3	27.7	30.0	68.0
5.5×10^{21}‡	BMI-24-18	Irradiated and annealed at 1800°F for 1 hr	27.4	65.0	28.7	31.7	68.0

*Tests made by Knolls Atomic Power Laboratory.

†Values based on $Fe^{54} \rightarrow Mn^{54}$ reaction.

‡Values based on cycle-to-cycle determination of $Ni^{58} \rightarrow Co^{58}$ reaction.

loop that operated in the ETR at the National Reactor Testing Station for about 17 months. The loop components from which the test samples were cut consisted of two basic capsules or tubes, an inner tube containing test specimens in a pressurized-water or -steam atmosphere, and an outer surrounding tube (or jacket)

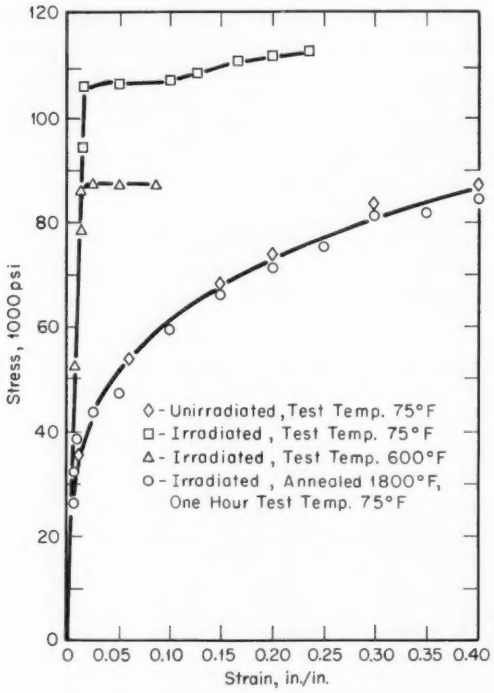

Fig. V-1 Stress vs. strain for AISI type 347 stainless steel before and after irradiation to 1.1×10^{22} nvt.

separated from the inner tube by a helium gas annulus. The outside of the outer tube was in contact with the 120°F process water. Thus the inner or pressure tube underwent irradiation at a temperature of about 750°F under significant pressure and thermal stresses, whereas the outer tube was exposed to the same irradiation but at a temperature of about 120°F with no significant stresses present.

The J-10 test loop was placed in service in the ETR in October 1959 and was removed on Mar. 16, 1961. During this time the loop was exposed to approximately 222 effective full-power days (approximately 38,800 Mwd) at an estimated maximum flux (above 1 Mev) of 3.8×10^{14} nv. The 36-in.-long section, which had resided in the ETR core, was removed from both inner and outer loop sections and was examined at Battelle.

The initial chemical and physical properties of the material from which the pressure tube and the gas jacket were fabricated indicated that the compositions and fabrication conditions of both the pressure tube and the gas jacket were similar, although forging of the pressure tube was accomplished at a higher temperature. The tensile strength of the inner pressure tube was slightly higher, and the 0.2% offset yield strength was appreciably higher than that of the gas jacket. The ductilities of both loop sections were approximately equal in the preirradiation condition.

Table V-5 gives the results of tensile tests on 3 unirradiated, and 18 irradiated, type 347 stainless-steel specimens that were machined from the inner and outer loop sections and tested at room temperature and 600 or 750°F. The procedure employed for the elevated-temperature tests was to heat the specimen to 600 or 750°F and maintain this temperature for 30 min before beginning the test. The unirradiated values listed in the table are for comparison and include handbook data, results of tensile tests from specimens machined from an uncontaminated outer loop section, and data from McInnes Steel Co. personnel who prepared the inner J-10 pressure tube.

All the test specimens fractured within the 2-in. gauge length and exhibited necking in the area of fracture. However, the inner loop specimens gave evidence of reduced ductility as shown by small uniform elongations, a severe reduction in total elongation, and decreases in the reduction in area. Tests made at room temperature on specimens from the outer jacket indicated that the yield strength and ultimate strength had been increased about 120 and 80%, respectively, over the unirradiated material. The total elongation and the reduction in area were decreased approximately 50 and 12%, respectively.

The outer jacket material when tested at 750°F showed about the same degree of increase in the ultimate strength, a slightly smaller increase in yield strength, and further decreases in total elongation and reduction in area as compared with unirradiated specimens. The decrease in total-elongation values as a function of increasing test temperature to about 900°F

Table V-5 TEST RESULTS OBTAINED ON IRRADIATED TENSILE SPECIMENS MACHINED FROM SECTIONS OF THE J-10 LOOP[5]

Specimen	Approx. peak irradiation test temp., °F	Fast-neutron (>1 Mev) exposure* 10^{14} nv	Fast-neutron (>1 Mev) exposure* 10^{21} nvt	Test temp., °F	Yield strength (0.2% offset), 10^3 psi	Ultimate tensile strength, 10^3 psi	Total elongation (in 2 in.), %	Reduction of area, %
Inner Loop, Initial Tests								
ST-3-L	510	1.0	1.9	75	132.0	132.0	4.25	53.5
ST-2-I	625	2.0	3.9	75	145.0	145.0	6.50	54.5
ST-2-H	735	3.7	7.1	75	149.0	149.0	10.30	58.2
ST-2-L	540	1.1	2.1	750	103.0	103.0	4.50	42.7
SB-2-I	740	2.7	5.1	750	115.0	115.0	1.50	40.8
SB-2-H	760	3.6	6.9	750	120.0	120.0	2.50	50.5
Control†				70	52.5 to 60.7	91.3 to 93	53 to 61	68 to 72
Handbook data‡				750	40 to 50	70 to 80	45 to 50	
Inner Loop, Duplicate Tests								
ST-7-L	540	0.87	1.7	75	130.0	134.0	6.5	59.1
ST-7-I	675	2.9	5.57	75	139.5	144.8	10.6	59.8
ST-7-H§	735	1.7	3.26	75	143.0	147.0	9.4	61.5
SB-7-L	700	1.2	2.3	750	115.3	115.3	4.2	64.0
SB-7-I	760	1.9	3.65	750	123.0	123.5	4.2	45.5
SB-7-H	760	3.4	6.5	750	125.4	125.8	4.1	40.5
Outer Loop								
LT-4-L	120	0.91	1.8	75	100.0	103.5	31.5	54.0
LT-4-I	120	1.8	3.5	75	95.2	101.3	26.0	57.0
LB-3-H	120	3.4	6.5	75	102.5	108.0	25.0	60.5
LT-3-L	120	3.1	2.0	750	62.5	66.7	13.3	54.0
LT-3-I	120	2.4	4.5	750	65.4	69.3	11.4	54.6
LT-3-H¶	120	2.7	5.1	600	71.8	73.3	12.5	48.3
Control 1**				75	46.8	99.7	50.4	61.8
Control 2**				750	36.5	67.6	26.2	62.9

*Exposures based on Mn^{54}.

†From McInnes Steel Co. reports on samples cut from as-machined J-10 pressure tube.

‡*Metals Handbook*, Vol. 1, 8th ed., p. 503.

§Less than 1 mg of sample was submitted for analysis; therefore the analysis may be inaccurate due to small weighing errors. On the basis of the location of the specimen, a value of $\sim 7 \times 10^{21}$ nvt would be expected.

¶Only 1.5 mg of sample was analyzed. Small weighing errors could have caused significant errors in analysis. It is believed that the actual value would duplicate LB-3-I since the specimen came from adjacent position.

**Samples cut from portion of J-10 pressure tube above reactor core.

is characteristic of unirradiated stainless steel and should not be considered a result of irradiation. However, the extreme difference between the results from the inner loop and outer jacket (much greater) at similar levels of exposure, at the same test temperature, does appear to be the result of irradiation under stress and/or temperature. The shape of the stress-strain curves for the inner loop and the outer jacket was entirely different.

The examination of the J-10 loop was of considerable value, since the data revealed the mechanical-property changes that occurred in a structural material under actual operating conditions of pressure, temperature, and neutron flux. Irradiation of encapsulated specimens can never duplicate *in situ* irradiations of reactor components, since the specimens are not subjected to variations in temperature and stress, two parameters that may contribute to property changes in irradiated structures. The data indicate that the stress state and irradiation temperature may play a very important role in property changes during irradiation.

References

1. M. J. Graber and J. H. Ronsick, ETR Radiation Damage Surveillance Programs. Progress Re-

port I, USAEC Report IDO-16628, Phillips Petroleum Co., Jan. 27, 1961.
2. D. O. Leeser, *Mater. Methods*, Manual 107, August 1954.
3. W. F. Murphy and S. H. Payne, Fast Neutron Effects on Tensile and Hardness Properties of Type 347 Stainless Steel, in *Symposium on Radiation Effects on Materials*, Vol. I, p. 162, American Society for Testing and Materials, 1956.
4. M. H. Bartz, Performance of Metals During Six Years Service in the Materials Testing Reactor, *Proceedings of the Second United Nations International Conference on the Peaceful Uses of Atomic Energy, Geneva, 1958*, Vol. 5, pp. 466-474, United Nations, New York, 1958.
5. W. E. Murr, F. R. Shober, R. Lieberman, and R. F. Dickerson, Effects of Large Neutron Doses and Elevated Temperature on Type 347 Stainless, USAEC Report BMI-1609, Battelle Memorial Institute, Jan. 21, 1963.
6. W. E. Murr and F. R. Shober, Annealing Studies on Irradiated Type 347 Stainless, USAEC Report BMI-1621, Battelle Memorial Institute, Mar. 6, 1963.

Section

VI

Power Reactor Technology

Operating Experience

Shippingport

A recent report[1] summarizes approximately five years of operating experience with the Shippingport Atomic Power Station: from its startup in December 1957, through the installation of, and the initial operation of, the fourth core seed, to the end of March 1963. Some 1650 reports are available on the Shippingport project and work related to it. The reports are listed in Ref. 2. A number of the previous reports on operating experience have been reviewed in past issues of *Power Reactor Technology*, 2(4): 74-77; 4(2): 52-58; 5(4): 61-72; 6(2): 64-67; and 6(3): 49-55. The Shippingport plant is described in detail in Ref. 3.

Figure VI-1 shows the operating history of the plant. Most of the nonroutine events cited on the figure have been covered in the reviews listed above. It is notable that the time required for refueling (with a new seed; the original blanket, called core 1, is still in place) decreased from five months for the first refueling to 44 days for the second and to 32 working days for the third. Most of this improvement is attributed to increased experience and improved planning, although 20 days of the first, long refueling period was devoted to modification of the vessel head instrumentation. The average load factor between refueling periods was 37% for the first seed, 70% for the second, and 77% for the third. If the periods used for testing and training are excluded, these factors increase to 75, 97, and 97%, respectively.

The third seed, which, like seed 2, initially contained 90 kg of U^{235} with 170 g of natural boron as a burnable poison, was operated for 7329 equivalent full-power hours (EFPH) during its lifetime. At the end of March 1963, the plant had delivered 1.225×10^9 net kw-hr of electricity and had operated for a total of 22,366 EFPH. The original core (i.e., the natural-uranium blanket) was still in operation, with seed 4. The average exposure of the blanket fuel was 9000 Mwd/metric ton of uranium, and its peak exposure was 30,100 Mwd/metric ton of uranium.

The five years of operating experience have demonstrated that the plant meets satisfactorily the operational requirements for practical integration into a utility system. These include: "...(1) the capability of operating as a base-loaded station for extending periods, (2) the capability of accepting its share of the load swings necessitated by system disturbance, and (3) the capability of operating on a peak-load basis when station-system efficiency conditions justified such use..."[1] Operation has shown that, when used as a peak-load facility, the station follows all system load changes in the power range; it can also be shut down and started up under controlled conditions at a faster rate than that of any conventional, modern station on the Duquesne system. In relation to the effectiveness of the station for base-load operation, it is significant that the frequency of safety shutdowns (scrams) has decreased with time, as indicated by Fig. VI-2. Some of the safety shutdowns are attributed to personnel error and some to equipment problems.

The fast-neutron exposure of the reactor pressure vessel is causing some increase in the ductile-brittle transition temperature, which places a limit on the permissible stress levels at temperatures below 250°F. These limitations are being observed by the control of operating procedures during plant startups and during the periodic hydrostatic testing. It is concluded, on the basis of present materials data, that neutron damage will not limit operation at normal operating temperatures at any time through the life of the second core.

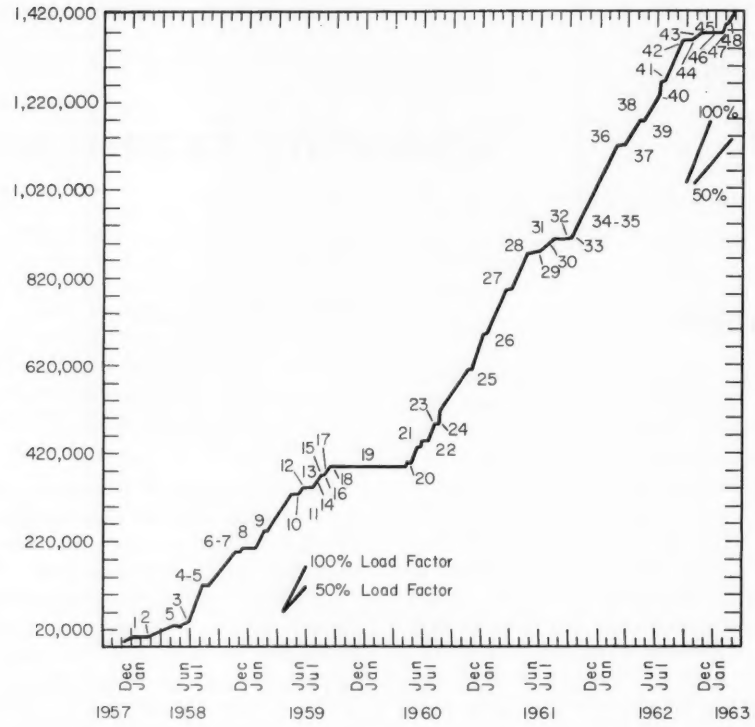

1. Reactor Shut Down for Test and Training
2. Leak Discovered in Steam Generator
3. Coolant Loop Pump Failed
4. First 1000-Hr Reactivity Lifetime Test
5. Shut Down for Maintenance and Testing
6. Second 1000-Hr Reactivity Lifetime Test
7. Shut Down for Maintenance and Testing
8. Moisture-Separator Failure Discovered; Plant Remained Shut Down Through January 1959
9. Repair of Turbine Governor
10. Periodic Operation for Training Purposes
11. Shut Down for Maintenance and Testing
12. Periodic Operation for Testing Plant Dynamic Response
13. Shut Down for Capacity Reduction and Hot Subpower Tests
14. Final Reactivity Lifetime Test; Final Run at Full Power for Core 1, Seed 1
15. Low-Power Physics Testing
16. 50-Mw Operation for End of Core Life Tests
17. Shut Down Because of Xenon Buildup
18. Final Power Run at 20 Mw
19. Shut Down To Replace Core Seed 1; Full Power Resumed
20. Low-Power Physics Testing
21. Maintenance—Replacement of E-12 Control-Rod-Drive Mechanism
22. Low-Power Physics Testing
23. Testing and Student Training
24. Return of 1-B Loop to Service
25. Low-Power Physics Testing
26. Low-Power Physics Testing and Maintenance
27. Low-Power Physics Testing—240-Hr Samarium Transient Test; Start of Final Full-Power Run
28. End of Seed 2 Ability to Override Equilibrium Xenon at 100% Power—Physics Testing
29. Testing, Maintenance, and Operator Training
30. Core Physics Testing—End of Seed 2 Life Tests
31. Start of Refueling and Replacing Seed 2
32. Initial Approach to Criticality, Seed 3
33. Full-Power Operation with Seed 3
34. Low-Power Physics Tests
35. A 3000-Hr Reactivity Lifetime Test
36. Shutdown Low-Power Physics Test, Rod Mechanism Test, Reactor Protection System Response Test
37. Student Training, Tests
38. Shutdown Xenon Transient Test
39. Operations Supervisor Training
40. Reduced Output on Generator Due to Feedwater Heater Outage
41. Shutdown Low-Power Physics Test—Rod-Mechanism Exercise
42. Shutdown End of Seed 3 Ability to Override Equilibrium Xenon at 100% Reactor Power
43. Operation at Reduced Power and Lower Average Coolant Temperature
44. End of Seed 3 Operation
45. Seed 3 and Seed 4 Refueling
46. Initial Approach to Criticality—Seed 4
47. Physics Tests
48. Shut Down for Testing and Begin 3600-Hr Reactivity Lifetime Test

Fig. VI-1 Operating history of Shippingport Atomic Power Station.[1]

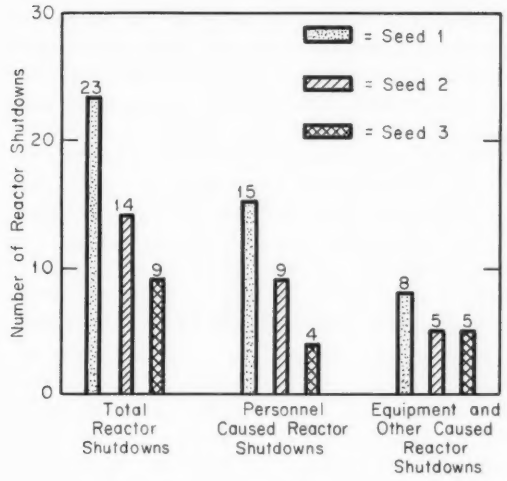

Fig. VI-2 Analysis of Shippingport safety shutdowns during operation with seeds 1 to 3.[1]

The history of power sharing between the seed and blanket is indicated in Fig. VI-3. The power fraction produced in the natural-uranium blanket during the first three seed lives averaged about 54%. Of the energy generated in the blanket, about half has been generated by the burning of plutonium in place, about 8% by the direct fissioning of U^{238}, and the remainder from the burning of U^{235}. The U^{235} content of the blanket has now decreased to about one-third its original (natural uranium) value. The temperature coefficient of reactivity (at rated power) has been nearly the same for all three seeds under comparable conditions of control-rod configuration. The coefficient becomes less highly negative as seed exposure progresses and control rods are withdrawn, as is to be expected. It changes from about $-2.0 \times 10^{-4}/°F$ for a new seed to about $-0.7 \times 10^{-4}/°F$ at the end of seed life.

During the operation of seed 1, asymmetries in the radial power distribution were observed to develop for certain configurations of control-rod insertion and to oscillate with a period of about 24 hr if no action was taken to control them. This phenomenon could be controlled rather easily by suitable manipulation of the control rods. Self-sustained oscillations of this type could not be generated in seed 2, even by deliberate unbalancing of the power distribution, and no oscillations were observed during seed 3 operation. Oscillation has, however, occurred in seed 4. The occurrence of the oscillation is presumably promoted by poor reactivity coupling of the various core regions in the azimuthal coordinate and is more apt to occur when the reactivity of the blanket is low than when it is high.

The performance of the blanket fuel elements has been very encouraging. Postirradiation examination of blanket rod bundles removed after seed 1, seed 2, and seed 3 operations has shown them to be in good condition. Detailed metallurgical examinations of elements removed at the second refueling have been made, and examination of a rod removed at the third refueling, with an estimated exposure of 23,000 Mwd/metric ton of uranium is under way. The examination of a rod removed, at the second refueling, with an exposure of 16,000 Mwd/metric ton of uranium, showed[1] that the average hydrogen content of the cladding was less than 80 ppm, that there was no abnormal cracking of grain growth in the UO_2, and that the 4-mil radial annulus between fuel and cladding was still intact. Reference 4 reports examinations of several elements removed at the second reloading and presumably includes the element mentioned above. The highest value of the estimated central temperature, for any of the elements, is 1320°F, corresponding to a time average heat flux of 152,000 Btu/(hr)(sq ft). For the blanket element diameter (0.411 in.), this heat flux corresponds to a conductivity integral ($\int k\,d\theta$) of 12.5 watts/cm..

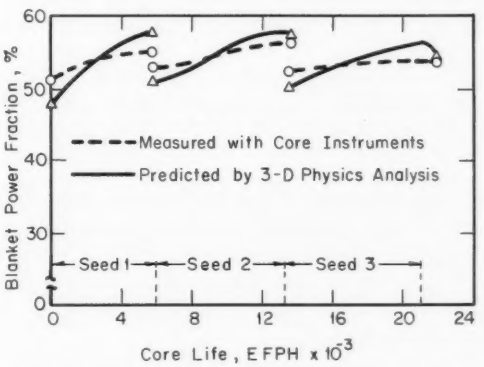

Fig. VI-3 Percentage of core energy from natural-uranium blanket during Shippingport core 1 life.[1]

Tests have been made of samples of the hafnium control rods removed after each seed life.

Figure VI-4 shows the changes in mechanical properties which were observed up to the end of life of seed 2. Excessive corrosion of the weld joint between the hafnium blades and the Zircaloy-2 control-rod hub was attributable to

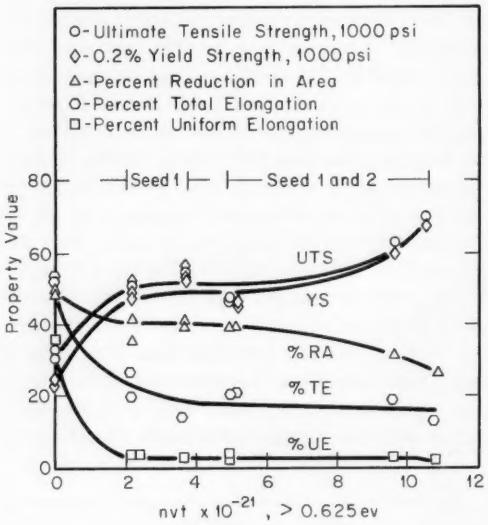

Fig. VI-4 Effect of neutron exposure on the 600°F tensile properties of Shippingport hafnium control rod after two seed lives.[1]

welding difficulties that resulted in contamination of the weld metal during rod manufacture. Improved welding procedures were developed, and all but two of the original rods (which showed low corrosion) were replaced at the second refueling.

The primary coolant water is demineralized water adjusted to a *p*H of 9.5 to 10.5 with lithium hydroxide. A hydrogen overpressure is used to give 15 to 60 cm^3 of hydrogen per kilogram of water and an oxygen content less than 0.14 ppm. These conditions have minimized corrosion of the reactor plant piping and components and have kept the crud concentration low (about 5 ppb). The control of *p*H by the ion exchanger has been excellent, with infrequent additions of lithium hydroxide of less than 0.5 lb every four to five weeks. The use of isotopically pure lithium (99.99% Li^7) was begun in December 1960 and has reduced the tritium concentration in the coolant from a maximum of 280 μc/liter to about 2 μc/liter. Until recent repairs to leaky relief valves, the rate of hydrogen addition was approximately 100 cu ft/week. No excursions of oxygen concentrations above 0.14 ppm have occurred during power operation.

Seed 4 is scheduled to operate for the remainder of its reactivity lifetime, at which time the entire core is to be removed and the reactor is to be modified to accept a core of new design. The new core will raise the reactor capability from 67 Mw(e) to 150 Mw(e)(gross). Part of the power is to be dissipated, since the station turbine is rated for only 100 Mw(e).

References

1. J. T. Stiefel, H. Feinroth, and G. M. Oldham, Shippingport Atomic Power Station Operating Experience, Developments, and Future Plans, USAEC Report WAPD-TM-390, Westinghouse Electric Corp., Bettis Atomic Power Laboratory, April 1963.
2. Westinghouse Electric Corp., Bettis Atomic Power Laboratory, The Shippingport Pressurized Water Reactor Project Catalog of Document Abstracts, USAEC Reports WAPD-PWR-1606(Rev.), December 1961, and WAPD-PWR-1606(Add. 1), May 1, 1963.
3. AEC Naval Reactors Branch, Westinghouse Electric Corp., and Duquesne Light Co., *The Shippingport Pressurized Water Reactor*, Addison-Wesley Publishing Company, Inc., Reading, Mass., September 1958.
4. L. R. Lynam, Examination of PWR Core 1 Blanket Fuel Rods for Microstructure Changes, Hydrogen Pickup, Burst Strength, and Fission Gas Release at the End of the Second Seed Life, USAEC Report WAPD-TM-326, Westinghouse Electric Corp., Bettis Atomic Power Laboratory, April 1963.

Section

VII

Power Reactor Technology

Specific Reactor Types

Seed and Blanket

The most recent operating experience with the Shippingport Pressurized-Water Reactor is reviewed in Sec. VI of this issue of *Power Reactor Technology*. The further work on seed-and-blanket technology by the Bettis Atomic Power Laboratory has been proceeding from this reactor in two main directions: the development of a second core for Shippingport and the study of large power reactors of the seed-and-blanket type (the Large Power Reactor Program). The following review covers three recent reports[1–3] relating to the second core program.

The Shippingport reactor is currently operating with its fourth enriched seed and with the natural-uranium blanket that was originally installed. The term "second core" refers to a replacement of the entire core, including the blanket, by a new core of different design. The replacement is to be made at the end of life of seed 4, which is expected early in 1964.

The new core is to yield large increases in both power output and total energy output, as summarized in Table VII-1. The major changes in design features are the following:

1. The fuel elements are to be of the plate type, composed of oxide wafers encased in Zircaloy-4 cladding, as illustrated in Fig. VII-1. The plates will be assembled into square fuel assemblies by welding at their edges. The blanket plates, which will replace rod type UO_2 elements in the present core, will be 0.140 in. thick and will contain natural UO_2 wafers 0.100 in. thick. The seed plates will be 0.076 in. thick and will contain wafers, 0.036 in. thick, of highly enriched UO_2 sintered with ZrO_2. They will replace the current seed plates of uranium-zirconium alloy clad with Zircaloy-2.

2. The seed of core 2 contains sufficient highly enriched uranium, compensated by lumped burnable poison, to achieve a lifetime of 10,000 EFPH for this first seed. The burnable poison is in the form of wafers of austenitic stainless-steel alloy containing 0.8% B^{10}. These wafers are used instead of the fuel wafers in some of the compartments of the seed fuel elements.

3. The fuel assemblies are to be somewhat larger in size and fewer in number (see Table VII-1).

4. The length of the core is to be increased from 6 to 8 ft. This requires lengthening of the pressure vessel by means of an extension ring, which also serves as a support flange for the core support barrel, clamped between the vessel proper and the head by the head bolts.

These changes were reviewed briefly in *Power Reactor Technology*, 5(4): 70-72. The most far-reaching change is the use of the plate type oxide elements. A long program of development has shown that these elements are capable of very long exposure lifetime if the center temperature of the fuel is not too high. When normal failure eventually occurs, it is as a result of excessive bulging of the walls of the plate compartment. Initially this bulging results from swelling of the oxide, due to the precipitation of fission gases within the oxide. Eventually, however, the pressure of the fission gas released by the oxide causes the compartment walls to bulge away from the oxide; the latter then overheats, releasing still more fission gas, and the process advances fairly rapidly to ultimate failure of the compartment wall.

The exposure lifetime has been found to vary with fuel operating temperature, internal porosity of the fuel body, and external fuel restraint, with the practical importance of the variables decreasing in the order named. Figure VII-2 shows the results of irradiation tests on elements comparable to those for the blanket of core 2. Figure VII-3 shows the results of tests in which

Table VII-1 COMPARISON OF CORE 1 AND CORE 2 DESIGN FEATURES, SHIPPINGPORT[1]

	Core 1	Core 2
Rating	231 Mw(t); 67 Mw(e) with three primary coolant loops	505 Mw(t); 150 Mw(e)* with four primary coolant loops†
Average power density, kw/liter		
Seed	75	157
Blanket	25	33
Total core	43	60
Design core lifetime, EFPH		
Seed 1	3000	10,000
Blanket	8000	20,000
Fuel elements		
Seed	Zircaloy-2-clad enriched metal alloy U-Zr plates	Zircaloy-4-clad enriched UO_2-ZrO_2 compartmented plates
Blanket	Zircaloy-2-clad UO_2 rods	Zircaloy-4-clad UO_2 compartmented plates
Fuel assemblies, number and size (cross section)		
Seed	32; 5.6 by 5.6 in.	20; 7.376 by 7.376 in.
Blanket	113; 5.5 by 5.5 in.	77; 7.376 by 7.40 in.
Number of coolant passes in core		
Seed	1	1
Blanket	1	2
Core height, ft	6	8
Nuclear control	32 rods and distributed burnable poison in the seed (seeds 2, 3, and 4)	20 rods and lumped burnable poison in the seed
Orifices	Fixed	Adjustable
Number of ports in reactor vessel head (for refueling)	10	1

*The 150-Mw(e) capability will be demonstrated by means of the existing 100-Mw(e) turbine plus a heat-dump system.

†New impellers and drive motors will be installed in the existing primary pump volutes to increase the head capability by 45%.

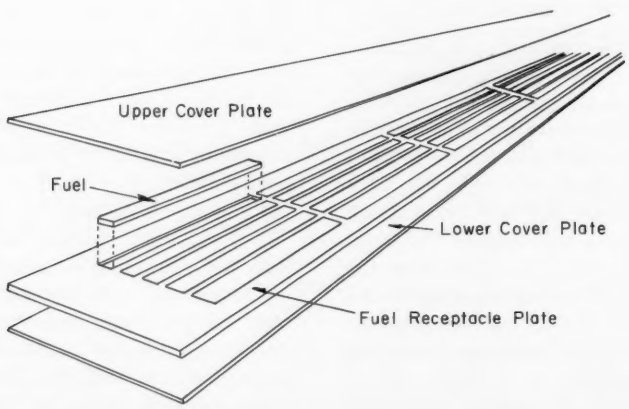

Fig. VII-1 Schematic representation of cladding and fuel components for a compartmented oxide plate type fuel element.[2]

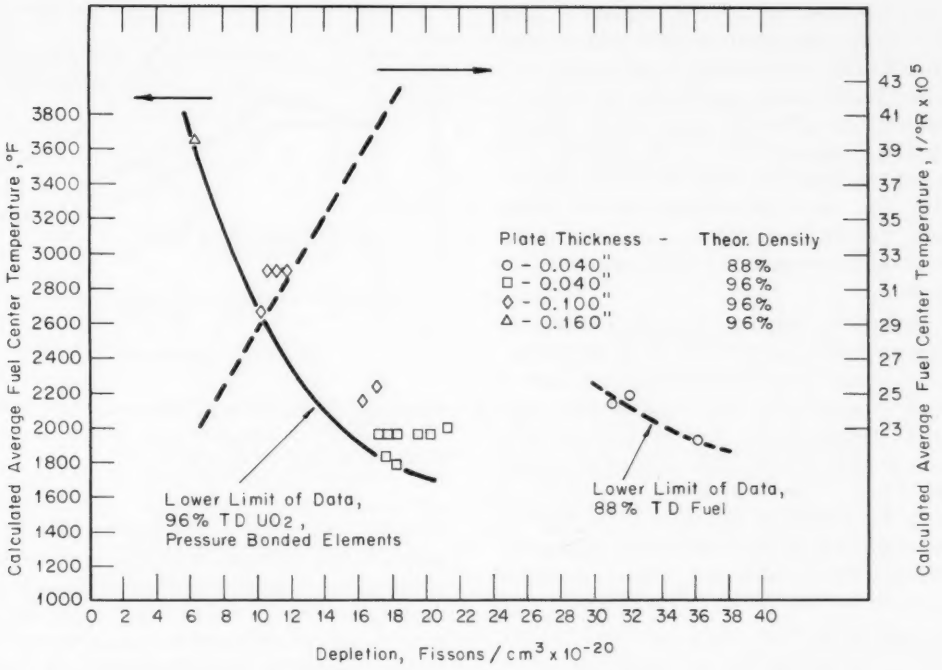

Fig. VII-2 Effects of center temperatures and oxide density on exposure lifetime of compartmented plate type UO_2 elements.[2]

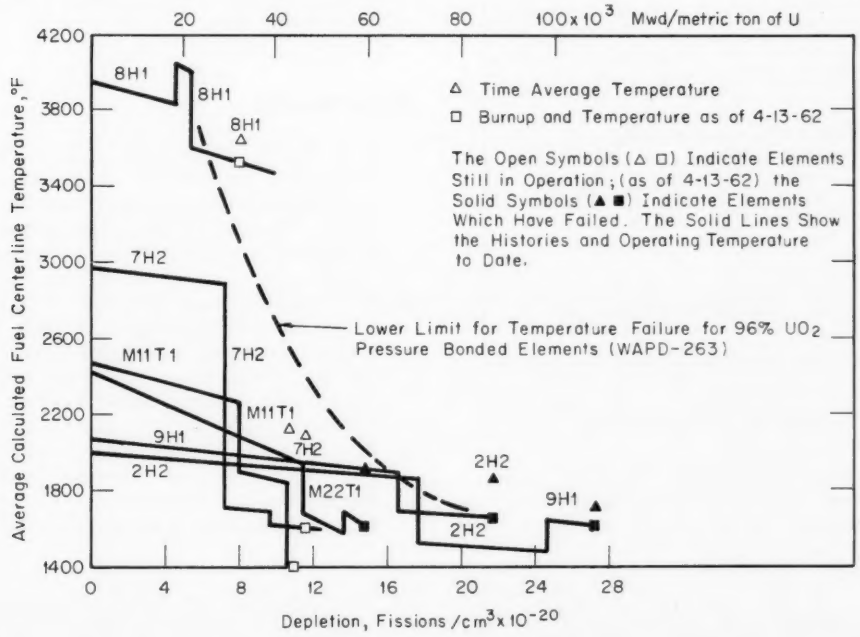

Fig. VII-3 Effects of temperature history on fuel-element life for 96% of theoretical density UO_2 fuel.[3]

elements operated for initial periods at high values of center temperature were subsequently operated at lower temperature (lower power density). The results show that the decrease of center temperature definitely improves the life expectancy and suggest that, within limits, it is reasonable to base an estimate of the life expectancy for such an element on its time-averaged center temperature—at least if the nature of the temperature variation is a decrease with time.

Figure VII-4 shows the calculated maximum exposure in the blanket of core 2 and the calculated fuel center temperature at the location of maximum exposure at the ends of four seed lives. The failure curve derived from the test program is also shown. The conclusion is that the blanket will last through four seed lives; at that time the maximum exposure in the blanket will correspond to about 70,000 Mwd/metric ton of uranium. The results of a similar analysis for the seed fuel are shown in Fig. VII-5.

It is clear from Figs. VII-4 and VII-5 that the fuel center temperatures in the Shippingport core 2 will be much lower than those customarily

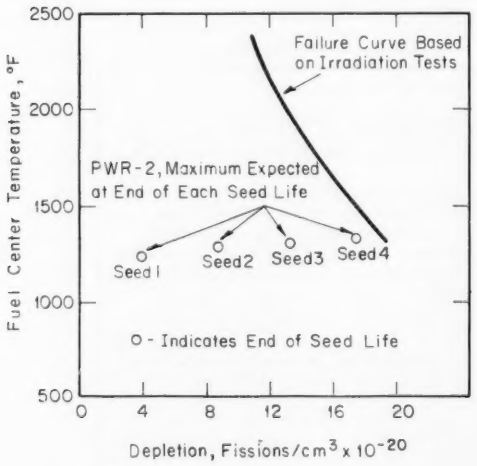

Fig. VII-4 Comparison of center-line fuel temperatures for failed UO_2 compartments with those expected in the Shippingport core 2 blanket.[1]

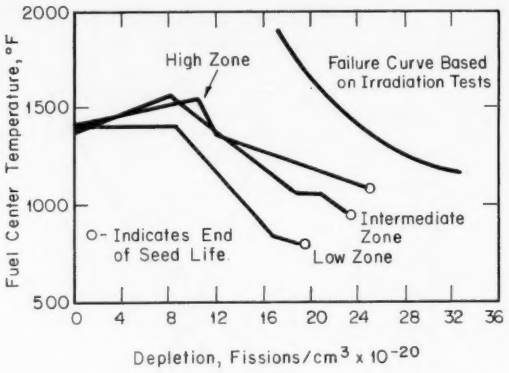

Fig. VII-5 Comparison of center-line fuel temperature in seed fuel elements tests with those expected for the Shippingport[2] core 2.

used in other reactors, which employ UO_2 elements of the rod type. The temperatures are, of course, low because of the thin oxide sections used in the fuel elements. The center temperature of one of the 0.10-in. oxide wafers in the blanket elements would be about the same as that of a rod pellet of 0.14-in. diameter if it were operating at the same specific power. The compartmented plates represent one method of utilizing very thin oxide sections in a structure of manageable size.

References

1. J. T. Stiefel, H. Feinroth, and G. M. Oldham, Shippingport Atomic Power Station Operating Experience, Developments, and Future Plans, USAEC Report WAPD-TM-390, Westinghouse Electric Corp., Bettis Atomic Power Laboratory, April 1963.
2. R. C. Daniel, M. L. Bleiberg, H. B. Meieran, and W. Yeniscavich, Effects of High Burnup on Zircaloy-Clad Bulk UO_2, Plate Fuel Element Samples, USAEC Report WAPD-263, Westinghouse Electric Corp., Bettis Atomic Power Laboratory, September 1962.
3. H. B. Meieran, Post-Irradiation Evaluation of a Plate-Type UO_2 Fuel Element, USAEC Report WAPD-TM-332, Westinghouse Electric Corp., Bettis Atomic Power Laboratory, January 1963.

NUCLEAR SCIENCE ABSTRACTS

The U. S. Atomic Energy Commission, Division of Technical Information, publishes *Nuclear Science Abstracts (NSA)*, a semimonthly journal containing abstracts of the literature of nuclear science and engineering.

NSA covers (1) research reports of the U. S. Atomic Energy Commission and its contractors; (2) research reports of government agencies, universities, and industrial research organizations on a world-wide basis; and (3) translations, patents, books, and articles appearing in technical and scientific journals.

Complete indexes covering subject, author, source, and report number are included in each issue. These are cumulated quarterly, semiannually, and annually providing a detailed and convenient key to the literature.

Availability of *NSA*

SALE *NSA* is available on subscription from the Superintendent of Documents, U. S. Government Printing Office, Washington, D. C., 20402, at $30.00 per year for the semimonthly abstract issues and $22.00 per year for the four cumulated-index issues. Subscriptions are postpaid within the United States, Canada, Mexico, and all Central and South American countries, except Argentina, Brazil, British and French Guiana, Surinam, and British Honduras. Subscribers in these Central and South American countries, and in all other countries throughout the world, should remit $37.00 per year for subscriptions to semimonthly abstract issues and $25.00 per year for the four cumulated-index issues.

EXCHANGE *NSA* is also available on an exchange basis to universities, research institutions, industrial firms, and publishers of scientific information. Inquiries should be directed to the Division of Technical Information Extension, U. S. Atomic Energy Commission, P. O. Box 62, Oak Ridge, Tennessee, 37831.

TECHNICAL PROGRESS REVIEWS may be purchased from Superintendent of Documents, U. S. Government Printing Office, Washington, D. C., 20402. *Isotopes and Radiation Technology* at $2.00 per year for each subscription or $0.55 per issue; the other four journals at $2.50 per year and $0.70 per issue. The use of the coupon below will facilitate the handling of your order.

POSTAGE AND REMITTANCE: Postpaid within the United States, Canada, Mexico, and all Central and South American countries except as hereinafter noted. Add $0.50 per year, or $0.15 per single issue for the *Isotopes and Radiation Technology* journal and $0.75 per year or $0.20 per single issue for the other four journals for postage to all other countries, including Argentina, Brazil, British and French Guiana, Surinam, and British Honduras. Payment should be by check, money order, or document coupons, and MUST accompany order. Remittances from foreign countries should be made by international money order, or draft on an American bank, payable to the Superintendent of Documents, or by UNESCO book coupons.

order form

SUPERINTENDENT OF DOCUMENTS
U. S. GOVERNMENT PRINTING OFFICE
WASHINGTON, D. C., 20402

Enclosed:
document coupons ☐ check ☐ money order ☐

Charge to Superintendent of Documents No. _____

Please send a one-year subscription to

☐ NUCLEAR SAFETY
☐ POWER REACTOR TECHNOLOGY
☐ REACTOR FUEL PROCESSING
☐ REACTOR MATERIALS
(Each subscription $2.50 per year; $0.70 per issue.)
☐ ISOTOPES AND RADIATION TECHNOLOGY
(Each subscription $2.00 a year; $0.55 per issue.)

SUPERINTENDENT OF DOCUMENTS
U. S. GOVERNMENT PRINTING OFFICE
WASHINGTON, D. C., 20402

(Print clearly)

Name _____

Street _____

City _____ Zone ____ State _____